8-22-2014

The Role of Metallothionein and Zinc Signaling in CD4+ T cell Activation and Differentiation

James M. Rice
University of Connecticut - Storrs, jamesmrice1@gmail.com

The Role of Metallothionein and Zinc Signaling in $CD4^+$ T cell Activation and Differentiation

James M. Rice, PhD

University of Connecticut, 2014

Metallothioneins (MTs) are small-molecular weight, high cysteine content proteins that bind and release zinc ions in response to redox signaling and oxidative stress. Although the precise cellular functions of MTs remain elusive, their upregulation in $CD4^+$ T cells following activation and during inflammation implicates their role in modulating immune responses. To understand the role of MT in $CD4^+$ T cells, MT expression and $[Zn^{2+}]$ were characterized under different cytokine environments during primary and secondary activation. Increased MT expression correlates with a higher intracellular $[Zn^{2+}]$ following activation, suggesting a potential mechanism of increased MT expression and a role for MT in the differentiation of the $CD4^+$ Tr1 effector phenotype.

$CD4^+$ T cells that do not express MT (MT-KO) exhibit a weaker increase in intracellular labile $[Zn^{2+}]$ following exposure to extracellular ROS or following T cell receptor activation compared with congenic wildtype controls (MT-WT). However, oxidation of ROS sensitive probes is equivalent in the presence or absence of MT, suggesting MT provides a redox sensitive mobilizable zinc reservoir but does not affect the total redox buffering capacity. These results suggest a role for MT in modifying intracellular signal transduction in CD4+ T cells by increasing intracellular $[Zn^{2+}]$ following ROS production.

The Role of Metallothionein and Zinc Signaling in $CD4^+$ T Cell Activation

James McDowell Rice

B.S. University of Connecticut, 2004

A Dissertation

Submitted in Partial Fulfillment of the

Requirements for the Degree of Doctor of Philosophy

at the

University of Connecticut

2014

APPROVAL PAGE

Doctor of Philosophy Dissertation

Investigating the Role of Metallothionein in
$CD4^+$ T cell Activation and Differentiation

Presented By
James M. Rice, B.S.

Major Advisor _____
Michael A. Lynes, Ph.D.

Associate Advisor _____
Adam Zweifach, Ph.D.

Associate Advisor _____
Lawrence K. Silbart, Ph.D.

University of Connecticut
2014

Acknowledgements

This thesis would not have been possible without the support of many people. First, I would like to thank my advisor, Dr. Michael Lynes, for being an excellent mentor. I have great respect for his innovative approach and tireless enthusiasm for science and without his guidance and encouragement this work would not have been possible. I would like to thank my associate advisor, Dr. Adam Zweifach. In addition to considerable time helping with experimental design and data analysis, his honest and objective critical insight helped me better address my experimental hypotheses. I would also like to thank my associate advisor, Dr. Larry Silbart, for his time and support and for teaching me to organize and focus my experimental results so they can be effectively communicated, which, ultimately, is the most important aspect of scientific research.

I would like to thank Dr. Carol Norris for her guidance and technical expertise in flow cytometry and microscopy. Her help in training me to collect and analyze my data and troubleshoot my experimental designs was instrumental to this work. I would also like to acknowledge Katherine Han who helped me with the ELISA based cytokine analyses as part of her undergraduate thesis and Gaurav Joshi who helped me with the confocal imaging.

An important component of this dissertation relied on the use of SPR based instruments designed and built by Ciencia, Inc. I would especially like to thank Arturo Pilar for his support and humor, which have always helped me maintain a positive

outlook. I would also like to thank Dr. Ernest Guignon for being an examiner and mentor and always being available for scientific feedback.

To my parents, James and Susan Rice, I thank you for your tireless support through all of my academic endeavors, along with your example of hard work and persistence, which has always motivated me to challenge myself. To my parents, Mukund and Meena Doshi, I thank you for your unwavering love and support. Finally and most of all, I would like to thank my wife, Dr. Bindi Doshi, for not only putting up with the late nights and long hours away from home, but for always encouraging me to be the best scientist and the best person I can be.

Table of Contents

Chapter 1

Introduction

Over the last decade, significant progress has been made in elucidating the roles of biological labile zinc and its effect on intracellular signal transduction. Because intracellular concentrations of labile zinc ions (hereafter referred to as [Zn^{2+}]) are maintained in the picomolar (pM) range in lymphocytes, investigating changes in [Zn^{2+}] was not possible until the development of suitable high-affinity fluorescent sensors. Following the widespread use of these sensors to investigate immune cell signaling, a paradigm of cellular fluctuations in [Zn^{2+}] as an important cellular signal has emerged. These fluctuations are associated with activation and cytokine receptor signaling and have significant and measurable effects on cell proliferation.

The spatial and temporal organization of zinc signals varies between cell types and signal origin. In $CD4^+$ T cells, zinc influx into the cytosol from both extracellular and vesicular spaces has been observed, resulting in an increase in cytoplasmic [Zn^{2+}]. This increase overlaps with cytosolic activation of phosphorylation dependent signaling networks, including MAPK and JAK/STAT pathways. Small increases (>1 nM) in cytoplasmic [Zn^{2+}] have the potential to modify these signaling networks by inhibiting phosphatase activity. Inhibition of phosphatases that are considered negative regulators of $CD4^+$ T cell signaling by zinc, including SHP-1 and MKP-1, are thought to be important regulatory checkpoints for cell proliferation.

The following work explores a novel mechanism for increased cytoplasmic [Zn^{2+}] in $CD4^+$ T cells that is independent of trans-membrane zinc movement through ion

transporters. Cytoplasmic pools of metallothioneins (collectively referred to as MT) serve as a redox mobilizable reservoir of zinc ions. The unique biochemistry of MT allows for the conversion of reactive oxygen species (ROS) into an increased cytoplasmic [Zn^{2+}], therefore converting a redox signal into a zinc signal. This can occur even in the overall reducing environment of the cytoplasm because of the low redox potential afforded to MT by its high cysteine content. The recent observations of ROS and RNS signals in $CD4^+$ T cells following activation provide a potential mechanism by which zinc release from cytoplasmic could affect intracellular signaling networks.

The central hypothesis in this thesis is metallothionein provides a redox mobilizable zinc reservoir in $CD4^+$ T cells following activation that affects intracellular signal transduction. This will be broken down into the following testable hypotheses:

1. MT is expressed in effector $CD4^+$ T cells
2. $CD4^+$ T cells that express MT exhibit a greater increase in intracellular [Zn^{2+}] following exposure to ROS compared to congenic MT knockout controls
3. $CD4^+$ T cells that express MT exhibit a greater increase in intracellular [Zn^{2+}] following T cell activation compared to congenic MT knockout controls
4. The increased zinc signal associated with MT expression increases activation of the p38 MAPK pathway in $CD4^+$ T cells
5. MT gene dose affects IL-10 secretion from $CD4^+$ T cells via regulation of intracellular [Zn^{2+}]

1.1 Thesis Overview

Chapter 1 provides a general review of metallothionein (MT) and its various biological functions with an emphasis on expression in $CD4^+$ T cells. This includes regulation of MT expression at the genetic level (transcriptional, post-transcriptional, epigenetic) and protein level (translation, degradation, trafficking). This is followed by a review of MT structure and how that contributes to its unique position at the intersection of redox and zinc signaling in biology. This is followed by a review of $CD4^+$ T cells and their contribution to adaptive immune responses through clonal expansion and differentiation. The role of labile $[Zn^{2+}]$ in modifying $CD4^+$ T cell signaling pathways following activation is discussed and a role for MT in modulating the labile $[Zn^{2+}]$ is proposed.

Chapter 2 describes the materials and methods used in the experiments described in this thesis. These include descriptions of the mouse models and the culture conditions used to generate the Tr1 and TH0 $CD4^+$ T cell phenotypes. Establishing a condition of robust MT expression in MT-WT CD4+ T cells using the Tr1 phenotype will allow experimental investigation into the effects of MT by comparing wildtype Tr1 cells with Tr1 cells from congenic MT knockout mice (MT-KO). Specific reagents and protocols are referenced.

Chapter 3 establishes the experimental foundation of how intracellular $[Zn^{2+}]$ is measured in $CD4^+$ T cells *in vitro*. This includes methods to manipulate intracellular $[Zn^{2+}]$ using zinc specific chelators or ionophores as well as control of intracellular $[Zn^{2+}]$ through addition of antioxidants or an extracellular $[Zn^{2+}]$. The subcellular localization of Zn^{2+} and the effect of MT gene dose on that localization is investigated by confocal

microscopy. Finally, the sensitivity of the p38 MAPK pathway to intracellular [Zn^{2+}] in $CD4^+$ T cells is demonstrated by western blot and flow cytometry.

Chapter 4 explores the effects of MT on the fluctuation of intracellular [Zn^{2+}] and MT expression in naïve $CD4^+$ T cells following primary activation through the T cell receptor (TCR). This is done in the presence (Tr1 inducing conditions) or absence (TH0 inducing conditions) of IL-27. The effect of MT gene dose on the redox mobilizable zinc pool and total redox buffering capacity in Tr1 cells is then investigated.

Chapter 5 examines the effects of MT on intracellular labile [Zn^{2+}] and effector function during reactivation of Tr1 cells. This includes the generation of ROS signals following TcR mediated activation and the subsequent increase in intracellular labile [Zn^{2+}]. The effect of this increase in intracellular labile [Zn^{2+}] on the p38 MAPK pathway and IL-10/ IFN-gamma secretion in Tr1 cells is then explored. Finally, the effect of MT gene dose on *in vivo* adaptive immune responses is assessed by isotyping the IgG response to type II collagen and by comparing the Treg frequency with $CD4^+$ T cell populations with MT gene dose.

Chapter 6 brings together a discussion of the experimental results and how they suggest a role for MT as a reservoir of redox mobilizable intracellular labile zinc in $CD4^+$ T cell activation. Finally, future directions for continuing to investigate the impact of MT on intracellular labile zinc signaling are proposed.

1.2 Metallothionein

Metallothioneins (collectively referred to as MT) are small-molecular weight, high cysteine content proteins that are ubiquitously expressed in most mammalian cells.

Although the precise cellular functions of MTs remain elusive, their upregulation in response to increases in metal or reactive oxygen species (ROS) or pro-inflammatory cytokines[1] suggests an important role during cellular stress responses. These conditions are present during adaptive immune responses where extracellular cytokines and intracellular redox and zinc ion signaling events precede the proliferation and differentiation of $CD4^+$ T cells. The unique biochemistry of MTs allows for the binding and release of zinc ions in response to redox signaling and may therefore play a role in shaping adaptive immune responses by directly influencing these signaling pathways.

Significant experimental evidence indicates that MTs are immuno-modulatory in both autoimmune disease and infection models, although the mechanisms underlying these effects remain poorly understood. Generally, inflammation and disease severity are increased in $CD4^+$ T cell mediated autoimmune disease models in MT knockout mice (MTKO) compared with wildtype controls [2,3]. However, MT expression is associated with increased inflammation in models of autoimmune inflammatory colitis [4] and EAE when $CD4^+$ T cells are adoptively transferred[5]. These divergent immunological consequences suggest that the effects of MT on the adaptive immune response are context dependent.

Intracellular zinc signaling has recently emerged as an important component of T cell activation and differentiation [6] and may play a role in MT mediated immunomodulation. Nanomolar increases in intracellular labile [$Zn2^+$] can have significant effects on signaling pathways originating from the T cell receptor [7], cytokine receptors [8] or toll-like receptors [9]. Increases in intracellular [Zn^{2+}] inhibit distinct sets of intracellular kinases [10] [11] and phosphatases [12] [13,14] that alter STAT and MAPK signaling

networks and affect transcription factor activity. Regulating the concentration of labile intracellular zinc, therefore, has the potential to dramatically impact the development of $CD4^+$ T cell effector function [15-17] and ultimately immune function and disease pathology.

MTs have the ability to bind and release zinc under physiologically relevant conditions and, along with cell specific Zn importers and exporters, are part of a network that regulates intracellular $[Zn^{2+}]$. The intracellular pool of MT is comprised of oxidized, reduced and zinc bound forms [18 19] whose dynamic equilibrium is positioned to release Zn in response to intracellular ROS generation and subsequently increase intracellular labile $[Zn^{2+}]$. Zn release is possible even in the reducing environment of the cytoplasm through reactions with selenium redox catalysts[20]. The 20 vicinal cysteine residues of MT impart a very low redox potential (-366 mV) which directs its preferential oxidation before other free thiols like GSH [21]. Additionally, three of the seven Zn binding sites of MT have an affinity for Zn ($\log K = 10 - 7.7$)[22] that allow Zn to be released and affect enzyme activity and signaling cascades[6]. These properties uniquely position MT to transduce ROS signals into Zn signals within the narrow range of redox and Zn fluctuations that occur during $CD4^+$ T cell activation.

In this report, the relevant state of the field for measuring intracellular labile $[Zn^{2+}]$ and [MT] and the development of protocols for measurement in lymphocytes is reviewed. Development of these methods forms the experimental foundation for investigating fluctuations in intracellular labile $[Zn^{2+}]$ and MT during primary $CD4^+$ T cell activation and differentiation into effector phenotypes. Furthermore, insight into the contribution of MT in this process will be gained by using an MT-KO model that does not express functional MT1 or MT2 proteins. Experimental manipulation of labile $[Zn^{2+}]$ will

also be investigated to determine the effect of MT gene dose on zinc mediated regulation of p38 MAPK activation and IL-10 and IFN-gamma secretion during secondary activation of $CD4^+$ T effector cell subsets. Finally, the broader immunomodulatory effects of MT will be examined by observing the humoral responses to type II collagen immunization as part of a mouse model of inflammatory autoimmune arthritis.

1.2.1 History and Occurrence

The first MTs were first isolated in 1957 from a equine kidney cortex after cadmium exposure [23] and is the only protein known to contain this metal [24]. The designation of metallothioneins, as its name suggests, comes from the combination of the high cysteine content and the ability to bind metals. MTs were originally characterized by the following characteristics: molecular weight of 6-7 kDa; high metal content: characteristic amino acid composition (high cysteine content, no aromatic or histidine residues); unique distribution of cysteine residues; and unique spectroscopic signatures associated with metal-thiolate bonds. At the First International Meeting on Metallothionein and Other Low Molecular Weight Metal-binding Proteins in 1978, the definition of metallothionein was adopted and any protein satisfying several of the criteria can be classified as MT. This classification strategy was revised in 1999 and is currently based on phylogenetic relationships between the protein and the nucleotide sequences of different isoforms[25]. The focus of Part 1 of this thesis will be to outline the unique structure of MTs and how that structure contributes to redox and zinc binding functions.

Metallothioneins, as defined above, can be found in both eukaryotes and prokaryotes and all vertebrate and invertebrate phyla except coelenterate (marine jellyfish). A comprehensive list of all the metallothioneins is beyond the scope of this thesis but for a review and comprehensive list of MT expression systems in different living systems see [26]. In mammals, 4 distinct isoforms of MT are expressed, of which MT-1 and MT-2 are the most abundant and are the only isoforms classes expressed in lymphocytes. MT1 and MT2 will be only isoforms discussed in this thesis and hereafter will be referred to collectively as MT. MT-1 and MT-2 differ by only a single negative charge that separates them during ion exchange chromatography, which led to the first distinction between MT1 and MT2. Within the MT-1 and MT-2 charge groups, many mammals (but not mice) express multiple isoforms with the same charge but distinct structures (see genetic organization below). MT-3 is found primarily in the brain and neurons [27] although its mRNA is expressed in the tongue, stomach, heart, kidney and reproductive tissues [28,29]. MT-4 is the least studied of the 4 isoforms and has been detected primarily in squamous epithelia [30].

Constitutive levels of MT expression can be found in most cell types, with certain tissues containing high levels of MT and others expressing significant less. In[31] adult monkeys, for example, the hierarchy of concentrations in tissues are kidney > liver > pancreas > intestine > testes > lung > heart [32]. There is considerable variation between species in concentrations of MTs in various tissues. For example, hepatic levels of MT ranges from 400 – 700µg MT per gram of liver tissue in humans, ~200 µg / g in monkeys, and 10µg / g in mice [33]. These amounts vary with differences in age, state of development, dietary regime, and other unidentified factors, underscoring the regulation

of MT as a dynamic component of tissues and cells that is under various regulatory controls.

Determining the presence and concentration of MT in blood cells and, in particular, lymphocytes is challenging because of the lower level of expression when compared with the liver or kidney. In general, MT protein concentrations in leukocytes are measured by Cd/ Hemoglobin Affinity assay, immunoassay (such as immunoblot or ELISA), or by immunofluorescence. Baseline estimates of MT expression place resting levels in human T lymphocytes at ~1.21nM with 4 times higher levels in B lymphocytes[34]. Activation of lymphocytes by mitogens, or exposure to inducing agents including Zn, Cd, or dexamethasone (a glucocorticoid analog) strongly induces the expression of MT in human lymphocytes. After 2 or 6 days in culture with extracellular ZnCl [125μM], T cell expression of MT increased 3-fold and 10-fold, respectively[34]. In mice, MT expression in lymphocytes and hepatic tissue is lower than in humans. MT protein levels are virtually undetectable in mouse splenocytes without induction. However, upon culture with Zn or stimulation with the T cell mitogen concanavalin A, MT is rapidly induced and can be measured by immunoblot in concentrations around 1.81nM and .381nM, respectively [35]. Interestingly, pathways of MT induction by mitogens or zinc are interrelated and can be a point of regulation during T cell proliferation [36].

1.2.2 Genetic organization

There are several distinct differences in the phylogenetic organization of MTs between humans and rodents. Rodents express 4 functional MT genes (*Mt1, Mt2, Mt3,*

and Mt4), which are clustered on chromosome 8. Humans express these 4 isoforms but have additional copies of *Mt1 and* Mt2*,* and all functional MT genes are clustered on chromosome 16 (16q13). In humans, there are 13 total copies of *Mt1,* 2 copies of *Mt2*, and one copy each of *Mt3* and *Mt4.* Of the 17 MT genes, 10 encode functional proteins (MT-1a, MT-1b, MT-1e, MT-1f, MT-1g, MT-1h, MT-1x, MT-2a, MT-3, MT-4) while 7 are classified as non-processed pseudogenes (*Mt1c, Mt1d, Mt1i, Mt1j, Mt1k, Mt1l, Mt2b)* according to the RCSB protein data bank (www.rcsb.org). For a thorough review see [37]. The MT-1 and MT-2 genes show a significant degree of sequence homology between mouse and human (Figure 1). All 20 cysteine residues between MT-1 and MT-2 in mouse and human proteins are perfectly conserved. Additionally, MT-1 and MT-2 from many species including human, mouse, rat, rabbit, dog, horse and fish are all cross reactive with anti-MT antibody (clone UC1MT) (http://www.abcam.com/metallothionein-antibody-uc1mt-ab12228.html)[38]demonstrating their shared antigenic structure. Taken together, these observations provide a reasonable basis for making inferences on the functions of human MTs based on mouse models.

To study the effects of MT in living systems, MT gene dose was manipulated in mice. Strains of mice that do not express (MT-KO) or overexpress MT (MT-TGN) were created and compared with congenic wildtype controls (MT-WT) in prospective studies to examine the role of MT in $CD4^+$ T cell activation and differentiation. To create a functional MT knockout strain, targeted disruption of the metallothionein I and II genes (*Mt1 and Mt2)* was achieved on a 129/SvCPJ background [39]. To create a functionally overexpressing strain (MT-TGN), 112 additional copies of *Mt1* (56 on each chromosome) along with distal regulatory elements (*cis-* and *trans-)* from the mouse MT

locus were cloned and introduced onto the 129/SvCPJ mouse background[40]. Both of the congenic strains described, hereafter, were produced by 8–9 generations of backcrossing these mice to the C57BL/6J background strain, followed by incrossing of the heterozygotes to produce homozygotes for each construct. According to the equation for the fraction of loci that are still heterozygous at the Nth generation $[(1/2)^{N-}1]$ the amount of residual donor genetic material that may contribute to observed phenotypic differences after 8–9 backcrosses is between 0.2 and 0.4% [41].

1.2.3 Basal Expression and Induction of MT Transcription

MT gene transcription is induced by many endogenous factors including metals, cytokines, oxidants, and glucocorticoids and exogenous factors including bacterial lipopolysaccharides (LPS) and mitogens including concanavalin A (for review see [37,42]). MT is upregulated under normal, healthy conditions in proliferating cells and under stressful conditions including infection, inflammation, and heavy metal toxicity, Because of the latter, MT is considered in many contexts to be a stress response protein because of its relatively fast induction (<2 hours) and small molecular weight; features it shares with other stress response proteins including heat shock proteins (HSPs). When MT is found in the extracellular environment it can even be considered a danger signal and can influence immune cell chemotaxis and the pathogenesis of inflammatory autoimmune colitis [4].

All MT genes in both mice and humans share similar regulatory elements that control their transcription. However, the preferential induction of certain MT isoforms under particular conditions indicates a high degree of regulatory control. In mice, for

example, metals and glucocorticoids equally induce MT-1 and MT-2[43,44]. In humans, metals induce all MT isoforms but preferentially induce MT-2a with 5 times greater efficiency that MT-1. Glucocorticoids induce MT-2a and MT-1e[45] but not the other MT-1 isoforms and with the same bias towards MT-2a. It is important to note that the presence of multiple copies of *MT1* genes as a result of gene duplication in humans has allowed for the mutation and evolution of the regulatory elements upstream of each gene copy, resulting in induction and expression patterns in humans that are cell and tissue specific. The multiple isoforms of MT1 and MT2 encoded by these genes, however, are so close in structure and sequence homology that they are considered functionally equivalent with regard to binding and releasing Zn. Furthermore, while MT1 expression patterns may differ between human cell types, the pattern of expression in mouse and human lymphocytes is the same. This includes the metal dependent coordinate regulation of MT-1 and MT-2 genes, which further supports using mice as a model system for studying MT post induction in lymphocytes. Below is a brief overview of MT expression and induction in humans and mice with a focus on lymphocytes.

The transcriptional regulation of MT genes is reflected in its physiological occurrence in response to metal stress and inflammation and the relevant regulatory elements underlying its induction are conserved between mice and humans. Directly upstream (*cis*-) of MT genes, in order of proximity to the transcriptional start site and strength of positive regulation are: metal response elements (MREs); antioxidant response elements (AREs); binding sequences for signal transducers and activators of transcription (STATs) which are part of extracellular receptor signaling pathways; and glucocorticoid response elements (GREs). Catecholamines and glucagon act via

second-messenger systems (Ca2+ and cAMP dependent protein kinases) and induce expression via *trans-* acting nuclear factors. For a comprehensive review, see [46]**.** The contribution of each of the regulatory elements is cell specific and can be synergistic, especially between non-metal induction pathways.

Basal MT Expression

Basal expression of MT genes is achieved through the presence of conserved TATA boxes that are 25 bp upstream of MT genes in all but 5 human MT1 isoforms (*MT1E, MT1F, MT1H, MT1J and MT1M)*. GC boxes are found in all MT promoters (human and mouse) and are often clustered close together near the transcription start site. This acts as a binding motif for Sp1 factors and can synergistically stimulate transcription. AP-2 related basal level enhancer sequences are found in most human MTs as well and can result in MT overexpression and acquired resistance to cisplatin[47]. Other important regulatory elements of basal MT expression in both mice and humans include general transcription factor II (TFII-I) and upstream stimulatory factor (USF) binding to an upstream E box which overlaps with the antioxidant response elements (AREs). Finally, metal response elements contribute to basal MT expression, primarily through a low level of constitutive metal transcription factor 1 (MTF-1) binding [48].

Induction by metals

The most potent inducers of MT expression are metals. In human peripheral lymphocytes, induction by metals has been demonstrated for Zn^{2+}, Cd^{2+}, Hg^{2+}, Cu^{2+}, and Ni^{2+}, but not Sn^{2+}, Pb^{2+}, Fe^{2+}, Co^{2+} and Mn^{2+} [49]. Metal induced MT synthesis is

mediated via *cis*-acting metal response elements (MREs) which are found in multiple copies in the promoter region of MT genes in both humans and mice and act as binding sites for MTF-1. MTF-1 binds to multiple, non-identical MRE sequences and a 7 bp core sequence (TGCRCNC) that is present in the promoter of MT genes. This variation of MTF-1 binding allows MT transcription to be differentially regulated by different metals[50].

MTF-1 activity is intrinsically regulated by multiple factors. It is a multiple zinc finger protein and Zn is an important co-factor of MTF-1 activity. Upon Zn binding, MTF-1 changes into an active conformation that effectively binds MREs and induces MT transcription. The activity of MTF-1 also relies on the CREB binding protein (CBP) and E1A binding protein, which are implicated in regulation of interferon-gamma production in human $CD4^+$ T cells[15] and regulatory T cell activation and signaling[51]. Oxidative stress has been found to activate MT[52], suggesting Zn release from cellular thiols upon oxidation may contribute to an important Zn signal that influences the cellular transcriptome. Because the amino acid sequence of MTF-1 is 93% identical between mouse and human, the role of MTF-1 in mouse studies can be considered to be a good model for human systems.

There are many proteins that act as transcription factors capable of binding MREs and positively affecting *Mt* gene transcription during induction. Many of these proteins are, themselves, induced by Zn^{2+} and are part of a regulatory loop that increases MT synthesis to maintain labile [Zn^{2+}] homeostasis. These include metal response element binding factor-I (MBF-1)[53], zinc activated protein (ZAP)[54], zinc regulated factor (ZiRF1)[55] among others. Many of these proteins have been observed in certain cell types and not others, suggesting that the regulation of zinc signaling is cell

type specific. In lymphocytes, the cell type that is the focus of this thesis, the most important signaling pathway for metal induction of MT is MTF-1.

Cd^{2+} and Zn^{2+} are the most potent inducers [56] of MT in all systems and can induce maximum MT expression in lymphocytes. Because Cd^{2+} and all other metals known to induce MT except for Zn^{2+} and Cu^{2+} are not biologically relevant under normal conditions, the remainder of this review will focus on Zn as the primary and most potent metal inducer of MT. Additionally, Cd^{2+} induction of MT is mediated, in part, through displacement of Zn from cellular ligands which confers a zinc signal, similar to induction by zinc itself. Of note, normal physiological concentrations of Cu^{2+} do not induce MT synthesis and therefore Zn can be considered the only relevant MT inducing metal. Because Zn signaling is an important regulatory component of many T cell processes, including but not limited to activation or exposure to oxidative stress (see Part 2 of the Introduction), the regulation of MT expression by Zn^{2+} should not be considered only in the context of environmental or nutritional excesses or deprivation, but rather as an important component of many signaling pathways.

Induction by stress, inflammation, and infection

When circulating $CD4^+$ T cell populations. When these extravasate through the blood vessels into sites of inflammation or infection, they become exposed high local concentrations of inflammatory mediators and oxidative stress, which are both strong inducers of MT synthesis. It is important to remember this temporal and spatial organization of $CD4^+$ T cell exposure to MT inducing conditions when evaluating *in vitro* models of $CD4^+$ T cell function. In general, activated and expanded T cell populations

that have exited secondary lymphoid tissues have been activated and expanded and have higher basal expression of MT than naïve cells. These populations also express higher levels of VCAM and other extracellular receptors that facilitate their chemotaxis into sites of infection and inflammation where they are likely to experience higher concentrations of molecular signals that further induce MT. This is in contrast to increased MT synthesis in naïve $CD4^+$ T cells that are exposed to increased systemic levels of cortisol or IL-6 in the peripheral blood, for example.

Transcriptional activation of MT genes following exposure to glucocorticoids (ex. cortisol), reactive oxygen species (ROS), and reactive nitrogen species (RNS) is independent of signaling through an extracellular receptor because these signals enter the cell through simple diffusion. This is in contrast to signaling though membrane-bound receptors where signals from many receptors are transduced via second messengers (cAMP, cGMP, g proteins, etc.) and the integration of these transduced signals results in transcriptional activation.

Glucocorticoids (GCs) and the synthetic glucocorticoid receptor agonist dexamethasone are strong inducers of MT in lymphocytes. In this receptor-ligand interaction, the cytosolic GC receptor binds cortisol that has diffused into the cell and becomes an active transcription factor capable of binding to GREs and upregulating transcription (for review see [57]). The human *MT2A* gene contains one GRE while murine *MT1* and *MT2* genes contain two tandem copies approximately 7 kb and 1 kb upstream, respectively. Consequently, GC induced expression of MT2A is significantly greater than MT1 in humans. In mice, the two isoforms are induced equally[58].

Transcription of MT genes following exposure to ROS is a consequence of the

activation of Nrf2 and upstream stimulatory factor (USF) and their subsequent binding to antioxidant response elements (AREs). AREs have been found upstream of murine *MT1* and human *MT1G* genes, the products of which are expressed following exposure to hydrogen peroxide or chemicals that induce oxidative stress[59]. An alternative pathway for induction by ROS has been demonstrated by the increased binding activity of MTF1 in cells treated with hydrogen peroxide [60], which is due to an increase in zinc redistribution in the cell following oxidation of cellular thiol ligands. Nitric oxide induces MT transcription in a similar manner. Exogenous addition or endogenous production (via inducible nitric oxide synthase) leads to zinc release and subsequent transcription of MT1 and MT2 genes [61,62] through MTF-1 activation. Alternatively, NO causes the nitrosylation of Keap-1 which actives Nrf2 and activates transcription via binding to AREs[63].

The fourth pathway of induction of MT transcription includes signaling through extracellular cytokine receptors. The four cytokines most strongly associated with MT induction are all considered pro-inflammatory and are secreted by immune cell populations in the context of infection and inflammation. These include IL-6, TNF-alpha, IL-1alpha and IL-1beta. IL-1 signaling is most likely mediated through glucocorticoids[64]. IL-6 signaling is achieved through activation and dimerization of signal transducer and activator of transcription 3(STAT3)[65]. These transcription factors bind IL-6 response elements (IL6RE) located in the 800 bp region upstream of all human and mouse *MT1* genes between GREs and AREs. Interestingly, there is a synergistic effect of IL-6 and GCs on MT1 induction, most likely due to the close proximity of IL6REs and GREs in the promoter region[66]. The heterogeneity of cytokine receptor expression on different

cells types and during different stages of cell activation results in pleiotropic cytokine mediated effects. TNF-alpha, in particular, which signals through TNFR1 and TNFR2, gives rise to different intracellular signaling pathways that are pro-apoptotic or pro-inflammatory, respectively. The cell dependent effects of TNF-alpha are evidenced by MT expression where MT-2 is preferentially induced in the liver and MT-1 is preferentially induced in the heart and lungs[67] following TNF-alpha exposure. Interestingly, MT expression in tissues following induction by IL-6 and TNF-alpha correlates with a marked decrease in plasma [Zn^{2+}] as part of an acute phase response to infection.

Inhibition of MT transcription also provides an important regulatory control for gene expression. Nuclear Factor 1 (NF1) suppresses both the constitutive and metal-induced activation of the MT1 promoter in both humans and mice[68] by binding to the MRE-c element. Dephosphorylation of the transcription factor C/EBPα following PI3K/AKT signaling is another mechanism of inhibition of MT expression. *Trans*- acting elements have been observed to be inhibited by a zinc binding transcription blocker PZ120, now called ZBTB11[69].

Epigenetic Regulation

Epigenetic regulation of MT genes is achieved through methylation of promoter regions in certain cell types or through modification of chromatin structure[31]. In contrast to unmodified regulatory elements, methylation of the 5 position of cytosine residues that occur as part of CpG dinucleotides can reduce associated gene expression. In MT promoter regions, CpG islands (defined as a region of DNA that is >60% CpG) have

been observed and are known to be hypermethylated in certain cancer cell types [70]. Chromatin modification is thought to also affect MT gene accessibility because addition of sodium butyrate, which is known to generate DNAse I hypersensitive sites, increases MT mRNA levels and renders the genes hypersensitive to metal induction[71,72]. In lymphoid cells, removal of DNA methylation by azacitidine treatment increases expression of MT-1F and MT-1G in response to zinc and MT-2A in response to dexamethasone, indicating a level of epigenetic repression that influences cell specific expression[31]. Given the high degree of chromatin remodeling that occurs during $CD4^+$ T cell activation and differentiation, chromatin structure may also play a role in lymphoid effector phenotype specific MT expression.

Although many mechanisms of MT gene specific activation and repression are cell type specific, they illustrate the complex nature of transcriptional regulation of MT genes. The organization and structure of the *cis*- and *trans- regulatory elements* suggests a level of regulation that is intimately involved with inflammatory immune processes and is tightly controlled by the interplay between zinc, ROS/RNS, and inflammatory cytokines. In lymphocytes, all of the following regulatory mechanisms contribute to MT expression. Hypermethylation of the MT-1 gene promoter in the thymus, for example, limits MT expression in immature thymocytes[44,73] but this repression is removed upon entry into the periphery. Zinc signaling, cytokine signaling, redox signaling, and chromatin remodeling are all essential components of $CD4^+$ T cell activation, differentiation, and development and are all intimately related to MT induction and feedback loops. Understanding the role of MT in influencing $CD4^+$ T cell differentiation relies upon an understanding of how different inducing conditions

contribute to the pool of intracellular MT and sets the stage for MT mediated effects on cell activation and signaling.

1.2.4 Translation, Degradation and Trafficking

Translation

There is strong evidence of post-transcriptional control of MT mRNA that is both metal and isoform specific[74,75]. Zn concentration affects the rate of *Mt1* and *Mt2* mRNA turnover and recruitment of *MT1* mRNA transcripts to the polysomes where the protein is synthesized[76]. Even though more *MT2* mRNA is expressed in most human cells, a greater proportion of *MT1* mRNA is associated with polysomes suggesting it is translated more efficiently. This difference in post-transcriptional control is a central reason MT mRNA levels are often not reflected by MT protein concentration within cells. This discrepancy emphasizes the need to measure protein levels in addition to RT PCR techniques that measure mRNA.

Post-Translational Modifications

The most common and well studied post translational modification is the binding of metal ions, which happens immediately after the protein is translated, and, to some extent, during translation itself. On human MT1 and MT2, there are 2 sites of potential phosphorylation (serine 6 and 12), 2 potential sites for acetylation (lysine 22 and 51) and 1 site for ubiquitination (lysine 43). Of these sites, only the K43 site is conserved between mouse and human. Acetylated and non-acetylated forms of MT2 both occur in relatively equal proportions in the human liver and plasma [77] but the biological

significance of this modification is not known. Furthermore, interactions between MT and glutathione[78] and ATP [79] have also been observed.

Degradation

The total cytosolic concentration of MT is a function of both its rate of expression and degradation. MT degradation takes place primarily in the lysosomes via the proteolytic action of cathepsins B and/or L[80,81]. On a more limited basis, MT degradation occurs in the cytoplasm via neutral, soluble proteases[82]. The rate of MT degradation is both metal and redox dependent and isoform specific. Metal bound MTs have a much longer half life *ex vivo, in vivo,* and *in vitro* than MTs that are not bound to metals (apoMTs) [83-85]. The type of metal bound and the degree of metal binding saturation are affected by the metal status of the organism as well as the redox poise of the cells themselves. Furthermore, other factors that affect MT-metal binding affinity, including pH, indirectly affect MT stability and degradation by affecting metal binding. This is a may be a contributing factor to lysosomal degradation of zinc bound MT, where the pH is significantly lower (3.6 – 5 vs. 7.2), being the predominant MT degradation pathway. Regarding isoform specific proteolysis, the alpha-domain of MT-1 and the beta domain of MT-2, but no other combinations, have been found in the liver form zinc treated rats[86]. This suggests that the different metal clusters of MT-1 and MT-2 may have different proteolytic degradation pathways, providing further control over the cell and tissue specific accumulation of the two isoforms beyond transcriptional and post-transcriptional regulation. It should be noted that the mechanisms described above were observed in cell and tissue systems that express large amounts of MT upon exposure to heavy

metals or zinc. In this way, MT is a primary metal detoxifying agent and a central player in the physiology underlying resistance of organisms to heavy metal toxicity. The focus of this thesis, however, will only cover fluctuations in zinc that occur within a normal physiological range and only in lymphocytes. It is important to remember that the degradation of large amounts of MT in liver cells following exposure to cadmium might not be an entirely relevant model for the degradation of MT in lymphocytes, where it is primary lysosomal and not significantly different for MT-1 and MT-2.

Nuclear Trafficking

MT is usually a cytoplasmic protein but exhibits preferential nuclear localization under several conditions. These include malignant tumor growth, fetal liver, in high glucose medium, and in proliferating and differentiating cells. Consequently, nuclear MT localization can be considered cell cycle and proliferation stimulus dependent. MT lacks a traditional nuclear localization signal (NLS) that would traffic the protein to the nucleus. Similar to calmodulin, which also lacks a NLS, MT transport into the nucleus is affected by wheat-germ agglutinin (WGA) treatment (which binds GlcNAc, glycosylated residues) and by ATP depletion[87]. Interestingly, there is conflicting data regarding temperature and MT nuclear transport. In SCC25 (squamous cell carcinoma) cells, temperature did not affect MT nuclear localization [88], while in HL-60 (lymphoblast) cells it prevented the protective effects of MT from taking place in the nucleus[21] indicating that the binding of MT to its receptor, but not the translocation process itself is energy dependent. This is different from the classical NLS-bearing protein translocation mechanism and indicates MT binds a nuclear translocation mechanism in an ATP dependent manner, and then

enters the nucleus by diffusion[89]. Evidence for this proposed mechanism is strengthened by the fact that MT is not retained in the nucleus after flushing with buffer. Further investigation has led to the discovery that MT nuclear localization requires the oxidation of a cytosolic accessory protein for efficient translocation[90], an effect which is prevented by excess glutathione. Taken together, this data suggests that MT is targeted to the nucleus by passive diffusion and retention with a non-diffusible nuclear binding partner, a process that would be compatible with a proposed role for MT that is closely associated with DNA replication. In the context of T cell activation and proliferation, increases in intracellular [Zn^{2+}] and [ROS] precede induction and sub cellular localization of MT to the nucleus, where it presumably plays a role in preventing errors in DNA replication by acting as an antioxidant. Increased expression of MT during $CD4^+$ T helper cell effector differentiation could therefore prime $CD4^+$ T cells for increased proliferative capacity.

Secretion

Extracellular pools of MT are observed in serum [91,92], urine[93], bronchoalveolar[94] and prostatic fluids[95], liver sinusoids and renal tubules[96], pancreatic ducts[97] and milk[98]. They are also considered an important extracellular danger signal with chemotactic properties that affect immune cell trafficking in the context of autoimmune colitis[4]. The mechanism by which MT leaves the cytoplasm is unknown but the high concentrations found in secretions and extracellular spaces, absent signs of necrosis or tissue damage, indicate that there is a biological mechanism responsible. Additionally, MT was found to be secreted from adipocytes in culture, and was observed in the supernatant before

other secreted proteins including leptin which strongly suggests it is actively secreted from cells. The vast majority of MT (>93% in rat liver) is translated on polysomes[99]. Most extracellular proteins have an N-terminal secretion signal (SS) that directs mRNA to the endoplasmic reticulum (ER) for co translational translocation and vesicle secretion via the Golgi apparatus. However, there exist many directed small molecular weight protein secretion mechanisms that lack this SS, including those for IL-1 alpha and IL-1 beta and HSPs. Like these proteins, MT may be secreted through lysosomal secretion pathways, exosomes, exovesicular membrane blebbing [100-102]or move directly across the membrane as is observed with IL-1[103].

Uptake from the Extracellular Environment

Extracellular MT can also be taken up by cells, as has been demonstrated in renal proximal tubules[104] and hepatocellular carcinomas cells (HepG2). This process appears to be dependent on surface expression of megalin[105] in the case of renal cells and on binding to albumin followed by clathrin-mediated endocytosis in HepG2 cells. In lymphocytes, MT has been found to bind to the extracellular membrane but not be endocytosed (unpublished data) and effect lymphocyte chemotaxis, most likely through a G protein coupled receptor mediated mechanism[106]. In summary, MT is primarily a cytosolic protein that is trafficked to the nucleus during DNA replication as part of proliferation and is secreted from certain cell types following stress exposure. The focus, hereafter, will be on the cytoplasmic role of MT where it is predominantly found in lymphocytes.

1.2.5 Structure

The introduction to MT structure presented below will focus on MT-1 and MT-2 in humans and mice (hereafter referred to as MT), which are structurally very similar and homologous in terms cysteine residues and zinc binding properties. The unique structure of MT is, in many ways, unlike any other mammalian protein.

The primary sequence of MTs is comprised of 61-62 amino acids (MW ~6kD) including 20 cysteine residues (except for MT-1B which has 21), 6-8 lysines, 7-10 serines, and a single acetylated methionine at the amino terminus. In general, MT is rich in the disorder producing amino acids (G, S, P) and has very few aliphatic amino acids (I, V, L) and no aromatic amino acids, both of which are order producing (http://www.rcsb.org/pdb/explore.do?structureId=1mhu)[107] (Figure 1). The MT1 isoforms are separated from the MT2 isoform during ion exchange chromatography based on the negative charge of MT-2 at position 11 where due to an aspartate residue. The human MT1 isoforms differ from each other by 3-13 amino acids [108] (Figure 2a and 2b). There is currently speculation in the field about whether the small differences in primary sequence between MT-1 and MT-2 isoforms impart a functional difference on the protein. The conservation of all 20 cysteines between all isoforms and the presence of similar amino acids at the other positions, however, suggests the primary function of metal binding and release also remains conserved and is not significantly different between the 2 isoforms.

The intrinsically disordered apo-metallothoinein (T) with no metal ligands occupies a large conformational space. This is evidenced by the lack of a clear band during SDS PAGE experiments using a reduced version of the protein. [109]. MT devoid of

metal ligands is only found *in* vitro, however, and MT isolated from biological samples is always bound with metal ligands. The affinity for divalent metal cation ligands comes exclusively from the 20 vicinal cysteine residues. These residues occur primarily in cys-cys, cys-x-cys, and cys-x-y-cys motifs. The free thiol R group of cysteines form thiolate bonds with divalent cations, most notably zinc and copper. In lymphocytes, in the absence of exposure to toxic heavy metals, zinc is the only metal found in a complex with MT [34].

Folding of the MT polypeptide chain around Zn^{2+} ions organizes the structure into two domains: a C-terminal alpha domain and an N-terminal beta domain, which resembles a barbell. The alpha domain contains 11 cysteine residues that can bind up to 4 Zn^{2+} ions. The beta domain contains 9 cysteine residues that can bind up to 3 Zn^{2+} ions. In the reducing environment of the cytoplasm, thiol groups (-SH) exist primarily as reduced sulfur atoms (S^-) and are capable of forming an ionic bond with cationic metals called a thiolate bond. In MT, Zn^{2+} ions are bound via thiolate bonds in a tetrahedral geometry (4 thiols per Zn^{2+}). Zinc-thiolate bonds are organized into two types: bridging and terminal. Thiols that interact with 2 Zn^{2+} ions are considered bridging and thiols that interact with one Zn^{2+} ion are considered terminal (See Figure 3). The alpha domain of MT contains 5 bridging and 6 terminal thiols; the beta domain contains 3 bridging and 6 terminal thiols. The alpha domain does not share a structural similarity to any other known protein while the beta domain shares some homology with histone lysine methyl transferases[110,111]. The cysteine residues and their coordinate Zn^{2+} ions are clustered, which results from the tertiary structure of the two domains putting cysteine residues in contact with Zn^{2+} ions in an order that is independent of primary sequence.

1.2.6 Redox Reactivity and Zinc Binding

Zinc is commonly used as a structural cofactor for protein folding and it is estimated that 3% of the nearly 19,000 human genes encode proteins with structural zinc sites with cysteine ligation[112]. In zinc finger motifs, where very tight zinc binding is preferential, combinations of nitrogen (histidine), oxygen (glutamate/aspartate) and sulfur (cysteine) are employed to form zinc binding motifs where the affinity is high (Kd < 10^{-12} ex. zinc finger domains) and is less reactive to oxidation[113]. In proteins that are subject to more dynamic regulation, where moderate affinity for zinc and a higher reactivity with oxidants is preferential, there are a higher proportion of cysteines in zinc coordination environments. This principle is illustrated in the Kelch domain of Keap1 protein binding to Nrf2 through coordination of a Zn^{2+} ion. Upon exposure to oxidants, cysteine ligands of Keap1 are preferentially oxidized, releasing Nrf2 to translocate to the nucleus and upregulate genes involved in antioxidant defense[114], including MTs.

The latter group of proteins with zinc finger motifs can be divided further into redox sensors and redox transducers. Redox effects are expressed at several levels in a signaling cascade through redox sensors: 1. Oxidative activation of matrix metalloproteins that proteolytically process receptors; 2. Regulation of phosphatase/kinase activity to affect phosphorylation state of proteins; 3. Interface of protein-protein binding interactions; 4. Regulation of transcription factor activity.[20]. MTs are hypothesized to be redox transducers, meaning they convert redox signals into zinc signals through oxidation of cysteine ligands and concomitant release of bound Zinc. In this way, the activity of MT after oxidation is not the important component of the

signaling cascade but rather, the effect of the released Zn^{2+} ions becomes the important cellular signal. Because intracellular [Zn^{2+}] is so low, even picomolar fluctuations caused by the release of free Zn^{2+} ions can act as a cellular signal in this manner.

Thiols or thiolates (-SH / S^-, or S-metal, respectively) react with electrophiles and become oxidized in the process. In general, thiolates have a lower pKa than thiols and are more reactive than sulfhydryls to oxidation, alkylation, and nitrosylation[18]. Generally, within the relatively narrow redox potential of mammalian cells, higher order oxidation of thiols (loss of 2 electrons) leading to sulfinic, and sulfonic acid are unlikely[20]. Instead, lower order reversible oxidation reactions resulting in disulfide bond formation are more likely[115]. Thus far, disulfides are the only oxidation states identified as the result of sulfur ligand oxidation in Zn-S sties.

In reactions of MT with biological oxidants, the presence of so many vicinal thiol groups imparts an extremely low redox potential (-366mV) [79] and makes higher order oxidation events even less likely. The reactivity of zinc bound thiolates to oxidation follows this order: $Zn\text{-}S_4 > Zn\text{-}S_3 > Zn\text{-}S_2 > Zn\text{-}S$. The underlying reason for this seems to be that the Zn^{2+} ions coordinate the sulfur atoms of sulfhydryl groups so they are in the correct orientation for disulfide bond formation before they are oxidized[116]. However, Zn^{2+} binding also affects entropic factors by electrostatically screening reduced thiols and protecting them from oxidation. Furthermore, H-bonding drastically affects the reactivity of sulfurs in proteins. Because different types of intramolecular forces affect Zn coordination environments, proteins can be “fine-tuned” to act as precise redox-zinc switches that change conformation and activity only at specific thresholds. Furthermore, parameters like temperature, pH, [Zn^{2+}], redox potential, and the nature of the oxidant

can all affect the threshold of zinc release/binding and allow redox-zinc switch proteins to react appropriately under different intracellular conditions. For example, the capacity of biological disulfides to release zinc from MT varies considerably. Cystamine release 93% of bound Zinc while oxidized glutathione (GSSG) releases 20% at the same molar concentration[117].

The combination of all of the factors affecting Zn-S binding in proteins makes empirical prediction of thiolate reactivity (and subsequent release of zinc) in a particular protein very difficult. For this reason, the 7 zinc binding sites in MT were originally thought to have a high affinity for MT [118] even though it is evident from ^{113}Cd NMR spectra that all seven zinc ions exist in unique environments within MT[119]. It has recently been revealed, however, that MTs have four sites with high affinity (logK=11.8), two sites with moderate affinity (logK=10) and one site with even lower affinity (logK=7.7) at pH 7.0 [120]. In reality, however, the relationship between zinc and MT in biological systems is more complicated and dynamic than a distribution of static logK values would suggest, especially in the context of redox signaling. It is important to note, that the binding sites with lower affinity prevent MT from being a thermodynamic sink for metal chelation, which is the case with Cd^{2+}. Instead, MT has the ability to transfer zinc to apoforms of zinc enzymes that have inherently lower stability constants for zinc[121]. Furthermore, this transfer is aided by the presence of both reduced glutathione (GSH) and oxidized glutathione (GSSG), when they are present together as a redox couple[79].

There are 3 distinct states of the sulfhydryl side chains of the cysteine residues; metal bound, reduced or oxidized. Metallothionein (MT) refers to the protein products of *Mt* genes that, once translated, are in a complex with metal ions. Thionein (T) refers to

apo- (metal removed) form of metallothionein, which can be further, differentiated by the redox status, reduced (T_R) or oxidized (T_O). Due to the dynamic nature of MT zinc binding and the redox state of intracellular proteins, single MT polypeptides may contain all 3 types of sulfhydryl groups simultaneously. Furthermore, intra- and inter MT zinc transfer happens rapidly [122] so it is not practical to consider any of the cysteine residues in a biological pool of MT to be in a static state. The 3 states of MT exist in a dynamic equilibrium that is reflected by their relative ratio in biological tissues or cells. Recent advances in chemical modification strategies have allowed the 3 states of MT to be measured simultaneously and, therefore, their relative ratios deduced. In both liver cells and tissue homogenate the ratio of T/MT is around 30%, which correlates with five of the seven metal binding sites being occupied by zinc[123]. Within the non-metal bound fraction of cysteine ligands, the ratio of T_R t: T_O is 2.75 : 1 in the liver and 1.5 : 1 in T29 human epithelial cells in culture, which most likely reflects the exposure of cells in culture to a higher partial pressure of O_2 and the resulting increased oxidative stress. Interestingly, introduction of a Ras oncogene that causes oxidative stress[124] increased the total amount of MT expressed by 20% but decreased the ratio of T_R : T_O (1:3). As the MT metal bound and reduced ligands were oxidized, the total ratio of T/MT also increased from 20% to 27%[123]. The observation that MT is not zinc saturated under cellular conditions underscores its position at the precipice of zinc and redox regulation in the cell and place it in a position to quickly respond to changes in redox or zinc status.

The interaction of biological oxidants with MTs is of particular importance in understanding the role of MT in modulating redox status. ROS and RNS have ability to react directly with MT to oxidize the protein and release Zn^{2+}[125]. ROS species including

superoxide radical, hydroxyl radical[126], and peroxides[21] all interact directly with sulfhydryl groups on MT to form disulfides. In the case of RNS, nitric oxide also reacts directly with MT[127], or reacts with superoxide to form peroxynitrite, one of the most potent biological catalyst for MT zinc release that has been reported [128]. The result of this reaction can be glutathionation[125], S-nitrosylation[129], transnitrosation[130], or disulfide formation[131]. Because the redox potential of MT is so low, it can also react with biological disulfides including GSH-GSSG, a process which is aided by catalytic selenols[132]. Furthermore, MT redox status is intimately associated with other redox pairs including thioredoxin[133]. The kinetics of reactions between biological disulfides and oxidants and MT are influenced by the concentration of enzymes including protein disulfide isomerase (DsbA)[121], glutathione peroxidase[122], and sulfhydryl oxidase[134] among others. The relative availability of these enzymes is believed to be responsible for the maintenance of differences in redox potential of different redox pairs within the cytosol.

1.2.7 Proposed Biological Roles of MT

MT has been referred to as a Sphinx [135] because of the difficulty in deciphering its elusive biological roles. More than 50 years of research have elucidated many immunological contexts in which MT appears to play a role. The biological roles of MT can be distinguished by their intracellular and extracellular modes of action. Extracellular pools of MT (reviewed previously [35,136,137]) have been shown to be potent mediators of leukocyte chemotaxis[106,138], CD8+ T cell cytotoxic function[139], $CD4^+$ T cell differentiation[2], dendritic cell function[140], T-dependent humoral responses [141], and

others. MT is hypothesized to modulate immune activity through interference with chemokine signaling or by acting as potent antioxidant and interfering with the positive feedback loop involving oxidative stress and inflammation.

The intracellular role of mammalian MT and its position at the juncture between redox and zinc metabolism has been well studied under normal and pathological conditions in various tissue and cell types. The very low redox potential and preferential oxidation of MT by ROS and RNS implicate MT in modulation of redox signaling pathways. In this way, oxidative signals generated by membrane bound enzymes[142], cytosolic enzymes[143], or mitochondrial enzymes[144] would be dampened in the presence of MT. MT's role as a negative regulator of oxidative signaling is reinforced by the presence of ARE elements in the MT promoter regions and strong induction of MT by oxidative stress. In addition to modifying the redox state of proteins, MT may directly interact with certain transcription factors including NF-κB and affect their DNA binding activity[145,146].

Of all the proposed mechanisms of MT mediated immunomodulation, MT's role in the management of intracellular labile [Zn^{2+}] may be the most notable. When considering the cumulative *in vitro* biochemical observations of MT function, evidence points to an integral, but context dependent, role in zinc homeostasis. On one hand, MT acts as a signal transducer that is preferentially oxidized (even in the presence of millimolar GSH) and releases a transient zinc signal. In the absence of an oxidative signal, MT acts as a general zinc buffer, binding and donating free zinc as part of metal homeostasis. Even during relative redox and zinc homeostasis, MT stabilizes the transition state between apo and metal bound forms of zinc proteins, thus facilitating

and regulating the use of zinc as a regulatory co-factor. The implications of this zinc mediated regulation of biological systems are immense and far reaching and have been the focus of several recent comprehensive reviews [18,133,147-149]. These interactions are not mutually exclusive, and depending on the MT concentration, cell type, and environmental context, particular mechanisms may play a more significant role in immunomodulation.

One of the most intriguing observations is the association of MT and its purported role in autoimmunity and inflammation. The positive feedback loop between inflammation and oxidative stress is well characterized, and in this context, exogenous addition or induction of MT appears to provide a potent redox buffer for the detoxification of potentially harmful ROS and RNS species. MT has been implicated in protection from several autoimmune diseases including collagen induced arthritis[2,150,151], type 1 diabetes[152], experimental autoimmune encephalomyelitis[3,153], and others. However, recent evidence suggests that disruption of endogenous production of MT using a genetic MT knockout can also prevent the onset of autoimmune disease, specifically EAE[5]. Further investigation into the responsible mechanism revealed that the development of immunosuppressive Type 1 regulatory T cells (Tr1) was increased in the knockout model, suggesting that MT plays a role in $CD4^+$ T cell development. Because this effect occurred both *in vivo* and *in vitro*, in the absence of antigen presenting or accessory cells, it is likely that intracellular $CD4^+$ T cell signaling following activation was influenced by MT gene dose.

1.3 Role of CD4$^+$ T Cells in Adaptive Immune Responses

A core component of adaptive immunity is the integration of signals that accompany the recognition of non-self molecular patterns and translating them into a beneficial response. This process is exemplified in CD4$^+$ T cells where parallel recognition of antigen and extracellular stimuli direct cell development into distinct effector phenotypes which go on to mediate appropriate adaptive immune responses.

1.3.1 CD4$^+$ T Cell Activation

For circulating naïve CD4$^+$ T cells that have exited the thymus, primary activation occurs following recognition of foreign or non-self peptides through the T cell receptor (TcR). Each unique TcR binds to an associated major histocompatibility complex II (MHC) molecule with a specific antigenic peptide (Signal 1). During this cellular binding event, other surface proteins on the antigen presenting cell (APC) and CD4$^+$ T cell interact including B7.1 (CD80) or B7.2 (CD86) on the APC and CD28 on the T cell (Signal 2). B7 expression on APCs is upregulated after exposure to pathogen associated molecular patterns (PAMPs) including LPS [154]or LTA[155]. The presence of B7 on the APC stimulates the activation of phosphoinositide 3-kinase (PI3K) and Akt based signaling pathway in T cells. Together, pathways downstream of Signal 1 and Signal 2 converge to result in CD4$^+$ T cell activation and proliferation. In the absence of PAMPs, APCs do not express elevated levels of B7, which upon recognition of peptide/MHC by the TcR, results in Signal 1 without Signal 2 and T cell anergy or apoptosis [156,157]. In this way, T cells can respond to the same antigenic peptide very differently, depending on co-stimulatory signals expressed by the APC.

Successful activation of primary $CD4^+$ T cells usually occurs in secondary lymphoid tissues following an interaction with a pathogen activated dendritic cell[158]. In addition to Signal 1 and Signal 2, $CD4^+$ T cells receive extracellular signals from both the contact APC and the extracellular environment. $CD4^+$ T cells express inducible costimulator molecules including ICOS, CD27, and CD154, and CD137 among others that all bind with cognate membrane-bound co-activating molecules on the surface of dendritic cells. Conversely, after a period of T cell activation, CD28 on the T cell surface is replaced by expression of CTLA-4, which activates an inhibitory pathway. This signal is transduced through SHP-2 and prevents T cell over-activation and influences the activation phenotype of the APC through an interaction with CD80 or CD86.

The process of T cell activation is complex and is an area of intense investigation. For the purposes of this introduction, the general mechanisms of T cell activation will be reviewed with an emphasis on the interactions that have the potential for MT mediated regulation. The series of events between the time the TcR recognizes its cognate peptide/MHC (Signal 1) and downstream gene regulation involve several parallel pathways initiate T cell activation. Upon recognition of the peptide/MHC complex by the TcR, intracellular phosphatases and kinases are brought within close proximity of one another and reach a density threshold. Subsequent phosphorylation of ITAMs on the intracellular domains of CD3 and ZAP70 triggers phosphorylation of LAT and activation of phospholipase-C (PLC), a crucial step in the signaling cascade and an area of integration with CD28 signaling (Signal 2). Activation of PLC cleaves phosphatidylinositol biphosphate (PIP2) to yield diacyl glycerol (DAG) and inositol trisphosphate (IP3). IP3 leads to a calcium signal that is a requirement for T cell

activation and underscores the importance of ionic signaling cascades in T cell activation. DAG recruits protein kinase C (PKC), for which MT2a is an observed substrate[159], and RasGRP which in turn activates Ras. Ras then activates the mitogen-activated protein kinase (MAPK) cascade that terminates with activation of several transcription factors, most notably AP-1 and NF-κB.

During the signaling through the T cell receptor (Signal 1) and CD28 (Signal 2), T cells also receive signals from extracellular cytokines (Signal 3). Cytokines signal through hetero-dimeric receptors on the plasma membrane, many of which use a γ common chain (IL-2, IL-4, IL-7, IL-9, IL-15) or β common chain (IL-3, IL-5 GM-CSF). Other heterodimeric cytokine receptors use unique chains for recognition and signaling (IL-13, IFN-γ, IL-10). These receptors signal through janus kinases (JAKs) that activate signal transducers and activators of transcription (STATs). Activated STATs may translocate to the nucleus and affect gene transcription or, in the case of STAT5, also activate MAPKs[160].

MAPKs fall into 3 families: c-Jun N-terminal kinases (JNKs), extracellular-signal regulated kinases (ERKs), and p38 mitogen-activated protein kinases (p38). Integration of STAT and MAPK signaling networks during and following TcR and CD28 engagement set the foundation for differentiation and $CD4^+$ effector T cell development[161]. Interestingly, p38 MAPK activity is increased following exposure to ROS [162], zinc [13], and glucocorticoids [163] and pro-inflammatory cytokines[164], all of which are important inducers of MT expression in $CD4^+$ T cells. This observation suggests negative feedback loops that may be important mechanisms of MT mediated immunomodulation in $CD4^+$ T cells. In the absence of MT, signaling through p38 MAPK

pathways would be sustained for longer periods of time, affecting activation of AP-1 and NF-κB and potentially cell differentiation and cytokine secretion.

The primary molecular mechanism underlying the propagation of Signal 1, Signal 2 and Signal 3 are the phosphorylation and dephosphorylation of signaling proteins, including signaling kinases and phosphatases themselves. This conservation of mechanism allows multiple signaling cascades to be regulated by zinc or redox status[165]. Increases in zinc, in general, inhibit cellular phosphatases which tends to increase phosphorylation and activation of signaling kinases in T cells [166]. Control of intracellular [Zn^{2+}], therefore, allows T cells to tune the threshold of signaling activation following Signals 1 and 2. Both zinc [12,167] and reactive oxygen species[168] are highly regulated during $CD4^+$ T cell activation and are under the direct influence of intracellular MT concentration and redox status, placing this protein at a central position for influencing T cell signaling. In addition to global regulation of phosphatase activity, it is important to note that intracellular phosphatases are differentially regulated by zinc and ROS and inhibitory concentrations of zinc (IC50) can vary by several orders of magnitude. Therefore, small decreases in ROS, and concomitant increases in labile zinc after oxidation of MT, could have a targeted effect on particular substrates including p38 MAPK, without needing to affect global phosphorylation patterns.

1.3.2 $CD4^+$ T Cell Differentiation and Development of Effector Phenotypes

Successful activation of naïve $CD4^+$ T cells *in* vitro results in proliferation and differentiation into an effector phenotype. This is marked by changes in expression of

surface markers of activation including CD44[169], CD62L, CD69, and CD25, and CD45 [170]. The effector function of differentiated $CD4^+$ T cells is influenced, primarily, by soluble cytokines that are present during the initial activation event (Signal 3)[171]. $CD4^+$ T effector cells fall into general categories and new categories are still being discovered. Of these categories, the 4 most well studied effector populations *in vivo* include Th1, Th2, Th17, and iTreg while stimulation of naïve CD4+ T cells *in vitro* without additional stimulation through cytokine receptors leads to a TH0 effector phenotype (Figure 1.4). These categories are generally defined by effector cytokine production and master transcription factor profiles. For a more thorough review see [172].

The dichotomy of the TH1 and TH2 groups were first discovered in murine cells and represent the most well studied paradigm of naïve $CD4^+$ T cell fate decisions[173]. Robust IL-2 and IFN-gamma secretion, in addition to many cells secreting TNF-alpha, characterize TH1 cells. IL-12 signaling during initial activation results in expression of the master TH1 transcription factor Tbet and controls the Th1 cell fate decision[174,175]. TH2 cells, on the other hand, are characterized by secretion of IL-4, IL-5, and IL-13 [176] and expression of the GATA-3 transcription factor. These cells are induced by IL-4 as part of a positive feedback loop that enhances TH2 responses[177]. The fate choice for TH1/TH2 is reinforced by the repression of transcription factor expression, where expression of one reciprocally inhibits expression of the other. This allows for coordinated cellular responses to immune challenges. In the case of TH1, this involves intracellular infections, whereas TH2 responses are required to clear extracellular bacteria and parasites such as helminthes.

A parallel dichotomy in $CD4^+$ cell fate lineage appears between Th17 and

inducible regulatory T cell (iTreg) $CD4^+$ cell lineages, which have been defined more recently. Th17 cells are characterized by their robust secretion of IL-17a, IL-17f, and IL-22[178] and the RORγt transcription factor. iTregs are characterized by secretion of IL-10 and TGF-β and expression of the FoxP3 transcription factor[179]. The dichotomy between these cells is defined by their functions, where IL-17 is responsible for controlling some extracellular bacteria and fungi and promotes inflammatory conditions while iTregs suppress T cell function and inflammation[180]. Furthermore, the conditions that induce these phenotypes are similar but distinct. The presence of TGF-β and IL-6 during primary activation result in the development of Th17 cells while TGF-β alone results in development of iTregs.

An alternative IL-10 secreting $CD4^+$ T cell subset is the *in vitro* or *in vivo* derived T regulatory Type 1 (Tr1) subset (Figure 1.4) These cells are similar to iTreg because they secrete IL-10 and are immunosuppressive, but do not require the expression of FoxP3 [181,182]. These cells can be induced by immunosuppressive drugs[183], certain soluble proteins[184] and peptide antigens[185], or by chronic stimulation[186]. Alternatively, Tr1 cells are induced in the presence of IL-27 during primary activation [187] and are an excellent model for studying the immunosuppressive functions of IL-10 producing cells[5,188].

1.3.3 The Role of Labile $[Zn^{2+}]$ in T Cell Signaling and Effector Function

Of the nutritionally essential transition metal ions, zinc ions have the most prevalent role in regulating protein strucutre[189]. The vast majority of biological zinc is

sequestered in proteins due to the high affinity of sulfur and other negatively charged atoms for zinc. This explains why total intracellular zinc concentration is in the range of a few hundred micromolar, while free or labile zinc concentration is only a few hundred picomolar. Interestingly, every metal ion in its "free" state is kept at a concentration that is commensurate with its binding affinity [190]. The compartmentalization of zinc is an important aspect of zinc biology and underlies the foundation of using zinc ions as molecular signals that affect cell behavior.

Briefly, zinc homeostasis in cells is achieved through the dynamic process of continuous export and import. Two families of proteins are implicated in the transport of zinc across membranes: the ZnT family (solute-linked carrier 30, SLC30A) is responsible for zinc export out of the cytosol while the Zip family (Zrt- and Irt-like proteins, SLC39A) is responsible for zinc import into the cytosol. For review see [191]. Cellular zinc homeostasis, on a smaller scale, is maintained through zinc buffering and muffling[192]. Specifically, these processes describe the binding and release of zinc from proteins and their transport into intracellular vesicles as strategies to maintain zinc homeostasis; both of these processes have been observed in lymphocytes[8,13,15]. MT is implicated in both of these processes, and is considered the most important intracellular zinc buffering mechanism[19,133].

Over the past 2 decades, significant but indirect evidence for the role of intracellular labile [Zn^{2+}] in $CD4^+$ T cell signaling has been observed. Unlike calcium ionic signaling, zinc ionic signaling events are difficult to measure because intracellular [Zn^{2+}] in human and mouse lymphocytes is a few hundred pM, which is about 3 orders of magnitude lower than calcium. Only recently have fluorescent probes been

developed that are capable of reliably measuring changes in labile [Zn^{2+}] during T cell activation[193 194]. However, since their acceptance as a research tool, the zinc probe Fluozin-3 (Invitrogen) has allowed the precise quantification of intracellular labile [Zn^{2+}] in cells *in vitro* and revealed a dynamic role for zinc in the regulation of T cell activation.

Zinc signaling can be temporally divided into two groups: early signals and late signals[148]. (Figure 5) Late signals involve transcriptional regulation of Zip (SLC39A) and ZnT (SLC30A) proteins and take place on the order of 30 minutes to hours after the initiating signal. Early zinc signals take place on the order of seconds to minutes and involve rapid mobilization of zinc from intracellular vesicles, extracellular space, or from zinc bound to cytosolic proteins including metallothionein. In $CD4^+$ T cells, both types of signals are associated with T cell activation. Late zinc signals include increased intracellular [Zn^{2+}] that is associated with the development of a lymphoblast phenotype and subsequent proliferation [36] and increased expression of Zip8 in T cell lysosomes[15]. Early zinc signals include influx from the extracellular environment after peptide/MHC recognition on an activated APC[7], release of Zn^{2+} from lysosomes following IL-2 [8] or IL-1 beta[195] cytokine signaling, or release of Zn^{2+} from metallothionein following exposure to heavy metals or oxidative stress[194]. The ability to induce zinc signals and, alternatively to terminate zinc signals, is negatively associated with increased age and is considered to be an important factor in decreased immune function in the elderly[36,196-198].

The reported effect of increased extracellular [Zn^{2+}] on T cell activation and function varies greatly. Increasing extracellular [Zn^{2+}] to 100µM alone is associated with increased T cell proliferation[199]. Increasing extracellular [Zn^{2+}] from 3-75µM during T cell

activation with APCs loaded with superantigen[7] is also associated with increased proliferation. However, studies using alternative mitogens including pokeweed mitogen (PWM), anti-CD3 antibodies[16] or concanavalin A (ConA) [17] reported reduced proliferation upon addition of ZnCl [100μM]. Additionally, strong zinc signals are associated with increased T cell apoptosis through regulation of Bim [200] and increased cytotoxicity following oxidative stress[201,202]. These conflicting reports underscore the context dependent nature of the effects of intracellular Zn on proliferation. It is important to note that these studies described above explored artificially high *in vitro* [Zn^{2+}] that is unlikely to be experienced by T cells *in vivo.* This makes interpretations of the biological significance of these observations less straightforward.

Another general paradigm that emerges from the large body of research involving the effects of zinc on T cell function includes the requirement of intracellular [Zn^{2+}] within a narrow window. In the case of dietary zinc deficiency, and resulting decreases in intracellular [Zn^{2+}], development of the Th1 phenotype[6,203] and secretion of IFN-γ[204] are impaired. This is the general mechanism of immunosuppression attributed to the relationship between zinc deficiency and viral infection[205]. However, like the studies described previously, dietary zinc deficiency is an extreme condition and the mechanisms underlying the influence of a severe cellular zinc deficit on immune function are likely different than those employed by zinc during “normal” cellular zincexposure.

In cases where zinc has been studied in a more concentration relevant context, increasing intracellular [Zn^{2+}] *in vitro* while maintaining viability still decreases production of cytokines including IL-10 and IL-17[16] while increasing IL-2[195]. These effects are

dependent on modulation of MAPK pathways by free Zn^{2+}, as described earlier. For example, MEK and ERK are both found to be activated in response to increased intracellular [Zn^{2+}] following IL-2 signaling [8], which results in increased expression of the transcription factor c-fos. This is due to zinc-mediated inhibition of MEK and ERK dephosphorylating protein phosphatases. Of the MAPK family, p38 is the most sensitive to changes in intracellular Zn in $CD4^+$ T lymphocytes during TcR signaling[13] and its increased activation by zinc is also attributed to inhibition of a MAPK-phosphatase[206]. This zinc-mediated effect on MAPK activity occurs within a physiologically relevant [Zn^{2+}] and affects IFN-gamma transcription and secretion as well as inhibitory activity of Treg[207,208]. It is therefore a likely mechanism for regulation of cytokine secretion and mediation of inflammation[209]. The mechanism underlying inhibition of phosphatase activity by zinc has recently been described in detail[12,167]. Interestingly, the regulation of protein tyrosine phosphatases by zinc overlaps considerably with the intracellular [Zn^{2+}] affected by MT expression and oxidation.

In addition to MAPK, zinc affects cytokine secretion by reducing the activation of STAT3[11]. Induction of IL-10+ Tr1 cells by IL-27 requires the activation of STAT3[210], which is increased in MT deficient lymphocytes[5] and is responsible for increased IL-10 expression compared with wildtype controls. However, the mechanism responsible for increased activation of STAT3 and subsequent increase in IL-10 expression in MT-KO mice remains unknown. One hypothesis is that a reduced intracellular zinc signal following T cell activation in MT-KO mice allows for a greater increase in STAT3 activation. This is supported by studies describing the presence of ROS during T cell activation[211] and the association of MT with higher concentrations of oxidant released

labile zinc[212].

1.3.4 CD4$^+$ T cell mediated effects on humoral immune responses

Effector CD4+ T cells influence both cell mediated and humoral immune responses. The coordination of effective immune responses to different classes of pathogens requires CD4+ T cells to integrate extracellular signals during differentiation of effector cells. Once cell fate has been decided and effector function has been gained, CD4+ T cells are poised to appropriately influence the activation both innate and adaptive immune cells through contact dependent and independent mechanisms. For adaptive humoral responses, CD4+ T cells influence B cell activation subsequent antibody secretion through both cell contact independent (ex. cytokine signals)[213] and cell contact dependent signals (ex. CD40L) [214]. During B cell activation and differentiation into an antibody secreting plasma cell, B cells commonly switch the class of antibody they secrete from membrane bound IgD to soluble IgG. The cytokine environment controlled primarily by CD4+ T cells influences the sub-type of IgG class. In this way, TH1 mediated immune responses are associated with higher levels of serum IgG2a [215] while TH2 responses are associated with higher levels of serum IgG1[177]. Alternatively, higher levels of TGF-beta associated with Treg mediated immune responses result in a higher level of IgG2b[216]. By measuring the IgG subtype of the humoral response to a specific antigen, it is therefore possible to draw conclusions about the cytokine environment and predominant type of CD4$^+$ T cell response.

BLAST Results Dot Matirx Plot of Human MT2A (P02795) vs Mouse MT2 (P02802)

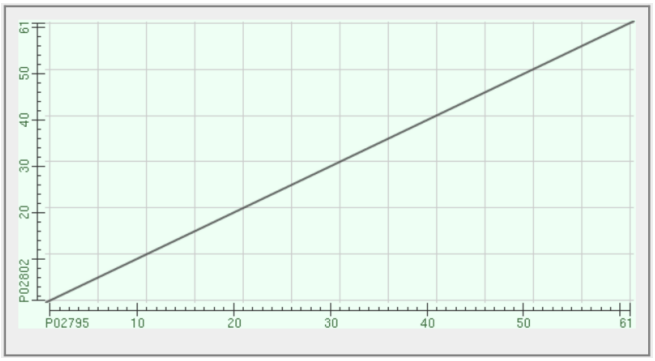

The human MT-2A sequence is represented on the X-axis and the numbers represent the bases/ residues of the query. The mouse MT-2 sequence is represented on the Y-axis and again the numbers represent the bases/residues of the subject. Alignments are shown in the plot as lines. Plus strand and protein matches are slanted from the bottom left to the upper right corner, minus strand matches are slanted from the upper left to the lower right. The number of lines shown in the plot is the same as the number of alignments found by BLAST.

Figure 1.2 Human Metallothionein Gene Comparison

A.

Human MT Isoform Sequence Comparison

```
                    10        20        30        40        50              60
MT1A        MDP-NCSCAT-GGSCTCTGSCKCKECKCNSCKKSCCSCCPMSCAKCAQGCICKG------ASEKCSCCA
MT1B        MDP-NCSCTT-GGSCACAGSCKCKECKCTSCKKCCCSCCPVGCAKCAQGCVCKG------SSEKCRCCA
MT1E        MDP-NCSCAT-GGSCTCAGSCKCKECKCTSCKKSCCSCCPVGCAKCAQGCVCKG------ASEKCSCCA
MT1F        MDP-NCSCAA-GVSCTCAGSCKCKECKCTSCKKSCCSCCPVGCSKCAQGCVCKG------ASEKCSCCD
MT1G        MDP-NCSCAA-GVSCTCASSCKCKECKCTSCKKSCCSCCPVGCAKCAQGCICKG------ASEKCSCCA
MT1H        MDP-NCSCEA-GGSCACAGSCKCKKCKCTSCKKSCCSCCPLGCAKCAQGCICKG------ASEKCSCCA
MT1R        MDP-NCSCAT-GGSCSCASSCKCKECKCTSCKKSCCSCCPMGCAKCAQGCVCKG------ASEKCSCCA
MT1M        MDP-NCSCTT-GVSCACTGSCKCKECKCTSCKKSCCSCCPVGCAKCAHGCVCKG------TLENCSCCA
MT1X (1L)   MDP-NCSCSP-VGSCACAGSCKCKECKCTSCKKSCCSCCPVGCAKCAQGCICKG------TSDKCSCCA
MT1Y        MDP-NCSCAT-GVSCACTGSCKCKECKCTSCKKSCCSCCPVGCAKCAHGCVCEG------ALEKCNCYA
MT2         MDP-NCSCAA-GDSCTCAGSCKCKECKCTSCKKSCCSCCPVGCAKCAQGCICKG------ASDKCSCCA
MT3         MDPETCPCPS-GGSCTCADSCKCEGCKCTSCKKSCCSCCPAECEKCAKDCVCKGGEAAEAEAEKCSCCQ
MT4         MDPRECVCMS-GGICMCGDNCKCTTCNCKTCRKSCCPCCPPGCAKCARGCICKG------GSDKCSCCP
```

B.

Number of amino acid variations within human MT-1 isoforms

	A	B	E	F	G	H	R	M	X	Y
A	0	10	5	9	7	8	6	11	10	11
B		0	5	9	9	8	7	8	8	10
E			0	4	4	6	3	8	7	8
F				0	4	8	7	10	10	10
G					0	6	5	10	8	10
H						0	7	11	7	12
R							0	10	9	10
M								0	10	6
X									0	13

Figure 1.3 Zinc Binding Motifs of Metallothionein

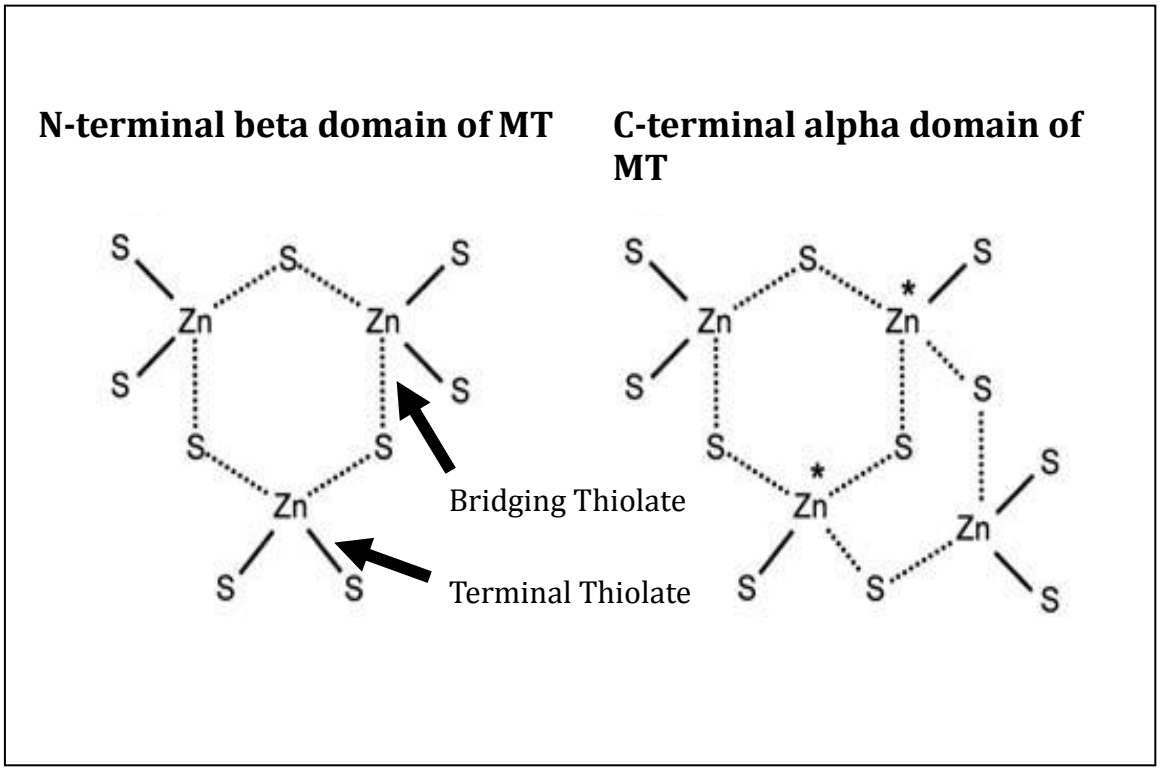

Adapted from [20]

Figure 1.4 CD4+ T Cell Differentiation

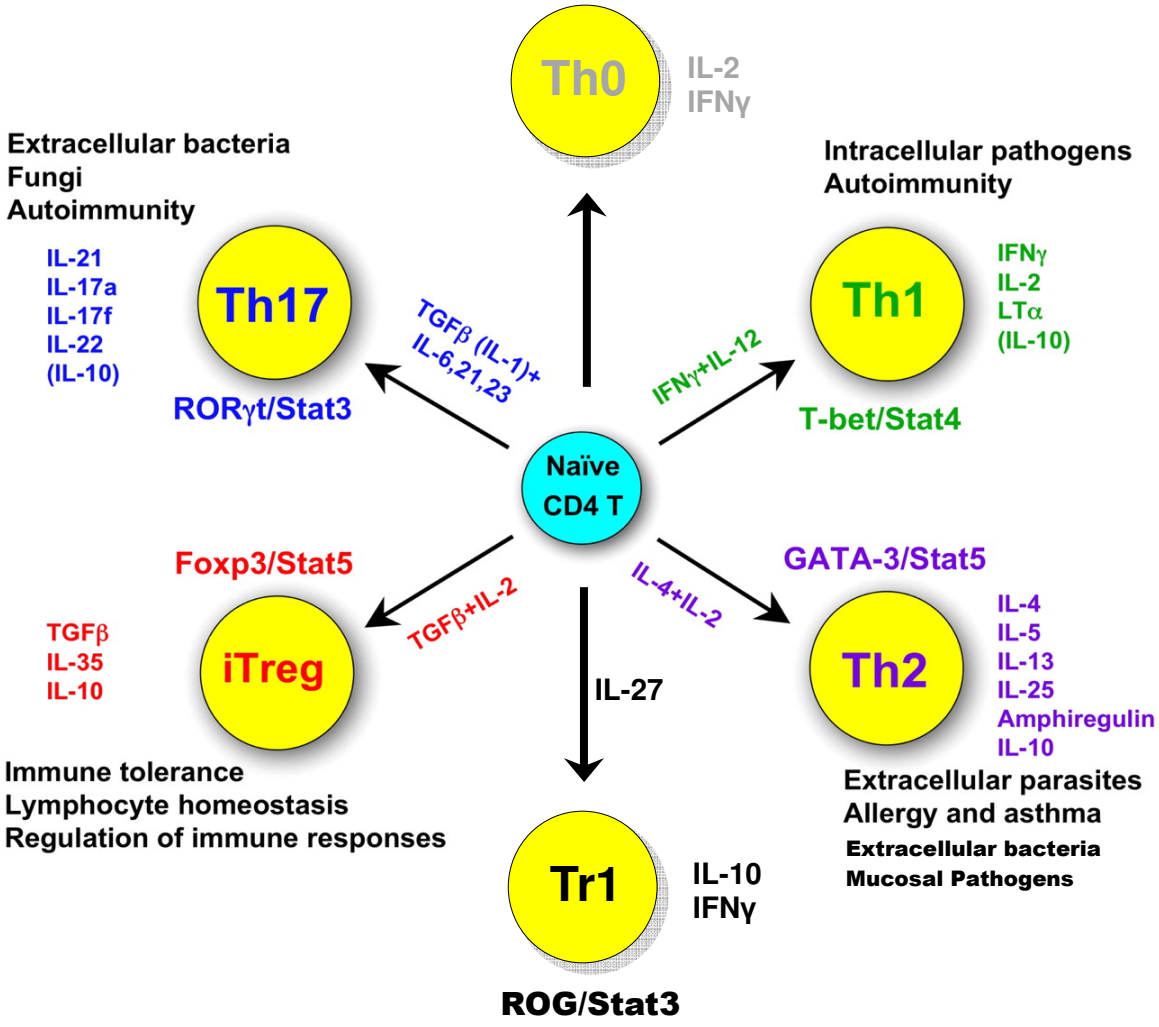

Adapted from [160]

Figure 1.5 Early and Late Zinc Signaling

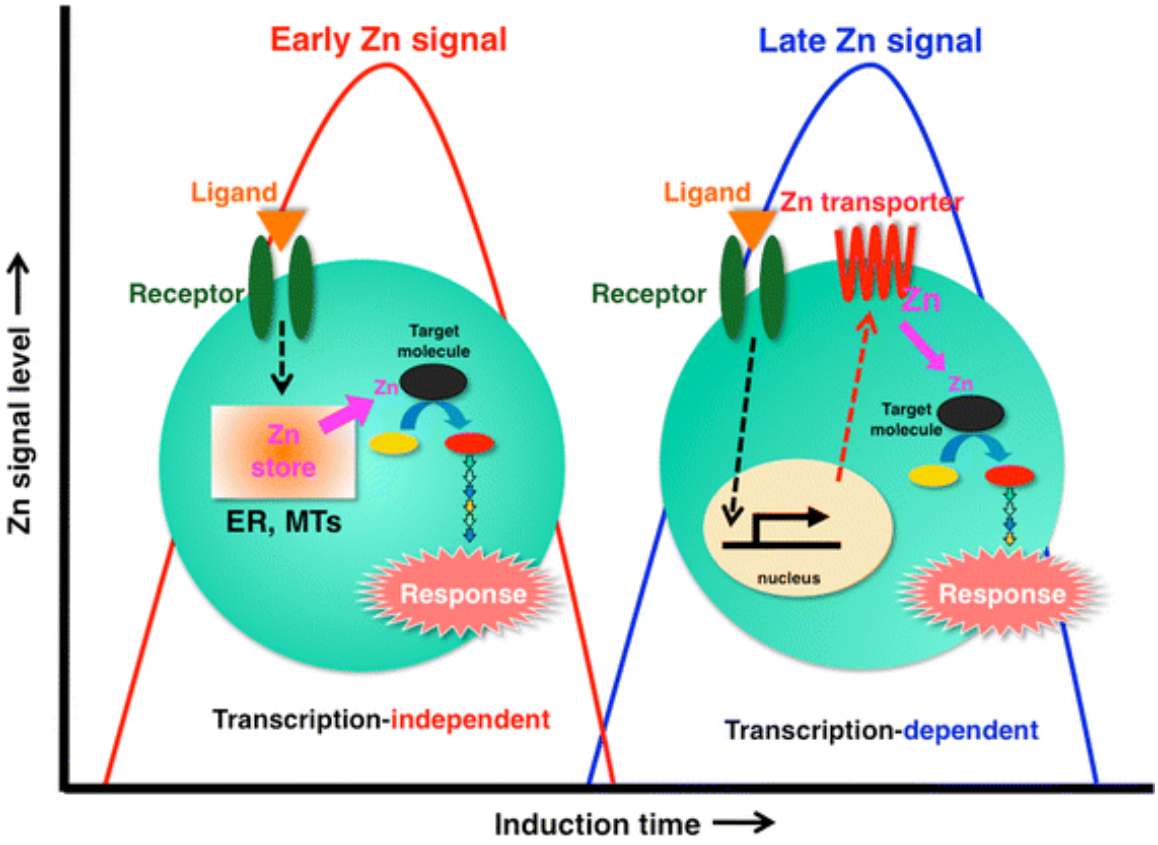

Adapted from [148]

Chapter 2

Materials and Methods

2.1. Mouse Strains

All *in vitro and in vivo* studies were performed using mice bred and housed at the University of Connecticut in accordance with the University of Connecticut Institutional Animal Care and Use Committee (IACUC) guidelines. The congenic MT-1/2 knockout mice and the congenic MT1 transgenic mice were derived from the original strain constructs (129S7/SvEvBrd-*Mt1*^{tm1Bri} *Mt2*^{tm1Bri}/J [12] and STOCK Tg(Mt1)174Bri/J [40] that had been obtained from the Jackson Laboratory (Bar Harbor, ME). The Jackson Laboratory provided Genotyping protocols for the selection of heterozygotes at each generation. Both of the congenic strains were produced by 8–9 generations of backcrossing to the C57BL/6J background strain, followed by incrossing of the heterozygotes to produce homozygotes for each construct. According to the equation for the fraction of loci that are still heterozygous at the Nth generation [(1/2)^(N-1)], the amount of residual donor genetic material that may contribute to observed phenotypic differences after 8–9 back- crosses is between 0.2 and 0.4%[41]. Strain production was done at the University of Connecticut, where these strains are maintained. (C57BL/6J, abbreviated WT; C57BL/6-*Mt1*^{tm1Bri} *Mt2*^{tm1Bri}, abbreviated MTKO; and C57BL/6-Tg(Mt1)174Bri, abbreviated MTTGN) mice were age and sex matched for each independent set of experiments. Mice between 9 and 24 weeks were used for all studies. Mouse genotype was confirmed by PCR prior to beginning studies.

2.2. Cell Culture and Treatment

2.2.1 Cell Isolation

For PBMC isolation, ~200µL of blood was collected by sub mandibular bleed into lithium heparin lined BD Microtainer tubes (BD Biosciences). Blood from 3-4 mice was pooled to create one sample. Blood was then mixed 1:1 with DMEM and layered over 2mL of Histopaque 1083 (Sigma) and spun at 300g for 30 minutes with no brake. The PBMC layer was removed and washed 2x in DMEM "Benchtop" Media (see recipe below).

For buffy coat isolation, ~50µL of blood was collected by retro orbital bleed into heparinized Micro-Hematocrit Capillary tubes (Fisher Scientific) and spun at 300g for 20 minutes. Tubes were cut below the bufficoat line and cells were expelled into DMEM "benchtop" media before use.

For splenocyte isolation, mice described in section 2.1 were euthanized by cervical dislocation. Spleens were removed aseptically and single cell suspensions were created using frosted glass slides (Corning #2948) and passing resulting cells through an 18 gauge needle (2x) and through a 70µM cell strainer (Fisher Scientific) into DMEM benchtop media.

For mouse $CD4^+$ T cell isolation, cells were isolated using a negative selection magnetic isolation column (Miltenyi Biotec) according to manufacturer instructions. The Jurkat E6 $CD4^+$ T cell line was obtained from the American Type Culture Collection (ATCC #TIB-152). The CH7C17 $CD4^+$ T cell line has been described previously[217].

Cells were counted using a hemocytometer or Z2 coulter counter (Beckman Coulter) using the limits T_U: 12 and T_L: 5 for viable lymphocytes.

2.2.2 Media

The Jurkat E6 $CD4^+$ T cell line was obtained from the American Type Culture Collection Benchtop Media: During isolation or for prolonged treatment outside of a CO_2 incubator, mouse cells were kept in DMEM containing 4.5g/L glucose, sodium pyruvate and 2mM L glutamine (Gibco) supplemented with 10% FBS (Hyclone), 25mM HEPES buffer, 1% penicillin/streptomycin (Gibco) and 50µM 2-mercaptoethanol.

Mouse Cell Culture Media: Mouse cells were cultured in DMEM containing 4.5g/L glucose, sodium pyruvate and 2mM L glutamine (Gibco) supplemented with 10% FBS (Hyclone), 1% non-essential amino acids (GIbco), 1% penicillin/streptomycin (Gibco) and 50µM 2-mercaptoethanol. Cells were kept in 96 or 24 well tissue culture treated plates (Fisher) at 1 x 10^6 cells/mL for $CD4^+$ T cell culture and 2x10^6 cells/mL for splenocyte culture at 37 ℃ and 5% CO_2.

Jurkat Cell Culture Media: Cell lines were maintained in RPMI 1640 (Invitrogen) supplemented with 10% FBS (Atlanta Biologicals) and 4 mM l-glutamine, Penicillin/Streptomycin, and 25 mM HEPES buffer (Fisher Scientific) at 37 ℃ and 5% CO_2.

2.2.3 Cell Activation and Differentiation

Mouse $CD4^+$ T cell differentiation: To induce TH0 cells, mouse splenocytes or $CD4^+$ T cells were incubated in 24 well plates coated with 1µg/mL anti-CD3 (Biolegend)

and 1µg/mL soluble anti-CD28 (biolegend). For Tr1 cells 50ng/mL of IL-27 (R&D systems) was added according to [5]. For Th1 cells, 20ng/mL IL-2, 20ng/mL IL-12, and 10µg/mL anti-IL-4 (R&D systems) was added. For Th2 cells, 20 ng/mL IL-2, 100 ng/mL IL-4, 10µg/mL anti-IL-12 (R&D systems) was added. After 5 days, cells were counted and resuspended @ $1x10^6$ cells/mL in 75% new media (rested) for 2 days.

Mouse $CD4^+$ T cell re-stimulation: Rested cells were plated at 1x10^6 cells/mL in fresh media in 24 well plates coated with 5µg/mL anti-CD3 (Biolegend). For zinc experiments, filter sterilized $ZnSO_4$ [50mM] (Sigma) in 0.85% NaCl was diluted in media to indicated [Zn^{2+}]. TPEN (N,N,N′,N′-Tetrakis(2-pyridylmethyl) ethylenediamine) [20mM] in DMSO was added to 0.85% NaCl to indicated concentration. After indicated time points, cells were spun down (300g) and supernatant was stored at -80^{O}C until analysis.

Jurkat T cell differentiation: Jurkat E6 $CD4^+$ T cells were stimulated with immobilized anti-CD3 (2 µg/ml) and soluble anti-CD28 (5 µg/ml) in the presence of IL-12 (5 ng/ml) and IFN-gamma (2 ng/ml) for 48 h (TH1 inducing conditions), or immobilized anti-CD3 (2 µg/ml) and soluble anti-CD28 (5 µg/ml) plus IL-4 (5 ng/ml) and IL-10 (10 ng/ml) for 48 h (TH2 inducing conditions).

2.2.4 Treatments

For metal treatment, $CdCl_2$ (Sigma), $Hg(OAc)_2$ (Sigma), $ZnSO_4$ (Sigma) were diluted in 0.85% NaCl at [50mM] and diluted in media to appropriate final concentrations.

For cell activation treatments, Phorbol 12-myristate 13-acetate (PMA) (Roche), was reconstituted in DMSO to 1mM per manufacturer's instructions and diluted in media immediately before use. Phytohemaglutanin (PHA) (Roche) and concanavalin A (ConA)

(Sigma) was diluted in PBS to 1mg/mL and diluted in media immediately before use.

For cytokine treatments, recombinant CCL2 (also called MCP-1) and anti-CCL2 were part of a duoset sandwich immunoassay kit (R&D systems) and stock concentrations were created and stored per manufacturers instructions. Mouse IL-1 beta, IL-2, IL-4, IL-5, IL-8, IL-10, IL-12, IFN-gamma, and TNF-alpha recombinant proteins were all part of duoset kits (R&D systems).

For ROS, RNS, and antioxidant treatments, H_2O_2 (30% w/v) (Sigma) was diluted in PBS before use (See section 2.3.2). 3,3-Bis(aminoethyl)-1-hydroxy-2-oxo-1-triazene (NOC-18) (Sigma) was diluted in 0.85% NaCl to 100µM immediately before use. To release a bolus of NO, HCl (1M) was added to NOC-18 in a dropwise manner until pH 3.0 was reached, then brought up to pH 7.4 before being diluted for use. 2,2'-dithiodipyridine (DTDP) (Sigma) was diluted in PBS to 100µM before being diluted in media. N-acetylcysteine (NAC) was diluted in 0.85% NaCl and pH to 7.4 with NaOH (1M) before use.

For zinc treatments, 2-Mercaptopyridine *N*-oxide sodium salt (Pyrithione) (Sigma) was diluted in 0.85% NaCl to 50mM before being diluted before use. N,N,N′,N′-Tetrakis(2-pyridylmethyl) ethylenediamine) (TPEN) in DMSO [20mM] was diluted to indicated concentration.

2.2.5 Buffer Recipes

(H_2O for all buffers was purified using Nanopure system, 18mΩ)

1. NP-40 Lysis Buffer

0.5% NP-40 (v/v): EDTA [1mM]

2. Complete Buffer “C”

   9.375 mL Buffer C. : 1 Roche mini tab :10µL DTT [1M] : 50µL PMSF [100mM] : 500µL Na-beta-glycerophosphate [1M] : 25µL NaF [400mM] : 100µL Na-ortho-vanadate [100mM]

3. FACS Buffer

   PBS (pH 7.4) : 5% FBS

4. Staining Buffer

   PBS (pH 7.4) : 0.2% BSA : 0.09% NaN_3

5. (2x) Laemmli Buffer with 2-Mercaptoethanol

   4% SDS : 120mM Tris-Cl (pH 6.8) : 20% glycerol : 0.02% Bromophenol Blue : 5% 2-Mercaptoethanol

6. SDS-PAGE Running Buffer

   3.25g Tris Base : 14.35g Glycine: 0.1% SDS : 1 L ddH20

7. PBS (pH 7.2)

   160g NaCl: 4g KCl : 4g KH_2PO_4 : 23g NaH_2PO_4 : 20L ddH_2O

8. PBS-T (pH 7.2)

   160g NaCl : 4g KCl : 4g KH_2PO_4 : 23g NaH_2PO_4 : 4g NaN_3 : 5mL Tween-20 : 20L ddH_2O

9. Incomplete Freund's Adjuvant

   Heavy Weight Mineral Oil: 10% (v/v) Arlacel A

10. Complete Freund's Adjuvant

    100mg *M. tuberculosis*: 30mL Incomplete Freund's Adjuvant

2.3 Quantification of Intracellular Labile [Zn^{2+}]

2.3.1 Resting Levels

Mouse and human cells were loaded with 0.5µM Fluozin-3 AM (Invitrogen) in benchtop media for 30 minutes at 37^{O}C and 5% CO_2 according to manufacturer's protocol. Cells were spun and resuspended in benchtop media alone and incubated for an additional 30 min. Cells were spun again and resuspended in ice cold benchtop media and stained with antibodies against surface markers for 20 minutes on ice (see section 2.4). Cells were then washed 2x with FACS buffer (PBS pH 7.4 + 5% FBS + 0.05% NaN_3) and resuspended in 400µL benchtop media + 3µg/mL propidium iodide. Cells were then aliquoted into 3 5mL polypropylene tubes (100, 100 and 200µL) and kept on ice until analysis. 10 minutes prior to analysis, 100µL of cell sample was mixed with 100µL of [100µM] pyrithione + [200µM] $ZnSO_4$ in FACS buffer to generate an Fmax

sample. Similarly, 10 minutes prior to analysis the other 100µL aliquot of cell sample was mixed with 100µL of [100µM] TPEN in FACS buffer to generate an Fmin sample. Untreated sample was used to generate the F sample. The geometric mean of each population in the FITC channel was used to generate F, Fmax, and Fmin measurements. To determine intracellular [Zn^{2+}] the following formula was used: Zn2+ [pM] = 15000 x (F – Fmin) / (Fmax – F), adapted from [194].

To determine effects of treatment induced Zn release at indicated time points, cells were loaded with Fluozin-3 AM as described. After loading, cells were incubated with appropriate treatment for 30-60 min. Cells were then washed 1x with media and placed on ice for surface staining.

2.3.2 Kinetic Zn^{2+} Release Following Treatment

For kinetic experiments, cells were loaded and stained as described (see 2.3.1). 1x10^6 cells were resuspended in 800µL of media and kept on ice until analysis. 5 min prior to analysis, cells and treatment (400µL diluted to 2x concentration in media) were warmed in a water bath. Cells alone were analyzed for 3-5 minutes to determine a (F) baseline measurement. Cell sample was then removed and 400µL of cell sample was added to 400µL of 2x treatment and immediately placed back on the cytometer for an additional 15-20 minutes.

2.3.3 0-3 Hour Treatment

Cells were resuspended in a 96 well plate with appropriate treatment for indicated amount of time. Cells were then removed, spun down (250g for 5 min) and

resuspended in 0.5µM Fluozin-3 AM in media for 15 minutes. Cells were then spun again and resuspended in media + surface marker antibodies on ice for 15 min. Cells were then washed 1x with media and resuspended in media + PI and kept on ice until analysis.

For detection of Zn release and ROS production during restimulation, see protocols adapted from [218]. Briefly, cells were coated with anti-CD3 (553058, BD Biosciences) [5µg/mL] on ice for 30 min. Cells were then washed in FACS buffer (PBS + 5% FBS, pH 7.4) and resuspended in pre-warmed media containing anti-hamster IgG (01-22-06, KPL Bio) [10µg/mL] for indicated period of time . During the last 15 minutes of incubation, Fluozin-3 AM [1µM] was added to load the cells before spinning and staining on ice for surface markers (see 2.4.1)

2.4 Immuno-phenotyping

2.4.1 Surface Marker Staining

anti-mouse antibodies: anti-CD4-alexafluor647 (557681, BD biosciences), anti-CD4-FITC (553729, BD biosciences), anti-CD4-PE (553730, BD biosciences), anti-CD4-PerCP (553052, BD Biosciences), anti-CD8-PerCP (553036, BD Biosciences), anti-CD8-APC (553035, BD Biosciences), anti-CD8-PE (553033, BD Biosciences), anti-CD45R-PE (1665-09, Southern Biotech) anti-CD45R-alexafluor647 (557683, BD Biosciences), anti-CD25a-PE Cy7 (552880, BD Biosciences) anti-CD25-alexafluor647 (563598, BD Biosciences), anti-CD19-PE (553786, BC Biosciences)

anti-human antibodies: anti-CD3 (MAB100, R&D systems), anti-CD3-biotin

(555331, BD Biosciences), anti-CD28 (555726, BD Biosciences), anti-CD4 (MAB379, R&D systems), anti-CD4-alexafluor647 (51-0048, Ebioscience)

2.4.2 Intracellular MT Staining

The UC1MT hybridoma [141] was grown and IgG was purified by LC using protein A/G according to lab protocols. For immunophenotyping, IgG was labeled with alexafluor647 using a NHS-alexafluor647 labeling kit according to manufacturers instructions (A20006, Life Technologies). After surface marker antibody staining, cells were fixed and permeabilized using the "Fix and Perm Cell Permeabilization Kit" (GAS004, Invitrogen) according to manufacturer's instructions. Approximately 1.6µg of UC1MT-alexafluor647 antibody per 500,000 cells was used for intracellular staining. Mouse-MOPC21-alexafluor647 (400130, Biolegend) was used as isotype control. Cells were analyzed in FACS buffer (0.2% BSA in PBS + 0.09% NaN_3, pH 7.4)

2.4.3 Intracellular p38 Staining

Cells were fixed with 2% paraformaldehyde (Sigma) at 37C for 10 min and then brought to room temp. Cells were permeabilized in 90% methanol in staining buffer (according to Cell Signaling Phospho Staining Protocol) and stored overnight at -20^{O}C. Cells were stained with anti-phospho p38 (9211S, Cell Signaling) or anti-total p38 (9212, Cell Signaling), or isotype control rabbit anti-OVA (AB1225, Chemicon). Anti-rabbit IgG-FITC (554020, BD Biosciences) was used as a secondary antibody. Cells were analyzed in FACS buffer (0.2% BSA in PBS + 0.09% NaN_3, pH 7.4)

2.4.4 Intracellular FoxP3 Staining

PBMC from mice were isolated over a Histopaque 1083 gradient and used for FoxP3 staining. Cells were fixed, permeabilized, and stained using the Alexafluor647 anti-mouse/rat/human FOXP3 Flow Kit (320021, Biolegend) according to manufacturer's protocols. Additionally cells were stained with anti-CD4-FITC and anti-CD25a PE Cy7 for measurement of Treg cell populations by flow cytometry.

2.4.5 Flow Cytometry

Cell fluorescence measurements were made on a FacsCalibur Flow Cytometer (BD Biosciences). Cells were analyzed using FlowJo v9 software (TreeStar). All cells were gated on FSC-SSC and PI negative to ensure uniform analysis of live cell populations. For Zn measurements, cells were analyzed in PBS + 10% FBS or benchtop media (using DMEM without phenol red)

2.4.6 Confocal Microscopy

Confocal microscopy images were taken with a Nikon A1R Laser Scanning Confocal Microscope (63x objective) or an Andor Revolution Spinning Disk Confocal Microscope (63x objective). Cells were kept at 37^{O}C in a humidified chamber during image acquisition. Images were processed using ImageJ software.

2.5 Redox Measurements

2.5.1 Intracellular ROS Production

ROS production was measured by loading cells with CM-H_2DCFDA (C6827, Life Technologies) according to manufacturer's protocols or according to protocols described in [218]. Treatment with 200µM H_2O_2 for 20 minutes was used as a positive control for oxidation. Fluorescence was measured by flow cytometry (see 2.4.4)

2.5.2 Intracellular Free Thiol Concentration

Total free thiol measurements were made using a SpectraMax Plate Reader and SoftMaxPro software (Molecular Devices, Sunnyvale, CA) according to [219]. CPM (7-Diethylamino-3-(4'-Maleimidylphenyl)-4-Methylcoumarin) was acquired from Life Technologies (D-346). To generate a free thiol standard curve, reduced glutathione (039K1054, Sigma) was reconstituted immediately before use. Briefly, cells were counted and cells were lysed in a nonidet P-40 based lysis buffer (NP-40 0.5% v/v, EDTA 1mM). Cell lysates were assayed for total protein concentration using a micro BCA kit (23235, Pierce). GSH standard curve in PBS (10µM – 10nM) and cell lysate samples were assayed in triplicate.

2.6 SDS-PAGE / p38 Western Blotting

After treatment, cells were spun down and frozen on dry ice and stored at -80^{O}C. Cell pellets were resuspended in 25µL complete Buffer "C" (see section 2.2.5). Cell lysates were assayed by Bradford Assay (500-020, BioRad) to determine protein concentration. For each lane, load 24µg of cell lysate in Laemmli Buffer (1x) (preheated to 95^{O}C for 5min and cooled) into lanes of a 3% acrylamide stacking / 10% acrylamide

separating gel using the BioRad SDS-PAGE box in Running Buffer. Run gel at 150mV (DC) for 1 hour. Transfer gel to PVDF membrane using iBlot system (Life Technologies) according to manufacturers protocols. For total p38, block membrane with 5% non-fat dry milk in TBS-T and probe using anti-p38 (9212, Cell Signaling) according to manufacturers protocols. For phospho-p38 block membrane in 5% BSA and probe using anti-phospho p38 (9211S, Cell Signaling) according to manufacturers protocols. Anti-rabbit-HRP (s-2054, Santa Cruz) was used as secondary antibody. Chemiluminescent detection was achieved using SuperSignal West Pico Kit (34079, Pierce) and a Kodak 2000MM image station. For reference, Full Range Rainbow Molecular Weight Marker was used (GE Lifesciences).

2.7 Biomarker Quantification by ELISA

All ELISAs were conducted using Immulon H2B plates and were read on a SpectaMax 2 Plate reader at 405nM – 540nM for reference correction of HRP substrate and 450nM for AP substrates. Plates were washed in between steps using an ELX 405 automatic plate washer and PBS-T wash buffer.

2.7.1 Mouse Cytokines

Mouse cytokine quantification by ELISA was accomplished using duoset matched pair antibodies for IL-10 (DY417, R&D systems), IFN-gamma (DY485, R&D systems) and streptavidin HRP substrate detection.

2.7.2 Human Cytokines

Human cytokine quantification by ELISA was accomplished using duoset matched pair antibodies for IL-2 (DY202, R&D systems), IFN-gamma (DY285, R&D systems) and TNF-alpha (DY210, R&D systems) and streptavidin HRP substrate detection.

2.7.3 Mouse IgG

Detection of mouse IgGs were accomplished by serial dilutions (1:4) of serum (1:100 – 1:6400) in PBS. The following capture antibodies were used: anti-mouse IgG (31168, Pierce), anti-mouse IgG1 (1070-01, Southern Biotechnology), anti-mouse IgG2a (103-01, Southern Biotechnology), anti-mouse IgG2b (104-01, Southern Biotechnology). Anti-collagen specific IgG was captured using plate bound type II chicken collagen [5µg/mL] in 0.05 M Tris-HCl/ 0.2M NaCl. Mouse IgG was detected using anti-mouse IgG – AP (1030-04, Southern Biotechnology).

2.7.4 Human anti-CCP antibody

Anti-CCP autoantibody was measured from human serum of 48 individuals collected by the New York State Department of Health, Wadsworth Center. Serum was stored at -80^{O} C until testing. Samples were analyzed by an anti-CCP autoantibody ELISA kit (FCCP 100, Euro Diagnostica) using manufacturer's protocols. For comparison with SPCE based measurements, cyclic citrullinated peptide (H-HQCHQESTXGRSRGRCGRSGS-NH2) was synthesized by Abgent and detected with anti-human IgG-biotin (H10315, Invitrogen) and streptavidin-alexafluor647 (S1374, Life Technologies).

2.9 SPR / SPCE Assays

2.9.1 SPR and SPCE Instrumentation and Sensor Chips

The GCSPRI instrument used in these studies is an engineering prototype of the 8500 Flexchip Analyzer (HTS Biosystems, Hopkinton, MA) and has been described previously (Unfricht et al., 2005). GCSRPI sensor chips were provided by Ciencia, Inc. (East Hartford, CT). Assays requiring both GCSPRI and fluorescent measurements were made with a second generation GCSPRI/SPCE dual mode instrument designed and built by Ciencia, Inc. (East Hartford, CT). The second generation instrument is based on the same SPR principle as the 8500 Flexchip, but operates at a shorter wavelength that is compatible with the excitation of Alexa fluor 647 (Invitrogen, Carlsbad, CA) and CellTrace Far Red DDAO-SE (Invitrogen, Carlsbad, CA).

2.9.2 GCSPRI Sensor Chip Modification and Printing

Gold sensor chips were washed with 70% ethanol and rinsed with water (18 MΩ) and dried under a stream of filtered air. For dithiobis-succinimidyl propionate (DSP) surface modifications, DSP (Thermo Fisher, Rockford, IL) was resuspended in dimethyl sulfoxide (DMSO) at 4 mg ml^{-1} and contacted to the gold surface for 30 min. Chips were washed exhaustively with DMSO and water (18 MΩ) and immediately used for printing. 2-(pyridinyldithio) ethylcarbamoyl dextran (PDEC dextran) surface modifications were performed as previously reported (Li et al., 2008). Before printing on PDEC dextran surfaces, inter-heavy chain disulfide bonds of antibodies were reduced with 1 mM dithiothreiotol (DTT) for 8 h to expose sulfhydryl groups for covalent immobilization. For

neutravidin surface modifications, cleaned sensor chips were incubated with a solution of 1 mM 1,9 nonanedithiol (Sigma–Aldrich, St. Louis, MO) in ethanol for 2 h and then washed extensively with ethanol. Chips were then incubated with 0.3 mg ml^{-1} maleimide-activated neutravidin (Thermo Fisher, Rockford, IL) in PBS for 1 h and then washed exhaustively with water (18 MΩ) and dried under a stream of filtered air. All surface modifications were made at 25 °C.

Microarrays were printed on sensor chips using the OmniGrid Micro robotic spotter (Genomic Solutions, Ann Arbor, MI) or a SpotBot II robotic spotter (TeleChem International, Inc., Sunnyvale, CA) and an ArrayIt Stealth micro spotting pin, size SMP7B (255 µm spot diameter, 3.1 nL delivery volume) (TeleChem International, Inc., Sunnyvale, CA). Chips were maintained in high humidity (75–85%) at 25 °C during spotting and allowed to incubate for an additional 1 h in high humidity after spotting. Chips were then removed and fitted with a 0.02″ thick, double-sided adhesive gasket and 1/8″ thick glass window to form a 50 µl flow cell over the printed array. Once printed, chips were stored desiccated at 4 °C for up to 4 days before use.

2.9.3 Antibodies and General Reagents

Anti-human cytokine antibody matched pair sets for interleukin-2 (IL-2), interferon-gamma (IFN-gamma) and tumor necrosis factor-alpha (TNF-alpha) were purchased as duosets from R&D systems (Minneapolis, MN). Mouse anti-human CD3 and anti-human CD28 antibodies were purchased from BD Biosciences Pharminogen (San Diego, CA). Biotinylated mouse anti-human CD3 was purchased from Becton-Dickinson (Franklin Lakes, NJ). Superblock (in PBS) blocking agent was purchased

from Thermo Scientific (Rockford, IL). Bovine serum albumin (BSA) was purchased from Fisher Scientific Company (Morris Plains, NJ). BSA was biotinylated using polyethylene oxide–maleimide–biotin from Pierce (Rockford, IL) and diluted to 500 µg/ml in PBS for use on reference ROIs. CellTrace Far Red 9H-(1,3-dichloro-9,9-dimethylacridin-2-one-7-yl) succinimidyl ester (DDAO-SE) was used for fluorescent cell labeling and streptavidin Alexa fluor 647 were purchased from Invitrogen (Carlsbad, CA). For mouse cytokine microarrays, sensor chips were contacted with dithiobis(succinimidyl propionate) (22585, ThermoScientific) [4mg/mL] in DMSO for 30 min and washed exhaustively with DMSO and water before printing. Arrays were printed as described in section 2.11.2. For analyte detection, the following sandwich immunoassay sets were used: IL-ra (DY480, R&D systems), IL-1beta (DY401, R&D systems), IL-2 (DY402, R&D systems), IL-4 (DY404, R&D systems), IL-5 (DY 405, R&D systems), IL-6 (DY406, R&D systems), IL-10 (DY417, R&D systems), IL-12p70 (DY419, R&D systems), IL-13 (DY413, R&D systems), IL-17 (DY421. R&D systems), IL-18 (DO47-3 + DO48-6, MBL International) IL-33 (DY3626, R&D systems), CCL-2 (DY479, R&D systems), CD40L (DY1163, R&D systems), IFN-gamma (DY485, R&D systems), Osteopontin (DY441, R&D systems), TNF-alpha (DY410, R&D systems)

2.9.4 Peptide-MHC Monomer Complexes

The influenza hemaglutanin peptide abbreviated HA (PKYVKQNTLKLAT), and the tetanus toxin control peptide abbreviated TT (QYIKANSKFIGITE), presented in the context of DR1 (DRA*0101, DRB1*0101) have been previously described (Stone et al., 2005 and Zavala-Ruiz et al., 2004). Briefly, recombinant MHC proteins were prepared

by standard methods (Cameron et al., 2002). Soluble HLA–DR1 including a uniquely reactive cysteine engineered at the C terminus of the alpha chain was produced in Schneider S2 insect cells, and was chemically modified with polyethylene oxide–maleimide–biotin (Pierce, Rockford, IL).

2.9.5 Assay Procedure

Sensor chips were blocked by flushing 5 ml of Superblock (Pierce, Rockford, IL) or 2% BSA in PBS over the chip and allowing the blocking agent to incubate for 10 min. This step was repeated once. Next, 5 ml of complete RPMI 1640 with 10% FBS was flushed over the chip and allowed to incubate for 30 min. This step was repeated once. Cells were resuspended to 2×10^6 cells ml^{-1} in complete RPMI 1640 with 10% FBS before analysis. Complete RPMI 1640 10% FBS was passed over the chip surface for 5 to15 min at 200 µl min^{-1} to establish a baseline SPR angle measurement. Three ml of sample was recirculated at 200 µl min^{-1} for 15–30 min to allow for cell binding. Non-specifically bound cells were minimized by following the cell suspension exposure with a wash step consisting of complete RPMI 1640 media 10% FBS at passed over the chip at 1 ml min^{-1} for 10 min. For cytokine production assays, cells were allowed to incubate on the chip for 3 h before exposure to lysis buffer (20 mM Tris, 100 mM NaCl, 1 mM EDTA, 0.5% Triton X100, pH 7.4) for 5 min followed by a wash with PBS plus 0.0025% Tween20 plus 0.0002% NaN_3 (PBST) at 500 µl min^{-1} for 5 min. 2 ml of 0.1% BSA in PBST containing a cocktail of secondary matched-pair detection antibodies at recommended ELISA concentrations (R&D Systems, Minneapolis, MN) was recirculated over the chip at 500 µl min^{-1} for 60 min, followed by a wash with PBST at 500 µl min^{-1}

for 5 min, followed by streptavidin-Alexa fluor 647 in PBST at 800 ng/ml for 20 min and a final 10 min wash step with PBST before measuring fluorescence using SPCE. Chips were kept at a constant 37 ℃ for the duration of all experiments.

2.9 Collagen Induced Arthritis (CIA) Model

Induction of the Collagen Induced Arthritis model in C57Bl/6 mice was accomplished using protocols described in [220]. Protocols were approved by UConn IACUC (protocol number A08-065).

2.9.1 Pilot Study

7 male C57BL/6 mice (mean age 25 weeks) and 7 female C57BL/6 mice (mean age 29 weeks) were injected 2x with 50µL intradermal injections at the base of the tail with Chicken Type II Collagen (C9301, Sigma) in complete Freund's Adjuvant (CFA) (Treatment Group) . Alternately, 3 male and 1 female mouse were injected with CFA alone (Vehicle Control group). The Treatment Group was given a secondary booster injection 2 weeks later with Chicken Type II Collagen in incomplete Freund's Adjuvant (IFA). Mice were monitored and scored for inflammation in the hind paws over the 3 month course of the study. Blood samples were collected before immunization and at days +4, +16, +43, +55, and +80 post immunization. Mice were euthanized at day +55 or day +80 and spleens, inguinal lymph nodes, PBMCs and serum were isolated for further analysis.

2.9.2 Influence of MT on CIA progression Study

13 male C57BL/6 (MT-WT), 13 male MT-KO, and 10 male MT-TGN mice were immunized as described above (see section 2.10.1) Additionally, 3 mice from each group were treated with vehicle control. Changes to above protocol including addition of sterile PBS to primary immunization (which precipitates collagen into a salt), and 2 additional booster immunizations at 14 days and 58 days.

Chapter 3

Measuring Intracellular [Zn^{2+}] in Immune Cells

in vitro

3.1 Introduction

Total intracellular [Zn^{2+}] in eukaryotic cells is usually in the range of a few hundred micromolar[221]. Lysis of cells and removal of the zinc with low pH and heating allows the careful analysis of total intracellular zinc. However, the physiologically relevant concentrations associated with zinc signaling, where transient changes affect cellular processes, are much lower. In T cells, important signaling pathways including activation of Akt following IL-2 signaling, for example, are affected when intracellular labile [Zn^{2+}] is increased from 200 to 590pM [222]. Because of the vast repertoire of zinc binding motifs, zinc has the potential to affect protein structure and function across a significant concentration range. However, fluctuations within normal healthy immune cells during activation and signaling usually include an increase in intracellular [Zn^{2+}] from 200 pM up to about 1 nM. Interestingly, this is within the theoretical range of regulation by metallothionein (MT), given cytosolic concentrations of MT[34] in lymphocytes and MT's affinity for Zn^{2+} (log K = 11 – 8)[120]. Within this range, zinc mediated regulation occurs via 4 distinct mechanisms in lymphocytes: 1. Structural changes and transcription factor activation (ex. MTF-1) 2. Inter-molecular binding and activity (ex. CD4/LcK) 3. Enzyme activation (ex. PKC); Enzyme inhibition (ex. PTPase). Of particular importance in T cell signaling is the inhibition of protein tyrosine

phosphatases[223]. The vast majority of structural zinc in zinc finger transcription factors is not significantly affected in this range of fluctuation because these motifs are already saturated with zinc, given their high binding affinity (logK = 13-11). Likewise, activation of metalloproteases, which requires high nanomolar [Zn^{2+}] [224], would not be affected by these picomolar shifts (Figure 3.1)

3.2 Measuring Intracellular Labile [Zn^{2+}]

There are many factors to consider when choosing a fluorescent zinc chemo-sensor including optical ex/em wavelengths, affinity for metal, specificity for a zinc, different excitation spectra from metal bound or free sensor for ratio-metric comparison, activity in large pH range, etc. Many of the currently available zinc sensors have been recently reviewed[225]. Briefly, an ideal zinc sensor is nonfluorescent in the free-base form and highly fluorescent when coordinated to zinc. Furthermore, for determination of intracellular concentration, the sensor must be cell-permeable and, ideally, retained inside the cell after crossing the membrane. Various zinc sensors meet some but not all of the necessary qualifications for measuring picomolar shifts in intracellular [Zn^{2+}] *in vitro*[131]. However, the need for high specificity, high affinity sensor prevents this investigation using established zinc sensors including Zinquin (Kd_{zinc} =7μM)[226] [227]and Newport Green (Kd_{zinc} = 1-3μM)[228] .

The precise measurement of intracellular labile [Zn^{2+}] in immune cells has only recently become possible with the development of the high affinity fluorescent sensor Fluozin-3 and its acetoxymethyl ester derivative Fluozin-3 AM (Figure 3.2) The high affinity (Kd_{zinc} = 15nM) of this sensor allow changes in [Zn^{2+}] below 100 pM to be

measured. Furthermore, this sensor is highly specific and is not perturbed by high levels of intracellular Mg^{2+} or Ca^{2+}[229] which is of particular importance in T cell activation where an influx of Ca^{2+} is a necessary requirement [230]. Furthermore, Fluozin-3 is relatively unaffected by low pH or oxidants [231] which is important for studying zinc in lysosomes or its release following oxidative stress.

One of the drawbacks of Fluozin-3 is its lack of ratio-metric properties, meaning the total amount of free dye that is not complexed with zinc cannot be determined using a different excitation wavelength like other sensors (ex. Fura-2). This can be overcome experimentally by exposing cells to complete chelation or complete saturation with zinc [194] to generate a minimum fluorescent signal (Fmin) or a maximum fluorescent signal (Fmax), respectively. Using these parameters, the intracellular $[Zn^{2+}]$ can then be interpreted based on the relationship of Fmin and Fmax to the unperturbed fluorescent signal (F) and the known dissociation constant of Fluozin-3 (Kd=15nM) using the equation:

Equation 1:

Intracellular $[Zn^{2+}] = K_d * (F-Fmin) / (Fmax - F)$ [194]

To generate the Fmin signal, an excess of the cell permeant zinc specific chelator TPEN is added to the cell sample at least 10 min prior to analysis. Minimum Flouzin-3 fluorescence, measured in the FL-1 or GFP channel of the FACScalibur flow cytometer, is reached within 1 min of TPEN [10µM] addition[194] to cells in complete cell culture media. To ensure fluorescent minimum is reached, samples are incubated for at least 10 min with 50µM TPEN in PBS/media (1:1). It is important to note, if extracellular $[Zn^{2+}]$ in the experimental system is exceptionally high (100µM $ZnSO_4$ treatment, for

example) the concentration of TPEN must be increased accordingly. The 10min incubation at 50µM is considered a good standard for cells in normal culture media and does not affect signal from propidium iodide or forward/side scatter properties, indicating this treatment does not interfere with membrane integrity.

To generate the Fmax signal, the Fluozin-3 fluorescent probe must be saturated with Zn^{2+} ions, which occurs at about 5µM $ZnSO_4$ at pH 7.2 in isotonic buffer [19] as a reference. To accomplish this, an excess of $ZnSO_4$ [200µM] is added to the media containing cells along with the zinc specific ionophore pyrithione [50µM] and incubated with the cells for at least 10 minutes. Fmax is achieved within 1-2 minutes using these conditions with $CD4^+$ T cells (Figure 3.5) and can be achieved with as little as 1µM pyrithione and 50µM $ZnSO_4$[194]. Therefore, the use of 2-10 fold excess ensures Fmax is achieved reproducibly.

The protocol for determining the best method for Fluzoin-3 loading and sensor saturation/chelation was part of a systematic, iterative process to ensure the method used had as little effect as possible on the measurement. Literature [7,194] and manufacturer's protocols often call for long incubations with ionophore and chelator at $37^{O}C$. However, this causes a change in the distribution of fluorescent signal and scatter properties in immune cells from both Fmax and Fmin conditions. This also leads to greater inter-assay variation for the same population of cells measured multiple times in parallel (data not shown). To avoid this variation, the method of 10 min incubations on ice directly before measurement was developed to produce populations with scatter properties that were the same as untreated cells.

The method described above was applied to freshly-isolated peripheral blood

mononuclear cells (PBMCs) from a C57BL/6 mouse. PBMCs were isolated from heparinized whole blood by density centrifugation and loaded with Fluozin-3 AM. Cells were then stained with anti-CD4-alexafluor647 antibody and propidium iodide (PI). The cell sample was split into 3 aliquots: one aliquot was treated with Zn/pyrithione (Fmax); one aliquot was treated with TPEN (Fmin) ; one aliquot was left untreated (F). Lymphocyte FSC/SSC and PI negative gates were applied and the resulting Fluozin-3 fluorescence for the three samples is shown in Figure 3.3. The geometric mean of each population was then determined and used as the relevant value in Equation 1. For this sample, the $CD4^+$ T cell population had an average intracellular $[Zn^{2+}]$ of 202 pM, which is within the reported normal distribution for murine $CD4^+$ T cells.

To determine the optimal concentration of Fluozin-3 AM to use in subsequent experiments, the effect of sensor incubation concentration on the resulting fluorescent signal (F) was measured in Figure 3.4. Increasing the Fluozin-3 AM concentration above [1µM] did not significantly affect cellular fluorescence. When fluorescent compensation between several fluorophores is required, the negative and positive stained populations must fit completely within the scale of fluorescence that is measured on the cytometer (for example, 10^4 fluorescent units on the FACScalibur). This will be a requirement for when multiple cell populations from the same sample need to be identified ($CD4^+$, $CD8^+$ $CD25^+$, $CD19^+$, $CD45R^+$, etc.). In order to get the unlabeled and Fmax populations both within this range on the FL-1 channel, it is necessary to use a concentration of Fluozin-3 AM that is 0.5µM or lower. Additionally, the least amount of probe necessary to generate sufficient signal is always preferred because excess probe can have a zinc buffering effect on the cellular system[19]. For

these reasons, a concentration of 0.5µM was generally used for all experiments.

To measure the effect of influx of extracellular [Zn^{2+}] on Fluozin-3 fluorescence, $CD4^+$ T cells were loaded with Fluozin-3 and treated with different concentrations of extracellular $ZnSO_4$ and pyrithione (Figure 3.5). In the absence of pyrithione (magenta line), adding up to 50µM $ZnSO_4$did not increase fluorescence in the 30 minute time window of incubation, evidencing the ability of cells to maintain steep extracellular/intracellular zinc gradients. Addition of pyrithione alone (teal line) did increase intracellular fluorescence, indicating the residual zinc in either the pyrithione preparation or the 1% fetal bovine serum (FBS) was enough to increase intracellular labile [Zn^{2+}] when ionophore was added. Increasing [Zn^{2+}] from 400 nM to 50µM increased fluorescence, indicating the probe was not saturated, even when 10µM $ZnSO_4$ was added (red line). This was likely due to the buffering capacity of both the intracellular environment and the FBS. 10% FBS has been shown to sequester about 50% of added [Zn^{2+}] when 10% FBS was added to media[7]. Fluorescence did not increase when more than 50µM $ZnSO_4$ was added, indicating saturation of Fluozin-3 by zinc had occurred (data not shown).

In general, different types of cell and cells at different stages of cellular development (naïve, proliferating, effector) load the Fluozin-3 sensor differently[19]. Total Fluozin-3 loading efficiency can be derived from measurements following zinc saturation using excess zinc and pyrithione to generate a maximum fluorescent signal (see section 3.3). Within resting naïve lymphocytes, $CD19^+$ B cells exhibit higher Fmax signals than $CD4^+$ cells, which are higher than $CD8^+$ cells (Figure 3.6A). The same hierarchy of fluorescence was also observed for Fmin signals (due to background fluorescence of

the sensor), which supports the conclusion that B cells load Fluozin-3 more efficiently than T cells. This effect was observed over different days with both PBMC and spleen derived lymphocytes.

The efficiency of AM dye loading is the consequence of 2 separate processes: 1. Esterase activity that cleaves the AM group from the dye, making it polar and sequestering it inside the cell. 2. Efflux of the dye through ABC transporters and/or exocytosis[232]. In $CD8^+$ T cells (naïve or activated), and activated $CD4^+$ T cells, Fmax signals showed a wider distribution than naïve $CD4^+$ T cells, indicating the greater variation in the amount of dye retained in the cells. This distribution increased with time (data not shown), suggesting that the dye was actively being transported out of the cells. That this process was more highly active in activated $CD4^+$ T cells than naïve $CD4^+$ T cells (Figure 3.6A) is not surprising given the increased SSC parameter of activated $CD4^+$ populations, evidencing a greater number of intracellular vesicles, and the generally increased metabolism of proliferating lymphoblasts versus resting naïve lymphocytes. However, because the determination of intracellular $[Zn^{2+}]$ is derived from a ratio of F, Fmin, and Fmax signals, the degree of saturation of the dye remains the important parameter. This ratio is affected by labile $[Zn^{2+}]$ and is independent of dye concentration.

3.3 Resting Intracellular Labile $[Zn^{2+}]$ in Different Lymphocyte Populations

To determine the effect of MT gene dose on the resting intracellular $[Zn^{2+}]$ of mouse lymphocyte populations, the methods described above were employed to freshly

isolated PBMCs taken from male, age-matched MT-KO (n=4), MT-WT (n=4), or MT-TGN mice (n=4). Cells were stained with anti-CD8 ($CD8^+$ T cells), anti-CD4 ($CD4^+$ T cells) or CD19 (B cells) to differentiate cell populations. The Fluozin-3 signal (F, Fmin, and Fmax) for one representative mouse from each genotype / cell type is shown in Figure 3.6A. The intracellular labile [Zn^{2+}] from each genotype / cell type is shown in Figure 3.6B.

The same hierarchy of intracellular [Zn^{2+}] was observed in each of the 3 genotypes. $CD8^+$ T cells maintain the highest intracellular labile [Zn^{2+}] which ranges from 350 and 400pM. $CD4^+$ T cells maintain a significantly lower concentration that ranges from 140 to 220pM. B cells maintain the lowest concentration at 95-130pM. These concentrations represent resting cells, the vast majority of which are naïve cells, having never encountered their cognate antigen. These zinc levels can be considered a baseline at which normal cellular functions are maintained. However, influx of zinc from the extracellular environment or intracellular vesicles can quickly raise this concentration and act as a zinc signal as part of cellular activation.

MT genotype did not significantly influence ($p<.05$) the intracellular [Zn^{2+}] in any of the resting lymphocyte populations tested (MT-WT vs. MT-KO or MT-WT vs. MT-TGN). On one hand, this result is somewhat unexpected, given the influence of MT gene dose on total serum Zn concentrations in Figure 3.7. However, total serum Zn is buffered by plasma proteins, especially albumin [233] and the difference in the labile [Zn^{2+}] in serum is likely to be much less. Additionally, given how tightly intracellular [Zn^{2+}] is regulated by the ZnT and Zip families of proteins in lymphocytes, modest changes (<25%) to extracellular [Zn^{2+}] can be adequately addressed by small changes in

transporter activity or expression. Furthermore, baseline MT expression in resting naive lymphocytes, especially those from mice, is very low and protein levels are almost undetectable [34,35,234]. Therefore, it is likely that intracellular MT plays a much less significant role in determining intracellular [Zn^{2+}] than other homeostatic mechanisms.

Fluorescent compensation of overlapping excitation spectra from multiple fluorophores is an accepted method of determining relative fluorescence from distinct fluorophores. However, it is not without caveats and is based on assumptions including a linear relationship between fluorescent intensity and compensation. To make sure that fluorescent compensation and/or small sample size did not mask any MT gene dose related effects on the intracellular [Zn^{2+}] , $CD4^+$ T cells from mice sacrificed on different days over the course of several months were stained using an alexafluor647 labeled antibody. There is no spectral overlap between Fluozin-3 and alexafluor647, which negates the need for compensation and avoids any compensation derived artifacts. Additionally, it was important to validate that the source tissue from which $CD4^+$ T cells were taken did not affect intracellular [Zn^{2+}] . The results of this larger study (n=12) confirmed earlier findings that MT gene dose does not affect intracellular [Zn^{2+}] in resting $CD4^+$ T cells. Furthermore, cells derived from the spleen or peripheral blood displayed similar concentrations of intracellular [Zn^{2+}] .

3.4 Influence of Added Zn or Antioxidant to Culture Media

The resting concentration of intracellular Zn is tightly controlled primarily by ZnT1 and ZnT4 which are the predominant zinc exporters expressed in $CD4^+$ T cells[235]. To test the extent to which intracellular labile [Zn^{2+}] could be affected by extracellular

concentration, splenocytes from C57BL/6 mice (MT-WT) were cultured in complete media with 125μM $ZnSO_4$ for 24 hours (Figure 3.9) The increase in extracellular labile [Zn^{2+}] from this treatment is estimated to be about 25 fold. However, intracellular Zn increase was only about 50%, from ~200 pM to ~300 pM (Zn+/Zn+). The ability to experience only a small increase in intracellular [Zn^{2+}] is due to an increase in ZnT expression and is an established mechanism of zinc homeostasis in leukocytes.[195]. When cells were placed back in normal media for 30 minutes after 24 hour incubation with increased Zn (Zn+/Zn-), intracellular [Zn^{2+}] was lowered considerably, even below the concentration of cells cultured in normal media for the entire 24 hours (Control). This effect has been observed previously in T cells [196] and results from upregulation and expression of ZnT family zinc exporters. This observation emphasizes the fact that measurement of intracellular [Zn^{2+}] is affected by the [Zn^{2+}] in the media and buffers used during cell loading and analysis. For this reason, cells should be kept in media with an equivalent [Zn^{2+}] throughout experimental treatment and measurement.

Intracellular [Zn^{2+}] is intimately linked to redox potential because the additional electron on reduced sulfhydryls (as a free electron or part of the hydrogen atom) is a requirement for the coordination and binding of cationic zinc[236]. Oxidative stress or ROS signaling oxidizes intracellular thiols into disulfides that release bound Zn and prohibit further Zn binding until a reduced sulfhydryl is regenerated[20]. In this way, oxidative stress decreases the redox and consequent zinc buffering capacity of cells and makes them more susceptible to zinc toxicity[201]. This is especially important in lymphocytes where small changes in oxidative stress and zinc status are important for pro-apoptotic pathways[237,238]. For this reason, understanding the relationship of intracellular redox

potential during cell culture becomes critically important when measuring or manipulating the concentration of intracellular zinc. Removal of cells from the body, where partial pressure of oxygen is around 9%, and placement in atmospheric oxygen at 19% causes cells to experience an oxidative stress. To counteract this increase in redox potential, antioxidants are added to culture media to maintain intracellular reduced thiol concentrations [239]. For some cell types, 10% FBS adds enough redox buffering capacity to maintain healthy cells. However, given the sensitive nature of lymphocytes to oxidative stress, additional antioxidant in the form of 2-mercaptoethanol (2-ME) is often added. Maintaining an appropriate redox potential is critical to T cell functions including proliferation[240,241] and differentiation[242] and perturbation can exacerbate inflammatory autoimmune disease[243]. Furthermore, maintenance of extracellular free thiols has a significant role in shaping T cell responses[244-246].

To determine the effect of additional antioxidant on maintaining intracellular $[Zn^{2+}]$ concentration in $CD4^+$ T cells, splenocytes were isolated and cultured in standard cell culture media that includes 50µM added 2-ME, 50% antioxidant (25µM 2-ME) or no added antioxidant (Control) (Figure 3.9B). It is important to keep in mind that the 10% added FBS also acts as an antioxidant and redox buffer so control cells were not exposed to non-buffered oxidative stress (which leads to decreased cell viability). After 24 hours, there was a strong correlation with added antioxidant and intracellular labile $[Zn^{2+}]$ in $CD4^+$ T cells. Cells cultured in 50µM 2-ME maintained the same intracellular labile $[Zn^{2+}]$ as freshly isolated cells. Reducing the added 2-ME concentration by 50% resulted in 50% increase in intracellular labile $[Zn^{2+}]$ while excluding 2-ME altogether resulted in a 2 fold increase. After 24 hours, cell viability for cell cultures without added

2-ME began to decline, indicating the effect of the increased oxidative stress and zinc concentration led to programmed cell death. For this reason, cells were cultured in 2-ME for all T cell activation experiments to maintain normal physiological intracellular labile [Zn^{2+}].

Transcriptional control of ZnT1 is mediated through activation of MTF-1 and its subsequent binding to MREs in the gene promoter [247]. Addition of 125µM $ZnSO_4$ does not significantly affect the viability of $CD4^+$ T cells because of expression of compensatory Zn regulatory mechanisms [205]. Activation of MTF-1 is important for protection against zinc toxicity and involves induction of *MT1* and *MT2* as part of the cellular response to increased extracellular [Zn^{2+}].[248]. As a proof of principle experiment, we wanted to determine if differential MT expression could be measured in $CD4^+$ T cells from mice with disparate MT gene backgrounds in the context of zinc toxicity. Freshly isolated splenocytes from C57BL/6 mice (MT-WT) and MT overexpressing (MT-TGN) or MT knockout (MT-KO) congenic mice were cultured for 24 hours in the presence of different concentrations of $ZnSO_4$ (1-125µM). After 24 hours, cells were fixed and stained for CD4 and MT. Concentrations of zinc between 1 and 12.5µM had no effect on MT expression (Figure 3.9B). However, at 125µM added $ZnSO_4$, cells from mice with intact *MT1* and *MT2* genes were positive for MT expression with cells from MT-TGN expressing significantly more MT than MT-WT (Figure 3.9A). Cells from MT-KO appeared to express more MT after exposure to 125µM Zn. This is likely due to the expression a truncated non-functional peptide expressed in the MT-KO mice. The premature stop codon that disrupts MT1 and MT2 translation is inserted past the first N-terminal 5 amino acids of the protein and, consequently, MT-KO mice are able to

express a truncated protein with an antigenic epitope [38] that is recognized by the anti-MT antibody.

3.5 Sub-Cellular Localization of Labile Zn2+

The sub-cellular localization of Zn in lymphocytes is an expanding field that is only beginning to be understood (for excellent reviews see [191,192]). Like most ions, zinc is kept at a significantly lower intracellular concentration (~ 100 - 200pM) than serum concentration (5-10 µM). Furthermore, intracellular Zn is partitioned by ZnT proteins (SLC30A, Zn exporters) into intracellular vesicles, especially lysosomes or the poorly described "zincosomes"[235]. Release of zinc from vesicles with low pH in $CD4^+$ T cells following IL-2 stimulation [8] and in CD8+ T cells following TcR stimulation [15] has been reported. Following activation of CD8+ T cells, sub-cellular zinc is increased in the cytosol and almost completely released from vesicles via upregulation of Zip8 expression. During activation of $CD4^+$ T cells however, the degree to which Zn is compartmentalized and how this changes over the course of differentiation from naïve cell to lymphoblast to effector cell has not been characterized. Furthermore, Aydemir *et al*, speculated that increased expression of MT was responsible for no observed increase in cytosolic Fluozin-3 fluorescence in T cells following activation, even though the cytosolic [Zn^{2+}] had increased.

To investigate the sub-cellular localization of zinc in naïve $CD4^+$ T cells, freshly isolated splenocytes were imaged by confocal microscopy. Specifically, splenocytes were stained with anti-CD4-alexafluor 647 and loaded with Fluzoin-3 AM and Hoechst stain and to visualize the plasma membrane, zinc localization, and nucleus, respectively

(Figure 3.11). Naïve $CD4^+$ cells that were freshly isolated from the spleen of MT-KO or MT-WT mice both showed similar morphological characteristics including a round shape, and a tight ring of cytoplasm around the nucleus. Interestingly, the zinc distribution pattern indicates a low level of fluorescence in the cytoplasm with zinc (and sensor) being localized to punctate fluorescence points. Addition of zinc/pyrithione caused a bright fluorescent signal in all areas of the cell (data not shown) indicating sensor was present throughout. Both MT-KO and MT-WT cells showed a similar fluorescence pattern and these images reflect the finding of previous reports with both mouse and human naïve $CD4^+$ T cells[7].

To determine the localization of zinc in actively proliferating lymphoblasts, splenocytes were activated with anti-CD3/anti-28 in the presence of IL-27 to induce a Tr1 effector cell phenotype. Cells were monitored daily for changes in scatter properties and surface markers of activation (Figure 4.2A) by flow cytometry. On Day +6, the highest proportion (nearly 90%) of $CD4^+$ T cell populations of both MT-WT and MT-KO were at a dividing lymphoblast stage of development, determined by CD25+ surface activation marker, DDAO-SE^{low} (indicating dye partitioning and cell division), and FSC^{high} /SSC^{high} properties. Confocal images confirmed the flow cytometry data (Figure 3.11B). $CD4^+$ lymphoblasts were larger and morphologically irregular, showing a greater percentage of cytoplasm and an enlarged nucleus, all of which are expected during lymphoblast formation. Interestingly, cells maintained punctate zinc fluorescent patterns, indicating that intracellular Zn continues to be muffled (partitioned) into intracellular vesicles during activation and proliferation. In general, there were more punctate fluorescent vesicles in lymphoblast compared with naïve cells from both strains, which

was expected from their increased SSC properties. Furthermore, expression of MT was not a requirement of intracellular loading of zinc into vesicles, a mechanism that had been hypothesized recently. This does not mean that MT does not increase the kinetics or efficiency of the transport of zinc ions into intracellular vesicles, only that MT is not a requirement for this process.

To further investigate the distribution of zinc, $CD4^+$ T cells were removed from inducing conditions on Day +6. At this point, cells were proliferating but no longer being subjected to TcR mediated activation (1µg/mL plate bound anti-CD3 in the stimulation plate is degraded by day +6). Cells were spun down and resuspended in media alone (50% fresh media, 50% existing media) or media + plate bound anti-CD3 [5µg/mL] for 48 hours. Rested cells decreased their FSC/SSC properties, indicating they reduced their cell size but remained significantly larger than naïve $CD4^+$ T cells. Restimulated cells retained the lymphoblast phenotype. Both types of cells from both strains also retained the punctate zinc fluorescence pattern, indicating labile zinc remained, at least in part, in a compartmentalized state during naïve, lymphoblast, and effector cell differentiation states. Increased frequency of zinc containing vesicles has been reported to be polarized in T cells that have formed an immune synapse [7]. Interestingly, punctate fluorescent patterns also seemed to be polarized with punctate CD4 fluorescence in the majority of cells observed in our system. Given that clustering of immune receptors (including CD4) occurs during synapse formation, our data would support the finding that labile zinc-containing vesicles may localize to the immune synapse, where intracellular labile zinc has been observed to play an important role in modulating TcR inducing signaling.

3.6 Activation of p38 MAPK

The influence of zinc and the regulation of its availability during cell signaling is of particular importance in T cell activation. Previous work has described the influence of increases in free zinc inhibiting intracellular T cell phosphatases including SHP-1 [7], PTP1b [249], calcinuerin[15], phosphatase and tensin homolog deleted on chromosome 10 (PTEN)[222] and the dual specificity phosphatase MAP Kinase Phosphatase 1 (MKP-1)[13] which dephosphorylates the ERK1/2 and p38. MAPK pathways are of particular importance in T cell differentiation fate decisions and inhibiting or activating different MAPKs can "push" cells towards different effector phenotypes[250] including TH1[251], TH2[252], TH17[253] depending on context. Activation of p38 is also important in IL-10 expression [254]and Treg effector function[255,256]. Of the MAPK family of proteins, p38 is the most sensitive to changes in intracellular zinc[13] in human T cells.

To verify that zinc mediated activation of p38 is conserved in mice, we investigated the activation of p38 in mouse $CD4^+$ T cells from C57BL/6 (MT-WT) mice (Figure 3.12). p38 is activated by phosphorylation by MKK3/6 and inactivated by dephosphorylation by MKP-1. In resting naïve $CD4^+$ splenocytes, a baseline activation of p38 (p-p38) can be detected. Chelation of intracellular zinc with TPEN decreases the activation of p38. Increasing intracellular labile [Zn^{2+}] by increasing extracellular [Zn^{2+}] and adding the ionophore pyrithione significantly increases p38 activation. This was confirmed by western blot (3.12A) and flow cytometry (3.12 B and C). In the context of T cell activation, the diacyl glycerol analog PMA has been shown to activate protein kinase C (PKC) and p38 MAPK independent of TcR mediated signaling through LcK or

LAT[257]. To confirm this activation in mice, naïve mouse splenocytes from MT-WT or MT-KO mice were activated with PMA (100ng/mL) for 60 min. At determined time points, cells were fixed and stained for $CD4^+$ before being permeabilized and stained for activated p38 (p-p38). As expected, p38 is activated in a time dependent manner by PMA, with a peak activation at 15 minutes. After 60 minutes of treatment, activated p38 levels were significantly lower than starting levels. Interestingly, the activation of p38 in $CD4^+$ splenocytes from MT-WT mice was higher than MT-KO mice. Because p38 activation is sensitive to zinc concentration and intracellular Zn is increased in naïve $CD4^+$ T cells following stimulation by PMA[194], we hypothesize that the difference in p38 activation may be dependent on differences in intracellular Zn mediated by MT. We will address this hypothesis more thoroughly in Chapter 5.

3.7 Conclusions

The measurement of intracellular labile $[Zn^{2+}]$ within physiologically relevant parameters in live cells is an important tool for understanding the role of zinc in the regulation of T cell signaling. The use of Fluozin-3 and the zinc specific chelator TPEN and ionophore pyrithione allows the extrapolation of the intracellular concentration and comparison of data between experiments and between investigators. To avoid the measurement of intracellular labile $[Zn^{2+}]$ affecting the concentration itself, it is important to optimize experimental parameters to minimize the effect of the sensor or the manipulation of cells during preparation and measurement. An experimental protocol that is optimized through careful titration and iteration is an important first step in the experimental measurement of intracellular labile $[Zn^{2+}]$ in mouse $CD4^+$ lymphocytes.

The parameters described above allow for the detection of subtle changes in intracellular labile [Zn^{2+}] while permitting the immunophenotyping of different cell populations.

Resting levels of intracellular labile [Zn^{2+}] vary between $CD8^+$, $CD4^+$ and $CD19^+$ lymphocyte populations. Interestingly these three populations also load and export the Fluzoin-3 sensor differently, as evidenced by Fmax signal differences between cell types. However, because the determination of intracellular labile [Zn^{2+}] is relatively independent of sensor concentration, this differential loading does not interfere with the intracellular labile [Zn^{2+}] measurement. The fact that no significant differences in intracellular labile [Zn^{2+}] exist between lymphocyte subsets from MT-KO, MT-WT or MT-TGN mice suggests that under normal, resting conditions zinc homeostasis in lymphocytes is primarily maintained by MT independent mechanisms. Furthermore, the low expression levels of MT in naïve lymphocytes are unlikely to have an effect on total intracellular labile [Zn^{2+}]. Only under conditions of induction does MT in lymphocytes appear to play a significant role. This is in line with other studies of MT mediated immunomodulation where MT is considered to be a stress response protein and phenotypic differences between strains of mice with disparate MT gene doses is only revealed after stressful challenge.

This observation was supported by confocal images that did not show differences in intracellular labile zinc distribution between strains. The presence of zinc containing vesicles in $CD4^+$ T cells from both MT-KO and MT-WT mice, in all stages of cellular activation (naïve, lymphoblast, effector) indicate that cellular zinc is maintained in a non-steady state with both zinc muffling and buffering contributing to the dynamic control of

zinc availability. The small differences in zinc availability afforded by MT may be enough to affect intracellular phosphatase activity and the regulation of p38 MAPK. Alternatively, the small pool of available MT in naïve lymphocytes may affect the kinetics of zinc regulation by facilitating the transfer of Zn to apoproteins more effectively than can be accomplished by the free ion alone. p38 MAPK is centrally involved in T cell activation and the control of T cell effector function and is very sensitive to intracellular labile [Zn^{2+}], even in the absence of other cellular activators. The reduced activation of p38 MAPK in cells lacking functional *MT1* and *MT2* genes following stimulation of $CD4^+$ T cells with PMA suggests that MT plays a role in modulating T cell signaling, potentially by regulating intracellular zinc.

Adding to the complexity of measuring intracellular Zn is the importance of controlling for oxidative stress and extracellular zinc concentration during all steps of cell isolation, culture, and measurement. The close relationship between intracellular redox status and Zn^{2+} concentration and the role of MT in modulating this intersection is the focus of the research described hereafter. It therefore follows that carefully controlling experimental conditions involving redox and Zn is fundamentally important for allowing MT mediated differences in T cell signaling to be measured.

Figure 3.1 Regulation of Protein Function by Intracellular Zn Fluctuations

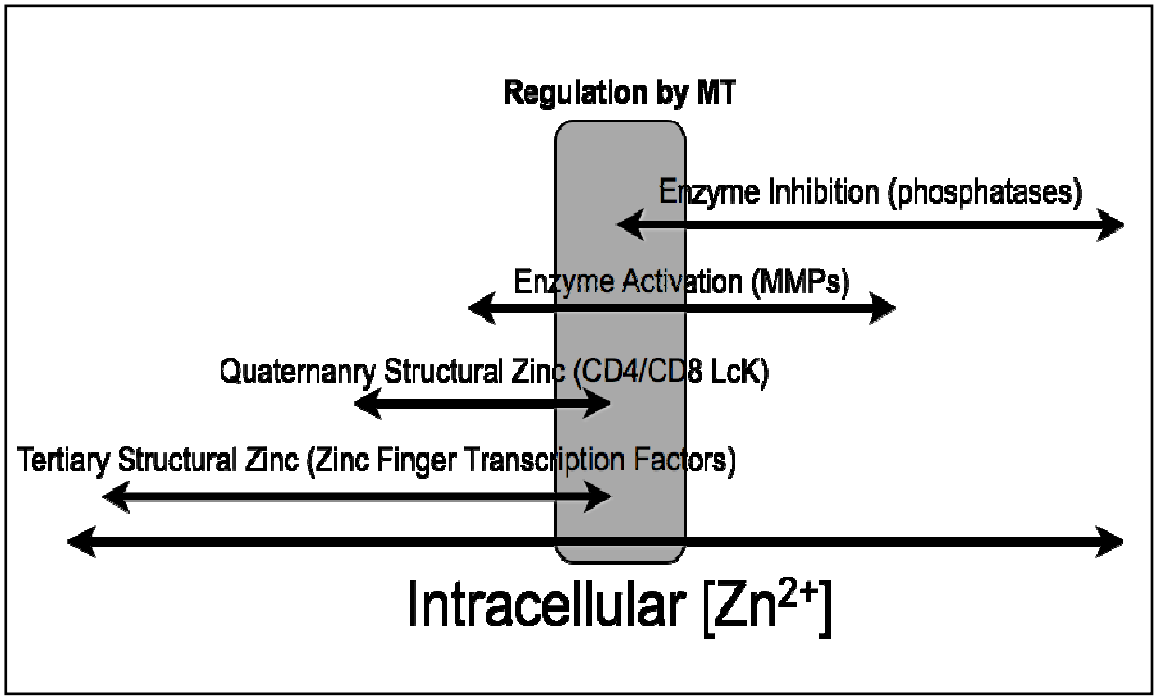

Different classes of enzymes and signaling proteins are differentially regulated by zinc based on affinity for the metal (Kd) and on/off rates (K on/off). The control of intracellular [Zn^{2+}] by metallothionein includes potential regulation of important signaling enzymes including phosphatases.

Figure 3.2 Structure and Emission Spectrum of Fluozin-3

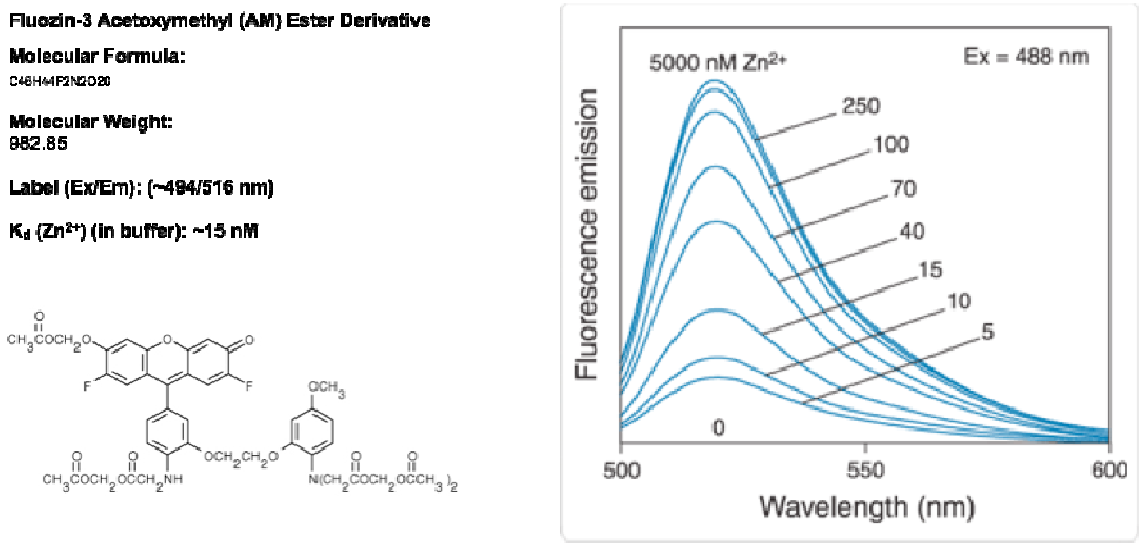

The structure, relevant specifications, and emission spectrum of the zinc specific fluorescent chemosensor Fluozin-3 AM. Figure adapted from website : http://www.lifetechnologies.com/order/catalog/product/F24195

Figure 3.3 Measurement of Intracellular [Zn^{2+}] in $CD4^+$ T Cells with Fluozin-3 AM

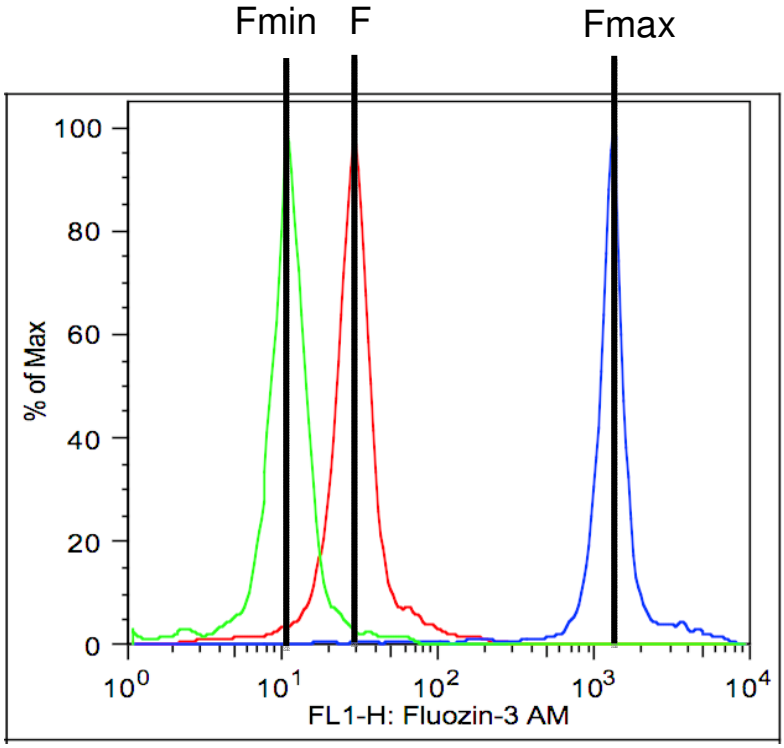

Peripheral blood mononuclear cells were freshly isolated from a C57BL/6 mouse. Cells were loaded with Fluozin-3 AM [0.5µM] and stained with anti-CD4alexafluor647 and propidium iodide. For the Fmin sample, cells were treated with TPEN [50µM] for 10 min on ice. For the Fmax sample, cells were treated with $ZnSO_4$ [100µM] / Pyrithione [50µM] for 10 min on ice. The Fluozin-3 signal for lymphocyte FSC/SSC, propidium iodide negative, $CD4^+$ cells are shown (Lines are representative and do not reflect the true geometric mean).

Figure 3.4 Effect of Fluozin-3 AM Incubation Concentration on Fluorescent Signal

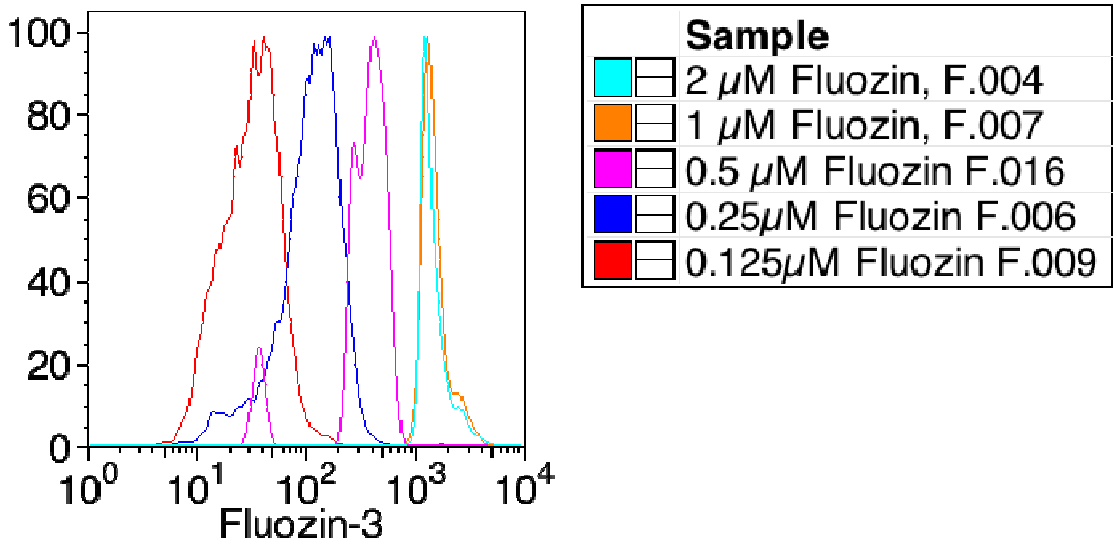

Freshly isolated PBMCs from a C57BL/6 mouse were incubated with different concentrations of Fluozin-3 AM in complete media for 30 min. Cells were then incubated without sensor for 30 min and stained with anti-CD4 alexafluor647 and propidium iodide. Lymphocyte FSC/SSC, PI negative, $CD4^+$ cells were gated and the effect of probe incubation concentration on the fluorescent signal in these cells is shown.

Figure 3.5 Relationship between Fluozin-3 Fluorescence and Extracellular $ZnSO_4$ with or without pyrithione

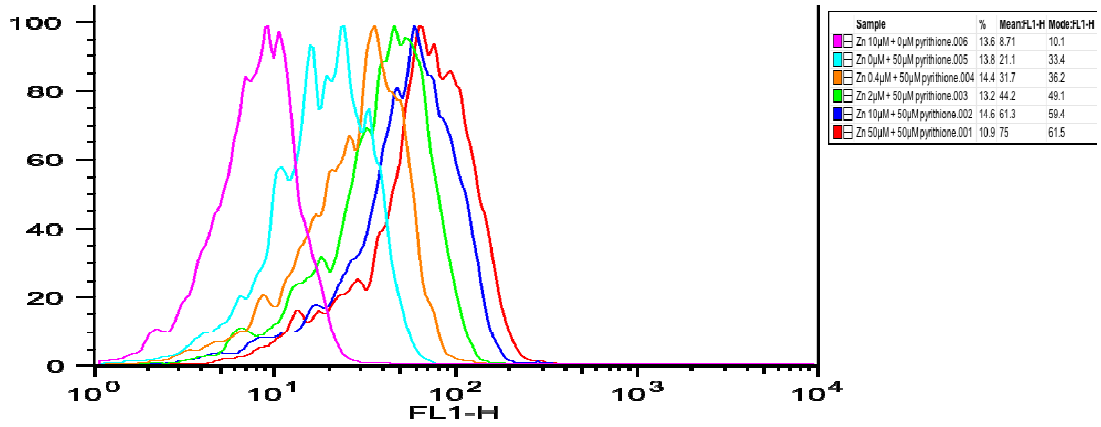

Mouse PBMCs were isolated by Histopaque1083 centrifugation and loaded with 0.5µM Fluozin-3AM. Cells were then treated with 50µM pyrithione (or control) and varying $ZnSO_4$ concentrations (0-50µM) in PBS + 1% FBS at 37C for 30 min. Cells were stained with anti-CD4 alexafluor647 and propidium iodide. Lymphocyte FSC/SSC, PI negative, $CD4^+$ cells were gated and the effect extracellular Zn or pyrithione on Fluozin-3 fluorescence was determined.

Figure 3.6 Effect of MT Gene Dose on Intracellular [Zn^{2+}] in Resting Lymphocyte Populations

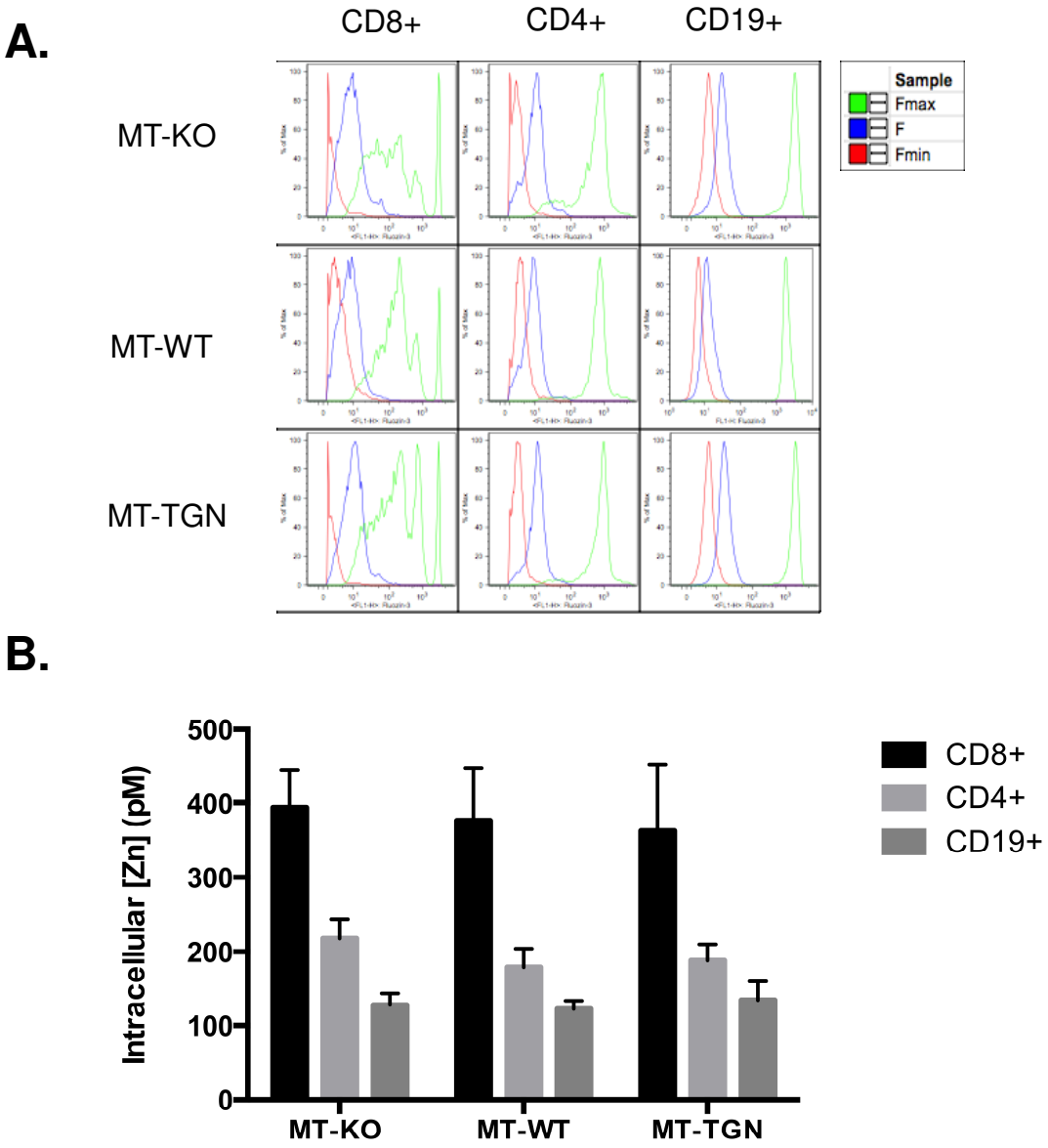

Freshly isolated PBMCs from C57BL/6 mice (MT-WT, n=4) or congenic strains that don't express MT (MT-KO, n=4) or overexpress MT (MT-TGN, n=4) were incubated with Fluozin-3 AM in complete media for 30 min as described in materials and methods. Cells were stained with anti-CD8 PerCP, anti-CD4 alexafluor647 or anti-CD19PE and propidium iodide. Lymphocyte FSC/SSC, PI negative cells, lymphocyte marker+ cells were gated and the Fmin, Fmax and F cell populations for one representative mouse from each genotype/cell type are shown in A. Intracellular [Zn^{2+}] was determined for each genotype / cell type. Bars indicate mean intracellular [Zn^{2+}]. Error bars indicate standard deviation.

Figure 3.7 Metallothionein Knockout Genotype is associated with decreased total serum zinc

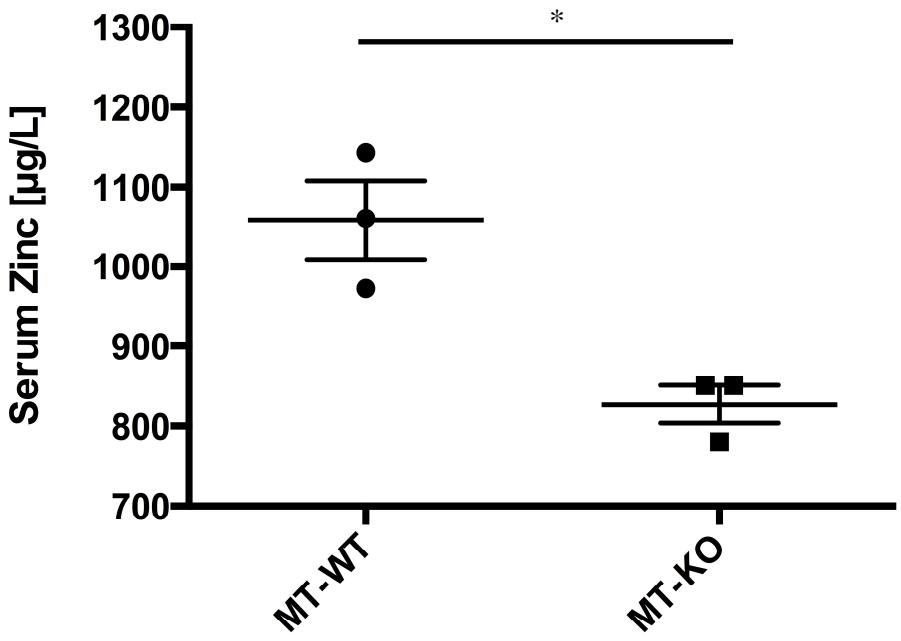

Serum was isolated by centrifugation from pre-clotted blood taken by sub-mandibular bleed from MT-WT or MT-KO mice (n=3). Total serum zinc was quantified using an Elan DRC (dynamic reaction cell) II quadrupole ICP-MS (inductively coupled plasma – mass spectrometer). Statistical significance was determined using a student's two-tailed T test. (*p<.05)

Figure 3.8 MT Gene Dose Does Not Affect Intracellular Labile [Zn^{2+}] in $CD4^+$ Splenocytes

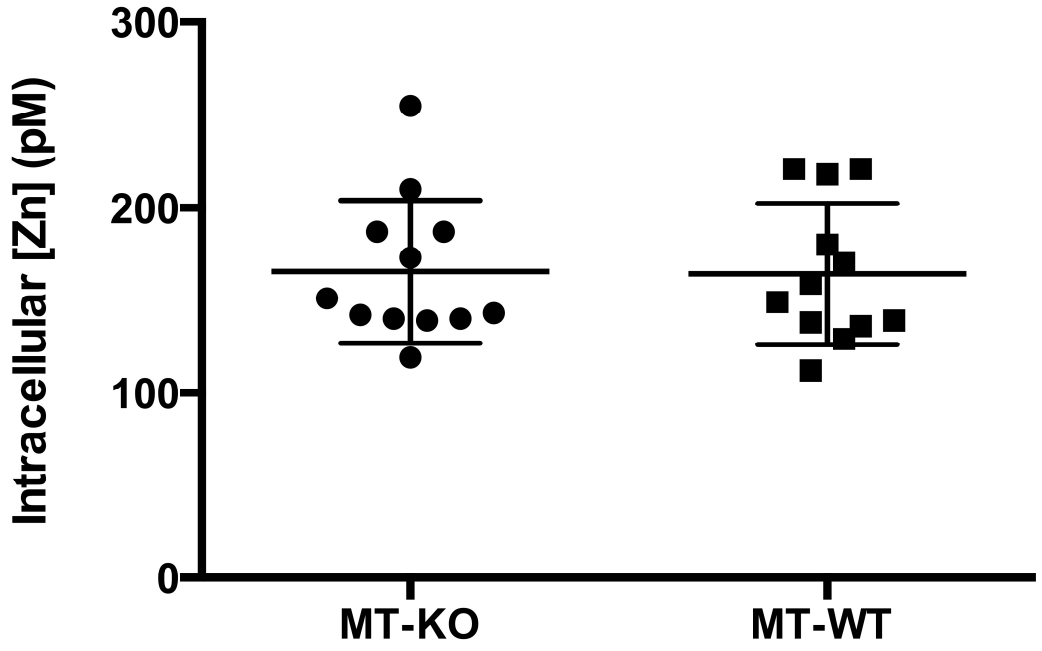

Intracellular labile [Zn^{2+}] was measured from freshly isolated $CD4^+$ splenocytes from MT-WT (n=12) or MT-KO mice (n=12) on four different days. Cells were loaded with Fluozin-3 AM as previously described. $CD4^+$ T cells were labeled with an alexafluor647 conjugated antibody to avoid the need for fluorescent compensation. Each point represents a different mouse.

Figure 3.9 Intracellular [Zn^{2+}] and Homeostatic Mechanisms are Affected by Extracellular Zn and 2-Mercaptoethanol in $CD4^+$ T cells

A.

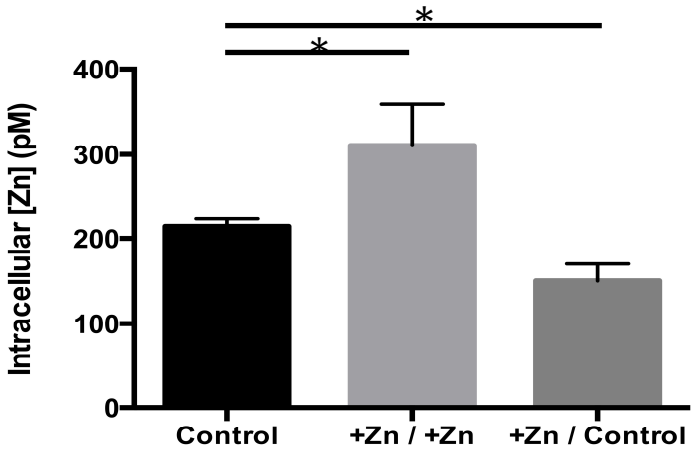

B.

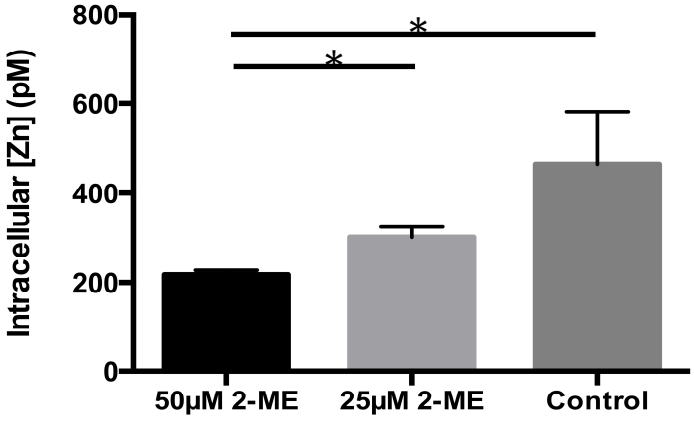

Splenocytes were isolated from C57BL/6 mice (n=3). (A) Cells were cultured in media containing 10% FBS (Control) or media with 125µM added $ZnSO_4$ for 24 hours. Zinc treated cells were loaded with Fluozin-3 AM and incubated for 30 min in media with added Zn (+Zn/+Zn) or control media (+Zn/ Control) while Control cells were kept in control media for the duration of the experiment. (B) Cells were cultured in standard cell culture media (50µM 2-ME) or media with reduced antioxidant (25µM 2-ME) or no antioxidant (Control) for 24 hours before intracellular [Zn^{2+}] was measured. Bars indicate mean of 3 separate experiments. Error bars indicate standard deviation. * ($p<.05$)

Figure 3.10 Extracellular Zn Induces Expression of Metallothionein in $CD4^+$ T Cells

A.

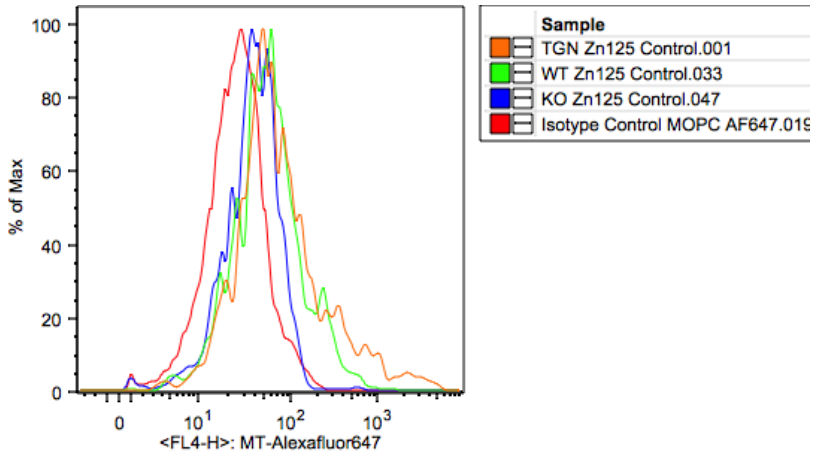

B.

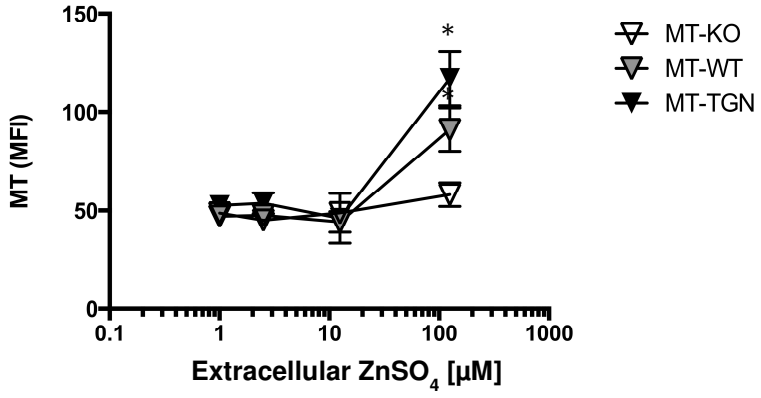

Freshly isolated splenocytes from MT-KO mice (n=3), MT-TGN mice (n=3) or MT-WT (n=3) wildtype congenic control mice were cultured in media with added $ZnSO_4$ (1-125µM) for 24 hours. Cells were fixed and permeabilized and stained for $CD4^+$ surface marker and intracellular MT using an alexafluor647 labeled anti-MT antibody (UC1MT) or isotype control (MOPC, red line. Expression of MT after 125µM $ZnSO_4$ is shown in Figure A for one representative mouse from each strain. Triangles represent mean MT MFI from 3 mice for each strain. Error bars indicate standard deviation. (*) indicates mean is significantly higher than baseline (1µM $ZnSO_4$) ($p<.05$)

Figure 3.11 Imaging Sub-Cellular Localization of Zinc in CD4$^+$ T cells from MT-KO and MT-WT Mice

A. Day 0

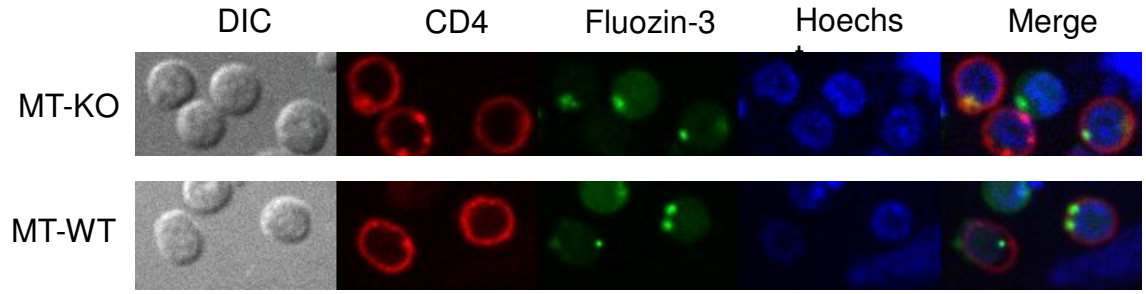

B. Day +6 (anti-CD3/anti-CD28 stimulation + IL-27)

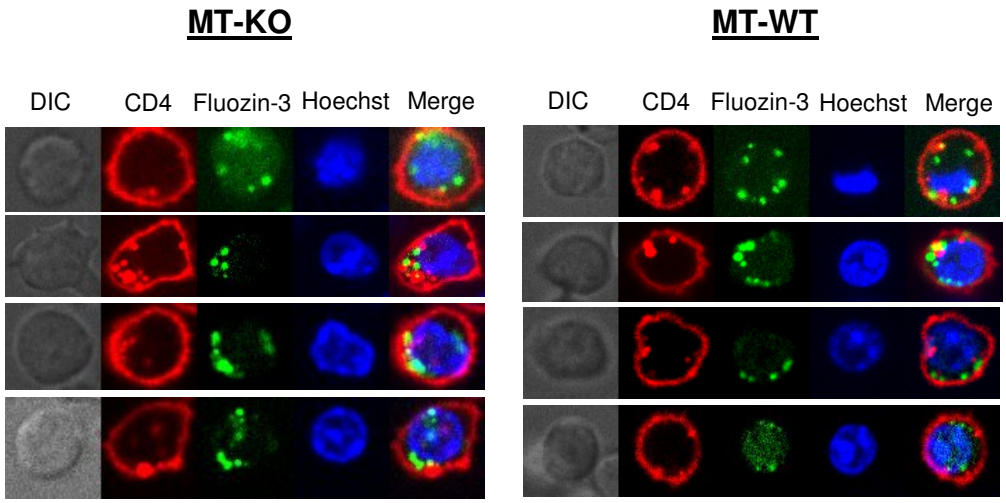

C. Day +8 (+6 days Stimulation, +2 Days Rested/Restimulated)

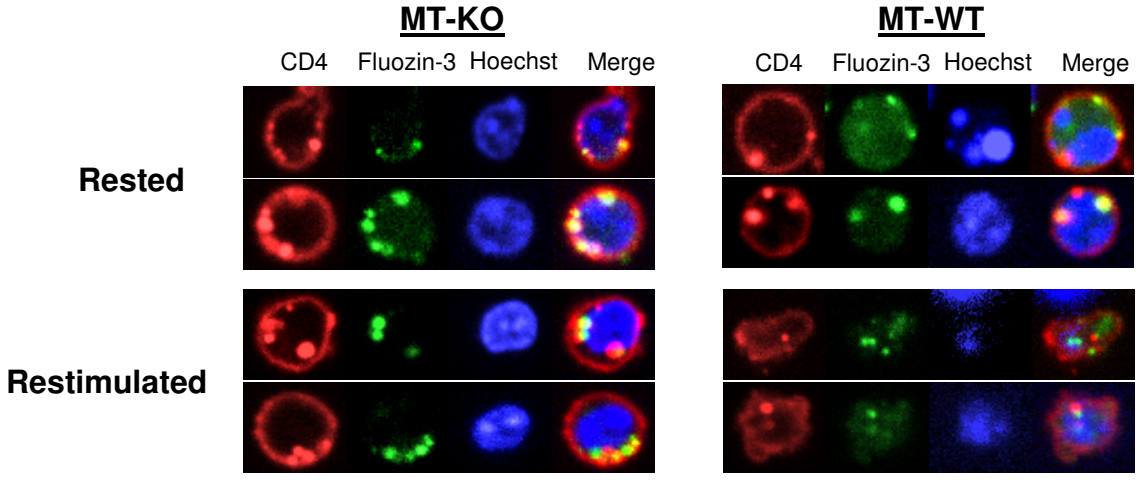

Splenocytes were isolated from MT-WT (n=4) or MT-KO (n=4) mice and stimulated under Tr1 inducing conditions for 6 days. Cells were then removed and rested in media alone or restimulated with anti-CD3 for an additional 2 days. (A). Freshly isolated splenocytes were stained for with anti-CD4 (red), and loaded with Hoechst stain (blue) and Fluozin-3 AM (green). Cells were then imaged by confocal microscopy. One representative field of view is shown for one mouse from each strain. (B) After activation and proliferation, cells were removed and stained as described for Day 0. One representative cell from each mouse (n=4) from each strain is shown. (C) At day 6, cells were either rested for 2 additional days in media alone or restimulated with anti-CD3. On day 8, cells were stained and loaded as described above. One representative field from 2 mice are shown for each condition / genotype.

3.12 Activation of p38 MAPK by Zinc or PMA

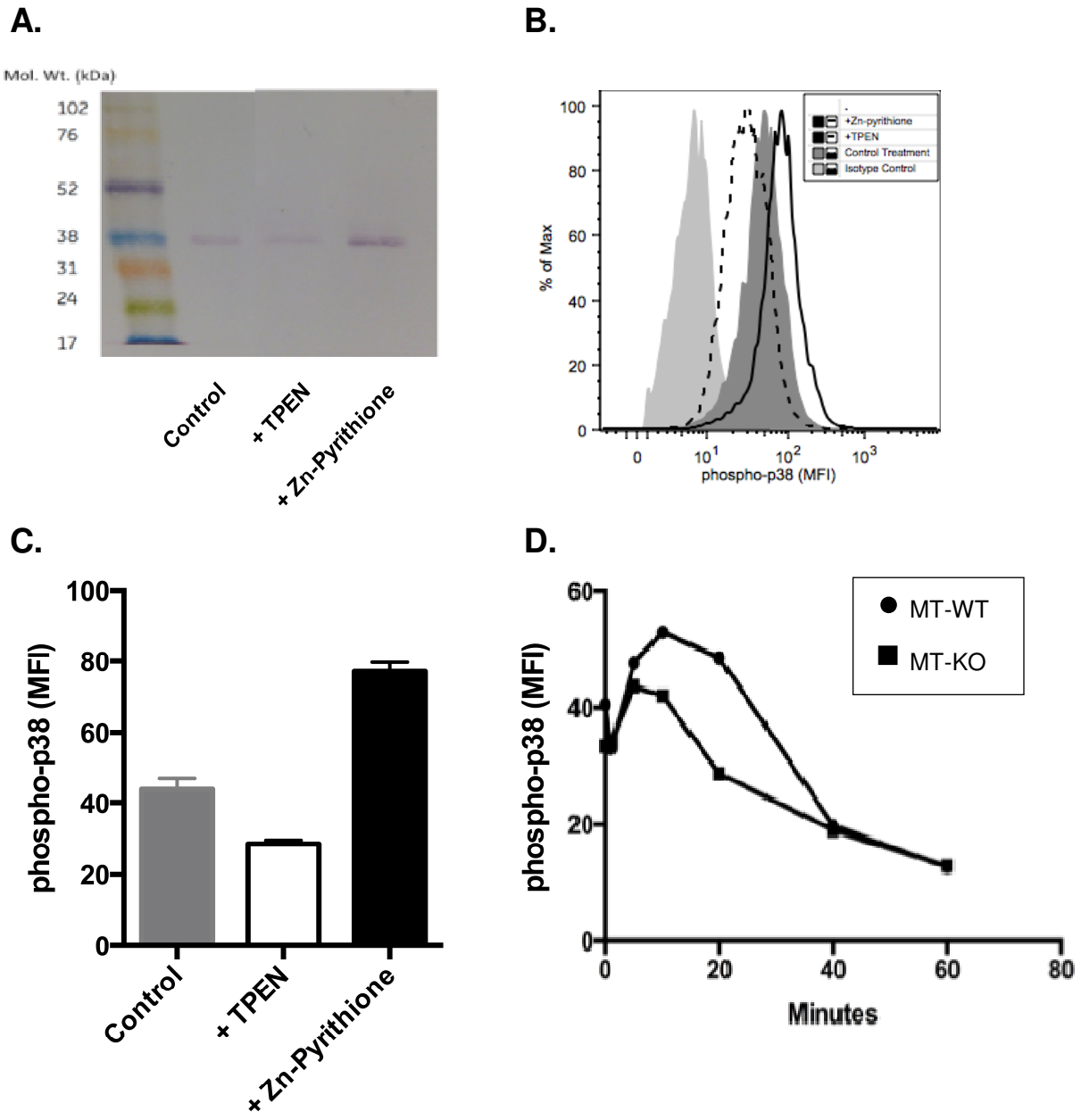

Naïve splenocytes were isolated from MT-WT (n=1) or MT-KO mice (n=1). Cells were exposed to 20µM TPEN or 100µM $ZnSO_4$ / 50µM pyrithione for 20 minutes before being lysed in buffer containing phosphatase inhibitors. Cell lysates were separated by SDS-PAGE and blotted for the presence of phospho-p38 (A). Alternatively, cells were fixed with paraformaldehyde after 20 min exposure and stained for CD4. Cells were then permeabilized and stained with anti-phospho-p38 or isotype control (B and C) and analyzed by flow cytometry. (D) To determine if PMA [100ng/mL] affects p38 activation, cells were stimulated before fixation and phospho-p38 was quantified in $CD4^+$ T cells by flow cytometry.

Chapter 4

Effect of MT Gene Dose on Primary $CD4^+$ T Cell Activation *in vitro*

4.1 Introduction

An increase in intracellular $[Zn^{2+}]$ [235] and metallothionein (MT) expression[35,36] are two measurable phenotypic changes that occur during the activation, proliferation and differentiation of naïve $CD4^+$ T cells. Manipulation of MT expression in $CD4^+$ T cells using genetic knockout/overexpressing mutants, or siRNA knockdown or knock-in,[5] affects signaling pathways and downstream effector function but the observations from different studies are often contradictory and inconclusive. For example, Huh *et* al reported restimulation of $CD4^+$ T cells from MT-WT mice (129S1/SvImJ) resulted in higher levels of secreted IL-10 than cells isolated from MT-KO congentic controls (129S7/SvEvBrd-$Mt1^{tm1Bri}Mt2^{tm1Bri}$) (following differentiation for 5-6 days under TH0 promoting conditions (plate bound anti-CD3 [10µg/mL] / soluble anti-CD28 [2µg/mL] [2]). Alternatively, Wu *et al* observed no IL-10 secretion from $CD4^+$ T cells differentiated under similar TH0 inducing conditions (plate bound anti-CD3 [1µg/mL] / soluble anti-CD28 [1µg/mL] from either MT-WT or MT-KO mice. However, addition of IL-27 promoted a Tr1 phenotype in $CD4^+$ T cells from both strains in their experiments, with MT-KO cells producing significantly more IL-10[5].

The body of research on the influence of intracellular $[Zn^{2+}]$ on T cell differentiation is also inconclusive. As discussed previously, much of the early work

involving metal influences on immune functions employed models of complete zinc chelation or addition of a 50 fold excess *in vitro* or *in vivo* which makes interpretation of biologically relevant influences of zinc within the normal, healthy range of fluctuation difficult. Recently, with the use of more sensitive zinc probes including Fluozin-3 AM, the effect of smaller changes in intracellular labile [Zn^{2+}] have been explored. In general, increased [Zn^{2+}] is associated with increased proliferative capacity[7] and increased signaling and expression of IL-2[8,222] and IFN-gamma[15]. However, these effects are still context specific and the role of zinc in T cell activation appears to be more nuanced than a simple positive correlation between [Zn^{2+}] and proliferation and TH1 differentiation.

To date there is no published study that carefully and systematically characterizes the changes in intracellular labile [Zn^{2+}] during naïve $CD4^+$ T cell activation through proliferation and effector differentiation. Our first specific aim is to test the hypothesis that MT gene dose affects intracellular labile [Zn^{2+}] during naïve $CD4^+$ T cell activation. This will be addressed by stimulating naïve splenocytes from MT-WT or MT-KO mice for 6 days with plate bound anti-CD3 and soluble anti-CD28 antibodies in the presence or absence of IL-27. The intracellular labile [Zn^{2+}], MT expression, and presence of the surface marker of activation (CD25a) will be assessed by flow cytometry every 24 hours to assess differences between strains and inducing conditions. After establishing the expression of MT, our second specific aim is to test the hypothesis that MT provides a redox sensitive mobilizable zinc pool in activated $CD4^+$ T cells. This will be addressed by measuring the release of bound intracellular zinc upon exposure to hydrogen peroxide and comparing the rate and amount of zinc released in

$CD4^+$ T cells from MT-WT and MT-KO mice. To determine if differences in release of intracellular zinc are due to total redox buffering capacity, intracellular thiols and the oxidation of an ROS sensor will be measured in $CD4^+$ T cells from each strain.

4.2 Effect of the Cytokine Environment on Intracellular $[Zn^{2+}]$ and MT Expression During $CD4^+$ T Cell Primary Activation

Primary activation of $CD4^+$ T cells is believed to occur primarily in in the secondary lymphoid tissues following interaction with pathogen activated dendritic cells [158]. Recognition of the unique peptide/MHC complex on the surface of the antigen presenting cell (APC) occurs by dual recognition and the strength of this interaction affects T cell signaling[258]. For T cell activation to proceed to proliferation rather than cell death, co-activation through expression of B7 on the APC signaling through CD28 on the T cell is a requirement[259]. To model these interactions *in vitro*, antibodies against molecular components associated with TcR (CD3) and CD28 are employed. Successful activation of T cells requires polarization of the TcRs and associated co-activating receptors to a single region of high density, often referred to as the immune synapse. This is replicated by the interface of the T cell and the plate bound anti-CD3 antibody. The bivalent nature of antibodies allows subsequent crosslinking of CD28 by anti-CD28[260].

The choice of concentrations of anti-CD3 and anti-CD28 are important when studying T cell signaling. Higher concentrations can overstimulate cells, leading to cell

death while lower concentrations can lead to insufficient levels of activation and proliferation. The choice of 1µg/mL anti-CD3 and anti-CD28 for activation of T cells *in vitro* in the following study was based on previous studies that revealed an effect of MT gene dose on T cell activation[5] and titration in the lab to assess the relationship between antibody concentration and cell proliferation (data not shown). The reasoning behind this choice of conditions was based on the risk of higher concentrations of antibody potentially masking differences in MT mediated effects by overstimulating cells and lower concentrations resulting in sub-optimal activation.

In addition to stimulation through the TcR and CD28, $CD4^+$ T cells receive signals about the status of their extracellular environment through cytokine receptors. As discussed in the introduction (1.2.2), integration of all three signals leads to a choice of T cell differentiation fate. Of particular interest is signaling through IL-27, which induces MT expression and results in a Type 1 regulatory T cell effector phenotype (Tr1).

Induction of the Tr1 phenotype via anti-CD3/anti-CD28 activation and addition of exogenous IL-27 [50ng/mL] was compared with induction of the TH0 T cell phenotype via activation through anti-CD3/anti-CD28 stimulation alone. Under both conditions, expression of the activation marker CD25a (high affinity receptor for IL-2) was increased within 24 hours and >95% of $CD4^+$ T cells were CD25+ after 5 days, indicating $CD4^+$ T cell activation is not delayed under TH0 conditions. (Figure 4.1A, 4.1B)) The increase in intracellular $[Zn^{2+}]$, however, is delayed under TH0 inducing conditions and is not significantly increased above naïve baseline concentration until day 6 (Figure 4.1C). This is in contrast to Tr1 inducing conditions where intracellular labile $[Zn^{2+}]$ was

significantly higher after day 4 and remained significantly higher than THO conditions through day 6.

Expression of MT following $CD4^+$ T cell activation has been reported for different stimulation conditions including concanavalin A[35], super antigen loaded APCs [36] and anti-CD3/ anti-CD28 [5,36]. To avoid confounding effects of post-transcriptional regulation of *MT* mRNA, we choose to verify the expression of MT by immunohistochemistry and flow cytometry. Similar to intracellular labile $[Zn^{2+}]$, MT expression was significantly higher by day 3 under Tr1 conditions (Figure 4.1E). Interestingly, the increase in intracellular MT preceded the increase in intracellular $[Zn^{2+}]$, indicating MT induction is not dependent on increased $[Zn^{2+}]$. However, the largest increases in MT and $[Zn^{2+}]$ under both inducing conditions appeared on day 6, suggesting a potential induction of MT when $[Zn^{2+}]$ reaches a certain threshold, similar to what was seen by MT induction in naïve $CD4^+$ T cells following addition of extracellular $ZnSO_4$ to the culture media (Figure 3.10). Interestingly, intracellular $[Zn^{2+}]$ was not higher in all Tr1 cells compared with TH0 cells, indicated by the considerable overlap of the distribution of Fluzoin-3 fluorescence (Figure 4.1D). This wide distribution of intracellular $[Zn^{2+}]$ illustrates the heterogeneity of the $CD4^+$ T cell population, even when all cells are stimulated under the same conditions.

The effect of IL-27 on the intracellular $[Zn^{2+}]$ and MT expression in $CD4^+$ T cells demonstrates that both of these parameters are potential points of regulation by cytokine signaling during activation. The expression of MT in the IL-27 treated cultures before a detectable increase in intracellular $[Zn^{2+}]$ suggests that MT may be induced by metal independent mechanisms. IL-27 is associated with pro-inflammatory effects[261] in

inflammatory autoimmune arthritis and may induce MT via pathways that are similar to pro-inflammatory IL-6. MT induction was not completely independent of zinc, however, and maximal MT expression coincided with the highest observed concentration of intracellular [Zn] under both conditions, underscoring the strong and direct relationship between zinc, MTF-1, and MT expression. It is important to note that induction of MT by IL-27 and Zn was complimentary and produced a T cell phenotype with an increased pool of intracellular MT (Figure 4.1F). This difference has the potential to position Tr1 cells to respond differently to oxidative signaling upon further reactivation.

4.3 Effect of MT Gene Dose on Intracellular [Zn^{2+}] and MT Expression During $CD4^+$ T Cell Primary Activation

Upon establishing the increase in intracellular [Zn^{2+}] and intracellular MT expression following activation of $CD4^+$ T cells, the effect of MT gene dose on intracellular [Zn^{2+}] was determined. Intracellular [Zn^{2+}] in MT knockout mice (MT-KO) and MT-WT congenic controls were compared during naïve $CD4^+$ T cell activation under Tr1 inducing conditions described above. Mice lacking functional *MT1* and *MT2* genes displayed the same pattern of activation as wildtype controls including increased FSC/SSC and CD25 expression (Figure 4.2A). Furthermore, there were no differences in the intracellular [Zn^{2+}] between the strains at any of the timepoints tested (Figure 4.2D), indicating MT did not significantly affect zinc homeostasis under these culture conditions. The expression of MT was verified by intracellular immunofluorescence (Figure 4.2C). In the MT-KO cells, the expression of non-functional truncated MT peptides is under the same transcriptional control as native *MT1* and *MT2* genes, and is

significantly increased by day 3. This supports the previous observation that MT is induced by IL-27 independently of zinc and this expression can be measured by day 3 after activation.

Ultimately, the intracellular labile [Zn^{2+}] in $CD4^+$ T cells associates very strongly with the developmental state ($p<.001$) (Figure 4.3) of the cells. When cells are removed from activation conditions and rested for an additional 48 hours, both the intracellular [Zn^{2+}] and MT expression decrease but remain significantly above levels seen in naïve cells. The observation that MT expression parallels intracellular Zn increases is expected given the established nature of Zn mediated regulation of MT. The observation that MT gene dose did not affect intracellular [Zn^{2+}] during primary activation implies that regulation of intracellular [Zn^{2+}] is controlled primarily by mechanisms that are independent of MT. However, the mechanisms underlying primary and secondary activation of T cells are fundamentally different. During secondary activation, effector T cells respond much more quickly to stimulation than naïve cells. Effector cells also require a lower threshold for stimulation and respond with intracellular redox signaling cascades (through the generation of ROS and RNS) that are more robust than those seen during primary activation. Taken together, this data suggests that MT does not play a significant role in affecting the ability of naïve $CD4^+$ T cells to become activated, develop into a lymphoblast phenotype, increase intracellular [Zn^{2+}] , or proliferate.

4.4 Effect of MT Gene Dose on Redox Mobilizable Intracellular Labile Zinc Pool

The increased intracellular pool of Zn-MT in the Tr1 phenotype provides a potential reservoir of redox mobilizable labile Zn. To assess whether this zinc pool could be released and affect intracellular labile [Zn^{2+}] in response to ROS, extracellular H_2O_2, as prototype oxidant, was added to Tr1 induced $CD4^+$ T cells loaded with Fluozin-3. Addition of H_2O_2 increased intracellular [Zn^{2+}] in a dose dependent manner over a period of 8 minutes (Figure 4.4A). This increase was unaffected by increased extracellular Zn during the time tested (data not shown), indicating the increased intracellular [Zn^{2+}] was not due to increased zinc influx. Additionally, H_2O_2 had no affect on the fluorescence of Fluozin-3 under the conditions tested based on Fmax measurements (data not shown.) The H_2O_2 induced release of Zn2+ was significantly greater in Tr1 cells from MT-WT mice compared with cells from MT-KO mice (Figure 4.4B). The effect of MT gene dose was significant for both the total increase in intracellular [Zn^{2+}] (Figure 4.4 C) and the fold increase when compared with baseline [Zn^{2+}] (Figure 4.4D) for the range of H_2O_2 tested. In addition to the differences in the total amount of zinc released, the rate of release (V_0) following initial exposure to H_2O_2 was greater in cells expressing MT (Figure 4.4E) for each of the concentrations tested. Taken together, this evidence supports previous observations that MT is preferentially oxidized in the presence of H_2O_2 compared with other Zn bound proteins[21]. It is important to note that cells were incubated in media containing 10% FBS (with no 2-ME) during oxidative release of Zn which acts as a buffer to reduce the concentration of H_2O_2 and subsequent oxidative stress experienced by the cells. This was necessary to avoid the confounding effects of decreasing intracellular [Zn^{2+}] when cells are moved from a normal [Zn^{2+}] (3µM) to a low

zinc environment (Figure 3.9A). This means that the intracellular release of zinc in response to extracellular oxidant is even more sensitive than the figures suggest.

To determine if the source of the released zinc was primarily reduced thiols, Tr1 cells from MT-WT and MT-KO mice were treated with the thiol specific oxidant DTDP [50µM] and the release of labile Zn2+ was monitored by measuring Fluozin-3 fluorescence. After 3 min of DTDP exposure, the increase in intracellular [Zn^{2+}] was significantly greater in cells that expressed MT (Figure 4.4F). The robust release of Zn upon oxidant exposure in cells that don't express functional MT indicates that MT is not the only redox sensitive mobilizable pool of intracellular Zn. However, the presence of Zn-MT ensures a greater increase in intracellular Zn following oxidant exposure and a more efficient transformation of an oxidant signal into Zn signal. The MT specific 0.3nM intracellular [Zn^{2+}] increase following exposure to 40µM H_2O_2 has the potential to significantly inhibit the intracellular phosphatase activity [8,12] that contributes to activation of MAPKs and affects downstream events including cytokine secretion.

4.5 Effect of MT Gene Dose on Cellular Redox Buffering Capacity

The influence of MT expression on oxidant induced zinc release could be explained by the preferential oxidation of zinc-thiolate bonds in MT, or by an increased redox buffering capacity in MT-KO cells. Either scenario would likely result in an increased release of Zn from MT-WT cells in response to oxidant. To examine the latter possibility, total free thiols in Tr1 cells from MT-KO and MT-WT controls were determined by CPM assay using reduced glutathione as a reference[243]. The

concentration of free thiols was within the range of previously reported for C57BL/6 mice[240] and was not significantly different between MT-WT and MT-KO mice (Figure 4.5A). This suggests that the expression of MT did not significantly affect the total free thiol status of the cell. This is not unexpected, given that reduced glutathione (GSH) is considered the primary intracellular redox buffer and is found in 100,000 fold molar excess compared with MT in T cells.

To determine if MT gene dose contributed to a difference in redox buffering capacity, MT-WT and MT-KO cells were loaded with CM-H_2DCFDA and exposed to 50µM H_2O_2 for 1 hour. This dye is sensitive to oxidation by different species of ROS including superoxide, hydrogen peroxide and peroxynitrite and is a good general indicator of oxidative stress[262]. MT gene dose did not significantly contribute to a difference in the total redox buffering capacity, evidenced by a similar level of oxidation of the fluorescent probe upon exposure to extracellular H202 (Figure 4.5B). As indicated by the similar levels of total thiols, this observation supports the conclusion that $CD4^+$ T cells maintain redox homeostasis primarily through non-MT based thiols, most notably GSH. However, the oxidation of GSH to GSSG controls the release of zinc from MT [263]. For this reason, when MT is present in the free thiol pool, it significantly changes the zinc release potential in response to ROS, even in the presence of a significant molar excess of GSH.

4.6 Conclusions

In vitro stimulation of $CD4^+$ T cells with anti-CD3 and anti-CD28 results in a predictable and reproducible activation and differentiation pattern that includes

development of a lymphoblast phenotype during proliferation. This metabolically active phenotype maintains a significantly higher intracellular labile [Zn^{2+}] than naïve or effector cells and this increase is not affected by MT gene dose but is affected by the presence of IL-27. Zinc alone does not control T cell fate decisions, however, and the increased labile [Zn^{2+}] is likely part of a larger pattern of activation including transcription factor expression and chromatin remodeling. The significant difference in intracellular [Zn^{2+}] between Tr1 and TH0 inducing conditions implicates Zn as a potential regulatory mechanism for the differentiation of the Tr1 phenotype. This observation has not been reported previously. Furthermore, the intracellular signaling events that precede the Tr1 phenotype occur in an environment of increased zinc beginning 2 days before significant proliferation occurs. This is in contrast to TH0 development where intracellular [Zn^{2+}] is not significantly increased until proliferation begins.

MT expression in the context of $CD4^+$ T cell activation and proliferation appears to be controlled by zinc dependent and independent mechanisms. Increased MT is generally associated with cell proliferation, most likely through the increased cellular redox potential that accompanies increased cellular metabolism [123]. In $CD4^+$ T cell activation, an initial increase in MT expression precedes an increase in intracellular [Zn^{2+}] and did not occur without the addition of IL-27. This indicates MT is regulated prior to cell proliferation and lymphoblast development, potentially influencing fate decisions of $CD4^+$ T cells before they gain effector function. Indeed, MT is associated with increased Repressor of GATA (ROG) and decreased expression of Tbet[2] during T cell activation, both of which would be regulated during the activation window that overlaps with MT expression.

Following the significant increase in intracellular [Zn^{2+}] that occurs on day +6 post activation in Tr1 cells, MT expression is robust. The overlap of increased MT together with an increased [Zn^{2+}] means the pool of readily oxidizable thiols (MT) is larger and is more significantly saturated with zinc. At this point, $CD4^+$ T cells are poised to release zinc in response to an oxidant signal. Indeed, exposure of these cells to ROS resulted in significant release of thiol bound zinc and a consequent increase in the intracellular labile [Zn^{2+}]. Although this effect is not specific for MT, and is observed in MT-KO cells, the expression of MT results in a significantly faster and larger zinc increase. Furthermore, the presence of MT during cellular redox signaling would facilitate the transfer of zinc to apo-enzymes more efficiently than in a system without MT [79,121]. This would amplify the effect of MT on zinc mediated regulation of signaling pathways and suggests a mechanism where even low nanomolar concentrations of MT could have a significant impact on signaling through both kinetic and thermodynamic control of zinc availability.

In terms of global redox regulation, the expression of MT does not appear to significantly contribute to the total free thiol concentration or the general redox buffering capacity of $CD4^+$ T cells, even after its induction by IL-27 and increased intracellular [Zn^{2+}]. This observation implies MT mediated effects on T cell signaling are not accomplished through the dampening of ROS or RNS signals through reaction with MT, but rather through the control of zinc in response to these signals.

Figure 4.1 IL-27 affects intracellular [Zn^{2+}] and MT expression in $CD4^+$ T cell during primary activation

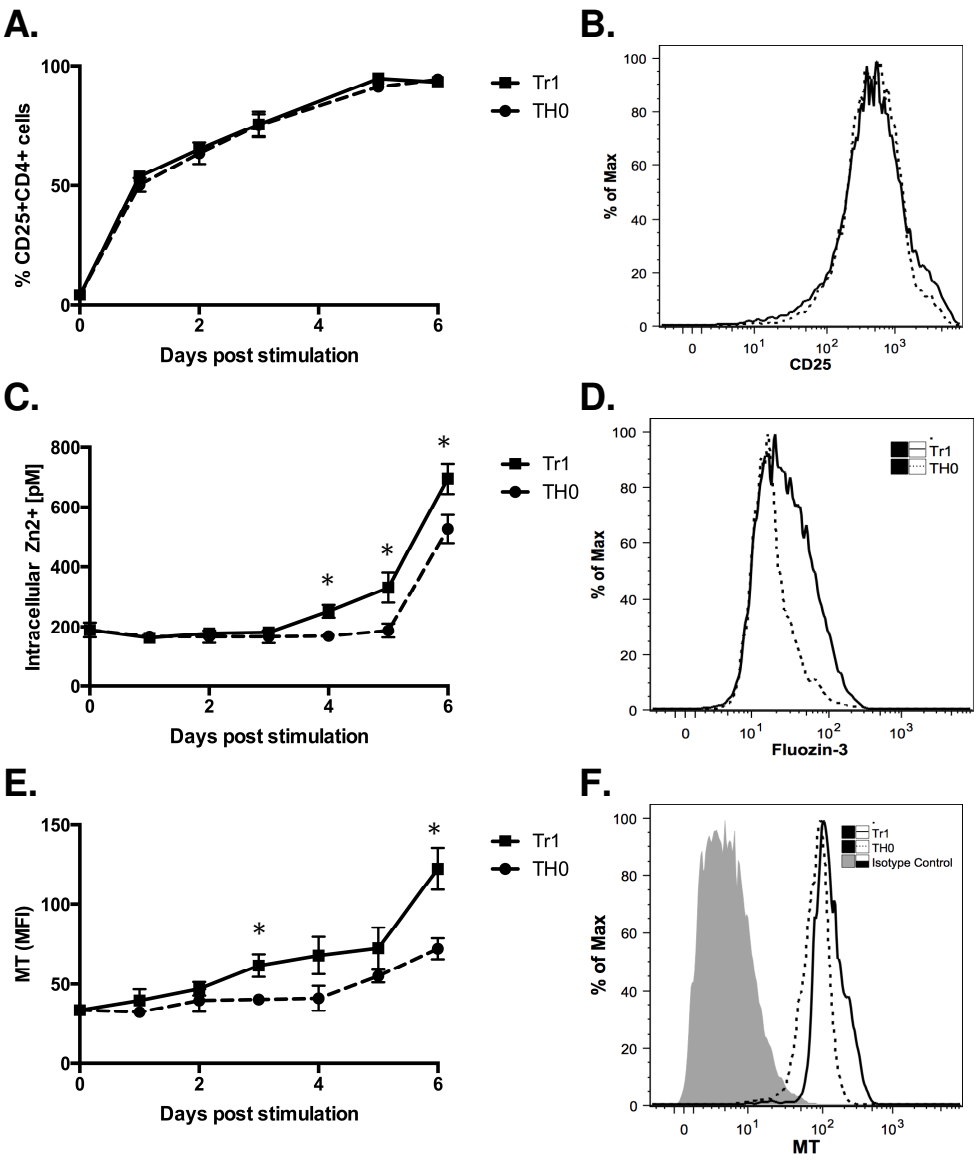

Mononuclear cells were isolated from spleens of C57BL/6 mice (n=7) and stimulated for 6 days in the presence of anti-CD3 and anti-CD28 with IL-27 (Tr1) or without cytokines (TH0). (A,B) Cell activation was monitored by measuring the frequency of CD25a expression within the $CD4^+$ cell population for 6 days. (C,D) Intracellular [Zn^{2+}] and (E,F) [MT] were measured from $CD4^+$ PI- cells every 24 hours for 6 days. Histograms are representative of 1 Tr1 and TH0 sample from day 6. Groups were analyzed by two-tailed T test followed by Bonferoni correction. *p<.05

Figure 4.2 Effect of MT Gene Dose on the Activation and Intracellular [Zn^{2+}] of $CD4^+$ T cells

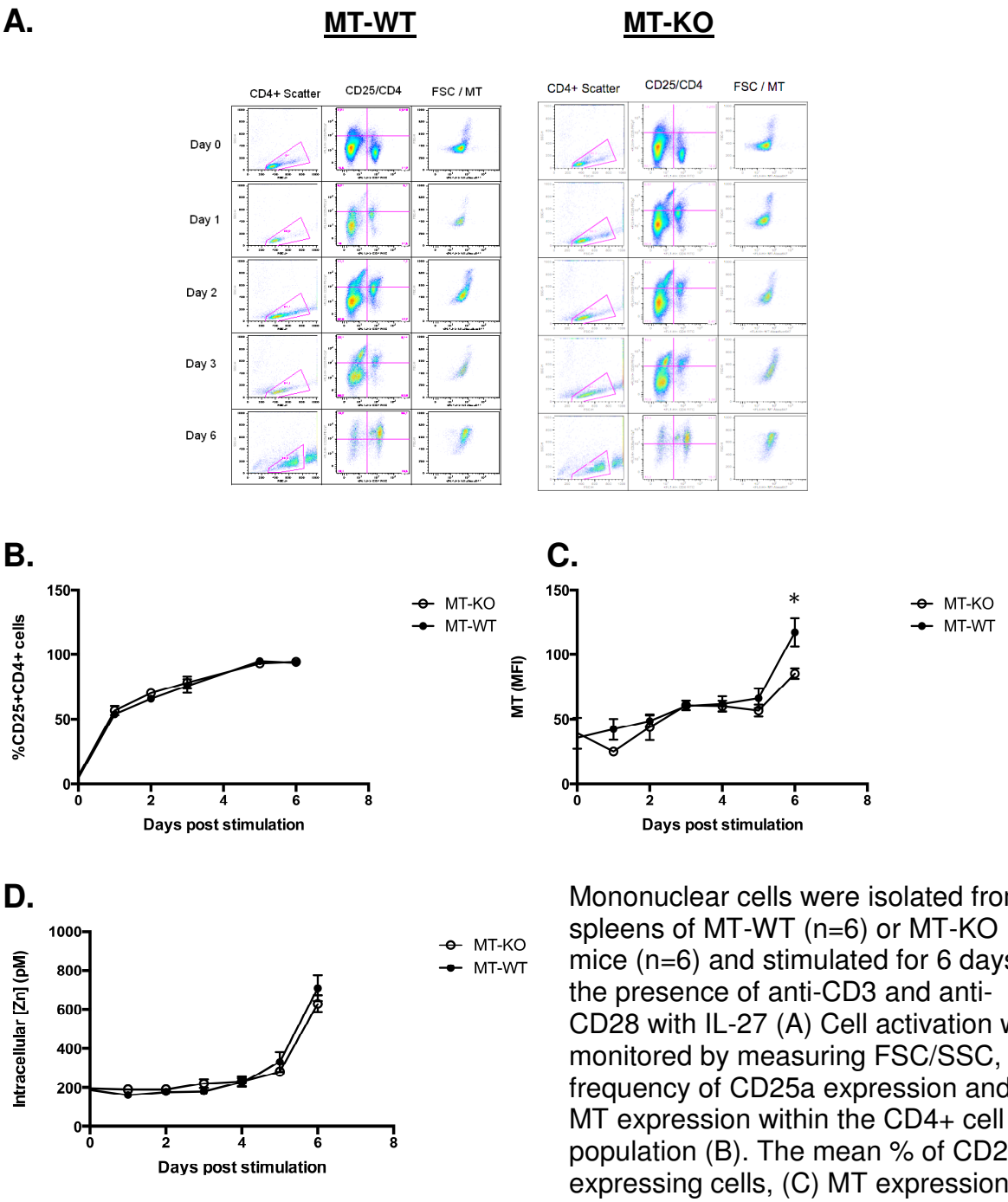

Mononuclear cells were isolated from spleens of MT-WT (n=6) or MT-KO mice (n=6) and stimulated for 6 days in the presence of anti-CD3 and anti-CD28 with IL-27 (A) Cell activation was monitored by measuring FSC/SSC, frequency of CD25a expression and MT expression within the CD4+ cell population (B). The mean % of CD25 expressing cells, (C) MT expression and (D) intracellular labile [Zn2+] for each strain over 6 days of activation is shown. Error bars indicate standard deviation. Groups were analyzed by two-tailed T test followed by Bonferoni correction. *p<.05

Figure 4.3 Developmental State but not MT Gene Dose Affects Intracellular [Zn^{2+}] in $CD4^+$ T cells

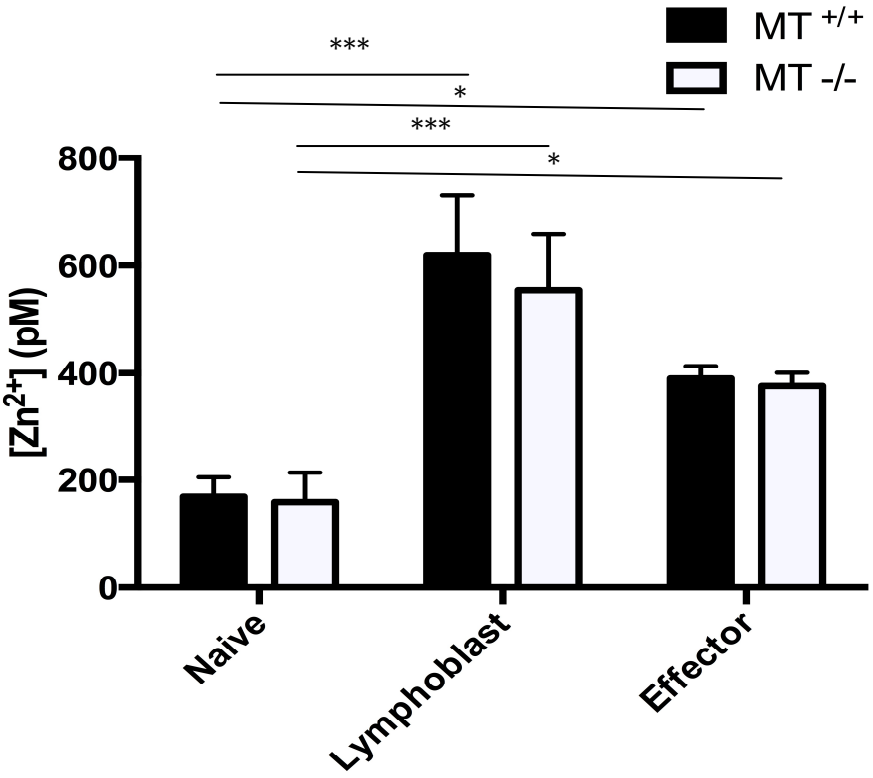

Mononuclear splenocytes from MT-KO mice (n=11) or MT-WT congenic wildtype control mice (n=11) were cultured under Tr1 inducing conditions for 6 days and then rested for an additional 2-3 days. Intracellular [Zn^{2+}] was measured at day 0, day 6, and day 8 corresponding to different stages of differentiation: naïve, lymphoblast and effector, respectively. Error bars indicated standard deviation. groups were analyzed by two way ANOVA followed by Tukey's test. *p<.05 ***p<.001

Figure 4.4 Metallothionein Gene dose Affects Thiol Oxidation Mediated Release of Zn in CD4$^+$ T cells

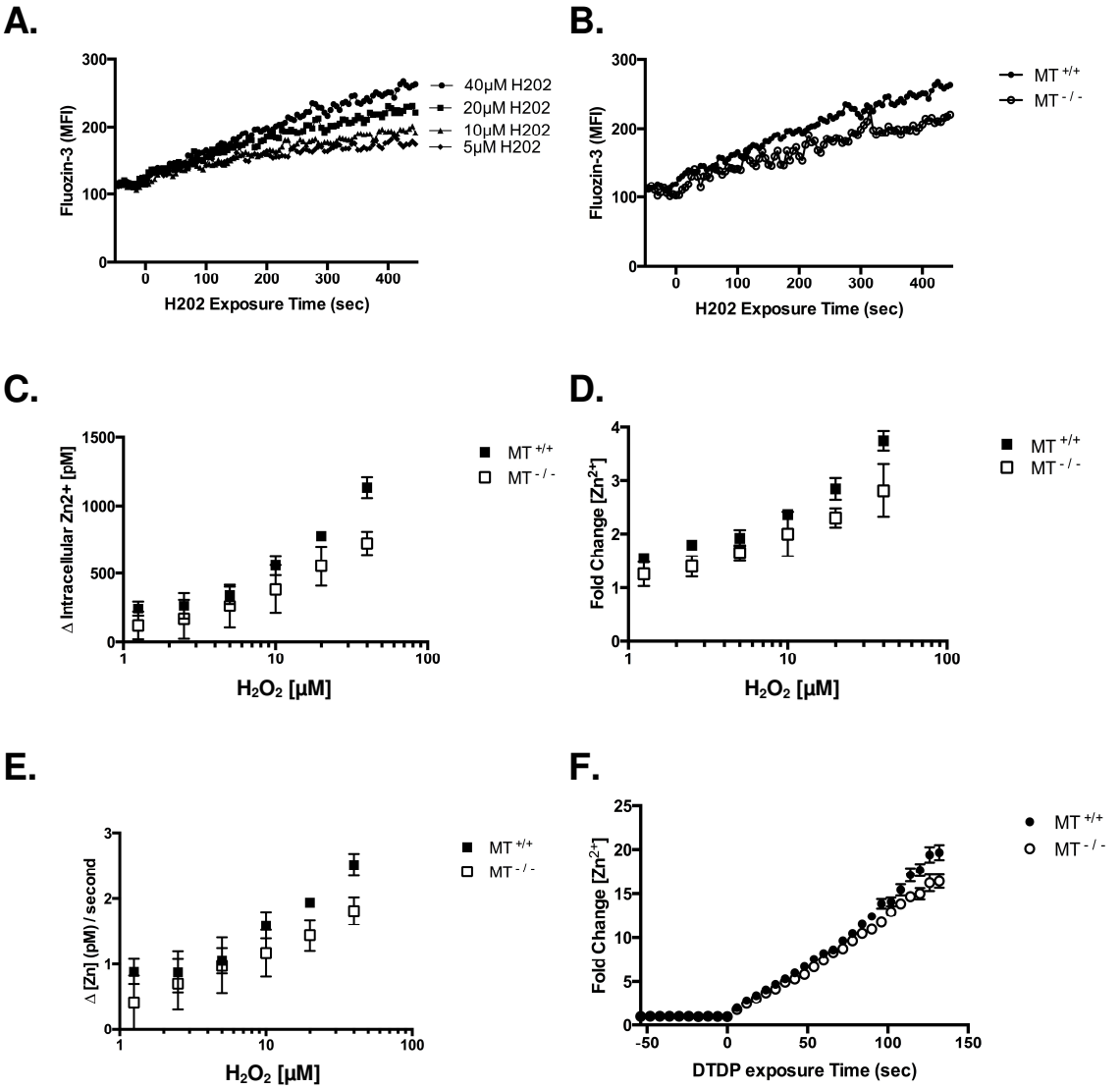

Intracellular [Zn^{2+}] was measured in Tr1 induced CD4$^+$ T cell lymphoblasts from metallothionein knockout mice (MT$^{-/-}$) (n=3) or congenic wildtype controls (MT$^{+/+}$) (n=3) exposed to different concentrations of H_20_2 for 8 minutes to determine the amount and rate of intracellular Zn^{2+} release. (a) The change in Fluozin-3 fluorescence from wildtype CD4$^+$ PI$^-$ cells before and after exposure to H_20_2 [40-5μM] or (b) for metallothionein knockout (MT$^{-/-}$) CD4$^+$ T cells compared with wildtype controls exposed to [40μM] H_20_2. (c) The average net increase or (d) fold increase in intracellular [Zn^{2+}] after 8 minutes of H_20_2exposure for each strain from 3 independent experiments is compared with H_20_2 exposure. (e) The slope of the increase in [Zn^{2+}] for the initial 60 seconds of H_20_2exposure is also compared. (f) The fold-increase in intracellular [Zn^{2+}] after 140 seconds of DTDP exposure [50μM] for each strain from 3 independent experiments is compared with H_20_2 exposure. Arrows indicate addition of treatment. *p<.05

Figure 4.5 Metallothionein Gene Dose Does Not Significantly Increase Total Redox Buffering Capacity of $CD4^+$ T Cells

A.

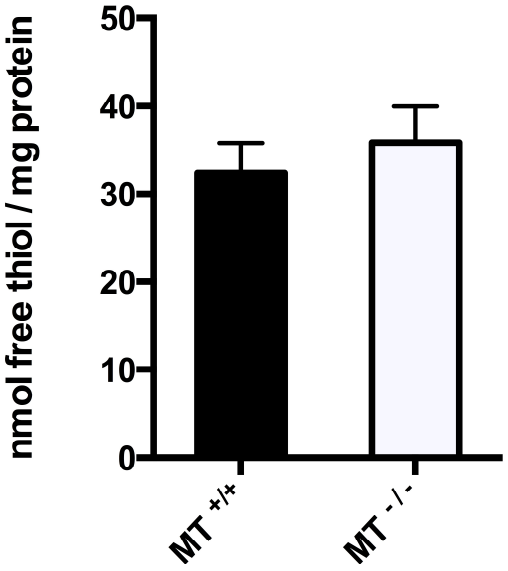

B.

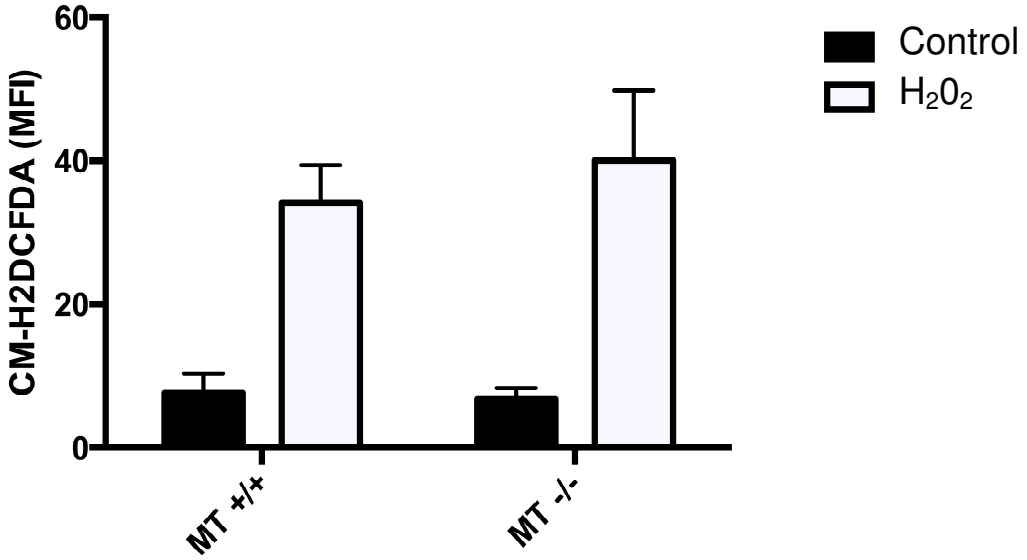

Mononuclear cells were isolated from spleens of metallothionein knockout ($MT^{-/-}$)(n=3) or wildtype controls ($MT^{+/+}$)(n=3) and allowed to differentiate into lymphoblasts under Tr1 inducing conditions. $CD4^+$ T cells were negatively selected by magnetic separation. (a) Tr1 $CD4^+$ cell lysate was analyzed for the presence of free thiols by CPM assay and total protein by BCA. (b) Cells were exposed to 50µM H202 to determine the redox buffering capacity. Bars indicate standard deviation.

Chapter 5

Effect of MT gene dose on reactivation of $CD4^+$ effector T cells *in vitro*

5.1 Introduction

The generation of ROS following TcR engagement is a critical component of effective T cell signaling and a requirement for proliferation and development of function[168]. $CD4^+$ T lymphoblasts produce superoxide and hydrogen peroxide through discrete enzymatic mechanisms following stimulation through the TcR. These ROS signals are separated temporally, as evidenced by differential oxidation of two different intracellular oxidation probes, DCFDA and DHF[218]. More recently, the source of these signals has been revealed to be a phagocyte-type p47 NADPH oxidase[264] and mitochondrial complex III[144]. The NADPH oxidase can be activated by a PMA dependent pathway in $CD4^+$ T cells [264,265] and is required for direct Treg mediated suppression of $CD4^+$ T cells[266], highlighting an important experimental model of ROS generation in $CD4^+$ T cells.

A hallmark of T cell activation is the increase in intracellular calcium following signaling through the TcR, first from intracellular stores and later through CRAC channels[230,267]. This calcium signal, in addition to activating calcinuerin, via calmodulin, is a requirement of inducible nitric oxide synthase (iNOS) activation in $CD4^+$ T cells[268,269]. The resulting nitric oxide (NO) signal is implicated in cytokine production [270,271] and

turning off Th17 T cell responses while increasing development of Th1 effector cells[272,273]. NO regulation in T cells occurs, in part, through the activation of soluble guanyl cyclase which up regulates cGMP[274]. NO can also affect cAMP and cGMP levels indirectly by releasing zinc signals which inhibit phosphodiesterases [6].

The ROS and RNS signaling pathways converge when they are converted or transduced into a zinc signal by interaction with MT, or alternatively through the interaction of superoxide O_2^- or hydrogen peroxide (H_2O_2) with NO [275] to form peroxynitrite which oxides MT even more readily. This mechanism of signal transduction is less studied than the direct interaction of ROS and NO with signaling proteins during T cell activation and differentiation. However, there is a large body of evidence that suggests NO and ROS induced changes in intracellular [Zn^{2+}] are mediated through MT[61,115,127,276-278]. In this way, by expressing cytosolic MT, $CD4^+$ T cells can poise themselves to effectively transduce ROS and RNS signals into Zn signals. The presence of MT also has a synergistic effect on this level of Zn regulation by lowering the kinetic barrier to Zn binding to apoenzymes[279]. This is supported by recent studies indicating that selenium promotes T cell responses following TcR stimulation[280,281] because selenium is an efficient catalyst for oxidant mediated Zn^{2+} release from MT and transfer to apoenzymes[121,132]. For redox signaling cascades to immediately follow TcR and co-stimulatory activation in T cells requires metabolic reprogramming and enzyme expression to already be in place at the time of activation. For this reason, naïve $CD4^+$ T cells do not immediately generate ROS following activation. However, as part of adaptive immunity and secondary immune responses, effector T cells express these proteins and remain poised to generate ROS signals.

The origins of redox signals in T cells are spatially and temporally separated, adding to the complexity of signal integration and suggesting a kinetic rather than a strictly thermodynamic component to oxidant reactivity. Enzymes associated with the plasma membrane generate three distinct types of ROS signals: 1. rapid hydrogen peroxide production independent of Fas or NADPH oxidase; 2. sustained hydrogen peroxide production dependent on both Fas and NADPH oxidase; 3. delayed superoxide production that is dependent on Fas ligand and Fas and independent of NADPH oxidase[264]. In addition to these ROS signals, mitochondrial signals originating from complex III[144] or an ADP-dependent glucokinase GDP2k[211] also produce superoxide required for efficient T cell activation.

Both ROS and RNS can directly modify signal transduction pathways through reversible oxidation or nitrosation of cellular target proteins. This process is important in regulating MAPK signaling[162,282], JAK/STAT signaling [283] and NF-κB signaling[284]. It is not clear, however, if MT affects ROS and RNS signaling directly by preventing oxidative modification of signal transduction pathways, or if MT acts indirectly by releasing intracellular Zn, which, in turn, modifies signal transduction pathways.

In specific aim 3 in this chapter, we address the hypothesis that the MT bound redox sensitive zinc reservoir is mobilized during T cell activation. This will be investigated by stimulating $CD4^+$ Tr1 cells from MT-WT and MT-KO mice and comparing the intracellular increases in ROS and $[Zn^{2+}]$ using appropriate intracellular sensors. In specific aim 4 we address the hypothesis that the consequence of an MT associated increased intracellular $[Zn^{2+}]$ during $CD4^+$ Tr1 secondary activation is a subsequent increase in p38 activation. This will be investigated by fixing cells at defined time points

following stimulation and measuring intracellular phospho-p38 by flow cytometry. Alternatively, cells will be lysed and intracellular total p38 and phospho-p38 will be analyzed by western blotting. In specific aim 5, we will address the hypothesis that MT gene dose affects cytokine secretion patterns in $CD4^+$ Tr1 cells and that these effects are mediated, in part, through zinc.

5.2 Tr1 Cells Produce ROS in Response to TcR or PMA Stimulation

To determine whether ROS production following TcR stimulation of $CD4^+$ Tr1 cells is affected by MT, we loaded cells with the oxidative sensor CM-H_2DCFDA and stimulated cells using anti-CD3 and anti-IgG as previously described [218]. Oxidation of the CM-H_2DCF probe was significantly higher after 30 minutes of stimulation and persisted for at least 2 hours, indicating cells produced a robust intracellular ROS signaling response following TcR stimulation (Figure 5.1A). Similar to the response to extrinsic oxidative stress, oxidation of the probe was not significantly higher in cells that did not express MT, supporting the previous observation that maintaining cellular redox buffering capacity does not require MT. Despite the similar strength of the ROS signal, the increase in intracellular zinc was higher in cells expressing MT by 1 hour of stimulation (Figure 5.1B). This increase was not affected by the addition of 20μM $ZnS0_4$ to the media for this time period, indicating the difference in zinc signaling was not due to differential zinc influx from the extracellular environment (data not shown). Taken together, these experiments reinforce the hypothesis that the total redox potential of $CD4^+$ T r1 cells is not significantly influenced by MT expression. This suggests that the

reversible oxidative modifications to signaling proteins including MAPK would not be directly affected by the presence of MT. The degree of oxidation under these conditions would be regulated thermodynamically by the redox state of the intracellular environment, which is influenced by intracellular antioxidants including GSH and thioredoxin (Trx). Furthermore, oxidation would be regulated kinetically by the presence of antioxidant enzymes including superoxide dismutase and catalase. The consequence of the oxidation of these intracellular thiols would eventually lead to oxidation of MT, given MT's extremely low redox potential (-366mV) and interaction with GSSG to release bound zinc[263]. When MT expression is high, as in the case of Tr1 cells, the concentration of zinc released from MT is sufficient to significantly effect total intracellular labile [Zn^{2+}]. During the initial reactivation of T cells, this process appears to dominate the control of intracellular [Zn^{2+}] before other mechanisms of zinc homeostasis are upregulated.

5.3 Effect of MT Gene Dose on p38 MAPK Activation

The co-stimulatory effect of zinc on p38 MAPK signaling in $CD4^+$ T cells has been observed following signaling through the T cell receptor[13], IL-1beta receptor [195] and IL-2 receptor [8,285]. To determine if increased p38 MAPK activation is associated with MT mediated zinc release, we activated $CD4^+$ Tr1 cells through the TcR and analyzed total p38 and activated p38 (phospho-p38) over a 2 hour time period by western blot (Figure 5.2A,B). The ratio of phospho-p38 / total p38 was slightly increased 20 min after activation before dropping off precipitously by 30 min in both strains. This

proof of principle study supports previous observations of increased p38 activation in MT-WT compared with MT-KO $CD4^+$ T cells (Figure 3.12D).

As an alternative strategy to investigate the mechanisms of MT dependent zinc mediated p38 MAPK activation, we employed the diacyl glycerol analog PMA. PMA does not induce a Zn influx from the extracellular environment but does induce ROS production in $CD4^+$ effector T cells[168,264,265]. Taken together, this model allows us to investigate the effect of ROS and zinc release from MT on p38 activation.

To further investigate p38 activation, Tr1 cells from MT-WT (n=4) and MT-KO mice (n=4) were activated with PMA [100ng/mL] over a one hour period (Figure 5.3A). Cells were fixed at different time points following activation and permeabilized to stain for intracellular phospho-p38 before being analyzed by flow cytometry[286]. Observed differences in phospho-p38 were not due to differences in total p38 between the strains or at different time points (Figure 5.2C). Activation of Tr1 cells led to a similar pattern of p38 activation compared with naïve cells, except that the peak activation was higher (5 fold increase in phospho-p38 compared with a < 2 fold increase) and took longer to occur (20 minutes compared with 10 min). Similarly, both MT-WT and MT-KO show equivalent levels of phospho-p38 before activation but Tr1 cells from MT-WT mice exhibit a significantly stronger activation of p38 by 20 minutes after treatment ($p<.05$) and maintain a higher level of activation at 60 minutes post stimulation.

The MT associated increase in p38 activation was prevented after pre-treatment of cells with the antioxidant N-acetylcysteine (NAC) [20M] which reduced p38 activation significantly in both strains (Figure 5.3B). Addition of NAC is associated with preventing oxidative Zn release from MT[287] and supports the hypothesis that the difference in p38

activation between MT expressing and MT-KO cells is due to increased zinc. The addition of 25mM NAC was chosen because it is a more than sufficient concentration to block ROS (and subsequent zinc release) signaling. The observation that p38 activation was still slightly increased in Tr1 cells in the presence of a large molar excess of antioxidant indicates ROS independent pathways, which have been reported previously[257], play a role in p38 activation.

To further investigate the mechanism responsible for the MT mediated increase in p38 activation, intracellular labile [Zn^{2+}] was chelated or increased to determine if the increased p38 activation phenotype could be rescued from MT-KO Tr1 cells or visa versa. Addition of modest concentrations of extracellular Zn [20μM] did not affect PMA activation in either strain (Figure 5.3 C). Typically, changes in extracellular Zn (<25μM) do not significantly affect intracellular [Zn^{2+}] within the one hour window of p38 activation unless cells are pre-exposed to periods of Zn depletion (and upregulate Zn importers) or activation is achieved through an activated APC presenting a strong agonistic peptide for TcR binding[7]. To overcome this membrane transport limitation, pyrithione was added in addition to increased Zn, which significantly increased p38, MAPK activation in both strains and rescued MT-KO Tr1 cells to WT levels of activation. Chelation of intracellular Zn with TPEN [5μM] significantly reduced p38 activation and prevented differential activation in the two strains. Like NAC pretreatment, addition of TPEN during PMA stimulation did not completely prevent p38 activation, providing further evidence for Zn independent pathways of p38 activation.

5.4 Effect of MT Gene Dose or Added Zn on Cytokine Secretion

Expression of MT has been linked to both increased and decreased expression of the important immuno-regulatory cytokine IL-10 [2,5]. To determine if the influence of MT on IL-10 secretion is Zn dependent, we measured the intracellular [Zn^{2+}] and cytokine secretion in Tr1 differentiated splenocyte cultures from MT-WT and MT-KO mice. Upon restimulation, in contrast to primary stimulation, the increase in intracellular [Zn^{2+}] in $CD4^+$ Tr1 cells was immediate (Figure 4b) and was significantly increased in the MT-WT cells from 0-6 hours post restimulation (Figure 5.1B, 5.4A). The metabolic reprogramming during primary activation and effector T cell development accounts for the faster response to secondary activation. This reactivation includes ROS generation and subsequent zinc release, which accounts for at least part of the initial increase in zinc. Tr1 cells display higher FSC/SSC and CD25+ expression than naïve T cells as well, indicating a change in phenotype that accompanies effector cell development. At later timepoints (12-48 hours), there were no significant differences in intracellular [Zn^{2+}] between the two strains. Redox control of zinc bound to protein-thiols becomes less important in determining intracellular labile [Zn^{2+}] as Zn influx through expression of Zip proteins becomes the driving factor in intracellular Zn homeostasis [15,36], which was seen during blast development in naïve T lymphocytes earlier.

Secretion of IL-10 was detected by 6 hours post stimulation and was greater in Tr1 induced $MT^{-/-}$ splenocyte cultures compared with wildtype controls (Figure 5.4B). This difference was significant after 6 hours, and again at 24 and 48 hours and represents a general pattern of increased IL-10 secretion in MT-KO cells[5]. Secretion of

IFN-gamma during the same time frame was not significantly affected by MT gene dose (Figure 5.5C).

To determine if differences in cytokine secretion between the two strains could be prevented by treatment with zinc, Tr1 $CD4^+$ T cell cultures were incubated in increased extracellular Zn for 48 hours during restimulation. 20µM $ZnSO_4$ represents the maximum [Zn] that does not affect Tr1 viability within a 48 hour period of cell culture (data not shown). Exposure to [20µM] $ZnSO_4$ during activation significantly increased the intracellular [Zn^{2+}] by 48 hours in the MT-KO $CD4^+$ Tr1 cells compared control [Zn^{2+}]. (Figure 5.5A). Interestingly, MT-WT cells maintained Zn homeostasis in the presence of increased extracellular Zn. The MT-KO Tr1 cell culture produced more IL-10 compared with MT-WT cells under conditions of normal zinc during restimulation, similar observations from splenocyte cultures, albeit with a higher final concentration of IL-10. The addition of 20µM $ZnSO_4$ and the resulting increase in intracellular labile [Zn^{2+}] in MT-KO Tr1 cells correlated with a significant decrease in IL-10 secretion (Figure 5.5B). This observation supports the hypothesis that an increased concentration of zinc can impair IL-10 secretion from Tr1 cells. In contrast to IL-10, IFN secretion was not significantly different between the strains under either of the conditions tested.

5.5 Effect of MT Gene Dose on Adaptive Immune Responses

Interpretation of the effects of MT gene dose on the development of $CD4^+$ T cell subsets *in vivo* during adaptive immune responses is difficult because of the complex nature of immune responses. The potential effects of intracellular versus extracellular pools of MT, which act to modulate intracellular zinc and influence chemotaxis,

respectively, compound this complexity. In this way, it is difficult to know whether the effect of MT gene dose on the development of $CD4^+$ T regulatory cells *in vivo* is mediated through the intracellular signaling within the cells, altered APC activity that differentially activates $CD4^+$ T cells, or even a modified extracellular chemokine environment that influences lymphocyte trafficking patterns. Furthermore, these mechanisms of action are not mutually exclusive and may all play a role in shaping the development of $CD4^+$ T cells during an adaptive immune response.

One of the paradigms that emerges from studies involving MT mediated immunomodulation is the association of MT with the control of inflammation and the reducing the pathophysiology of inflammatory autoimmune diseases[150,152,288]. Genome wide association studies (GWAS) have even revealed an association between 2 polymorphisms in the *MT1a* gene in an Italian Central female population that is associated with reduced induction of MT. The consequence of this reduced MT pool is lower inflammatory status in the population and increased longevity [197]. This observation supports the *in vitro* observations discussed above where decreased release of zinc from MT in MT-KO cells was associated with greater expression of the potent anti-inflammatory cytokine IL-10.

As discussed previously, one of the major sources of IL-10 *in vivo* is $CD4^+$ CD25+FoxP3+ T regulatory cells [289]. To determine if MT gene dose affects the circulating frequency of Treg cells *in vivo*, PBMCs were isolated from MT-KO (n=3), MT-WT (n=3) and MT-TGN mice (n=3) and the percentage of CD25+FoxP3+ cells within the total $CD4^+$ T cell population was determined (Figure 5.6) Even with a small sample size, a significant difference in circulating frequency of Tregs was observed between

MT-KO and MT-WT mice ($p<.05$). In line with *in vitro* observations, MT-KO mice had a significantly higher frequency of Tregs (1.7%) compared with MT-WT mice (0.9%). The frequency of MT-TGN Treg cells was closer to MT-WT levels, but the small sample size and large variation in the MT-TGN population limits the interpretation of this study.

An alternative, less direct way to study the effect of MT gene dose on $CD4^+$ T cell adaptive immune responses is to measure the humoral response to immunization with a T dependent antigen[290]. Immunization with type II chicken collagen is an established method for inducing an autoimmune arthritis phenotype in mice[220] and represents a T cell dependent antigen[291]. Age-matched male mice were grouped by MT gene dose. MT-KO (n=7), MT-WT (n=8), and MT-TGN (n=8) mice were immunized with type II sternal chicken collagen in complete Freund's adjuvant (CFA) (Day 0) and immunized with booster injections of collagen in incomplete Freund's adjuvant (IFA) on day +14 and day +55. Serum was collected by sub mandibular bleed on day 22, day 43, and day 77. Total IgG in the serum was not different between the strains at any of the time points tested (data not shown). On day 22, the anti-collagen specific IgG response was greater in MT-TGN compared with MT-WT (Figure 5.7A). Interestingly, this supports observations from a previous study where both MT-KO and MT-TGN mice develop more robust immune responses to challenge with *Listeria monocytogenes* [292].

Cytokines secreted by $CD4^+$ T cells affect the sub type of IgG expressed in response to antigenic challenge[293]. On day 43, serum was collected and the anti-collagen IgG sub type response was measured. The concentration of IgG1 and IgG2b sub types of anti-collagen IgG were significantly higher ($p<.05$) in MT-TGN mice than MT-WT while the IgG2a response was roughly equivalent for all three strains. Increased

IgG1 is associated with TH2 responses and is induced by IL-4 and inhibited by IFN-gamma[294]. Alternatively, increased IgG2a is induced by IFN-gamma and inhibited by IL-4 and is associated with TH1 responses.[215]. IgG2b is induced by TGF-beta and is selectively increased in the serum of individuals suffering from rheumatoid arthritis[216]. For MT-WT and MT-KO mice, the concentration of the 3 anti-collagen IgG sub-types present was not significantly different (.05µg/mL and .08µg/mL, respectively). The concentration of anti-collagen IgG2b in the serum of MT-TGN was the highest of any response tested.

The similar level of IgG2a response to collagen between the strains supports the *in vivo* $CD4^+$ cytokine secretion studies that indicate IFN-gamma secretion is not significantly influenced by MT. The observation that IgG1 and IgG2b responses were significantly greater in MT-TGN compared with MT-WT, but are not significantly greater than MT-KO responses, is difficult to interpret. The important mechanisms underlying MT mediated immunomodulation may be different for the different genotypes. For example, the important mechanism responsible for the influence of MT mediated differences in MT-KO $CD4^+$ T cells may be the lack of a redox mobilizable pool of intracellular Zn while in MT-TGN mice, it may be a sufficient concentration of extracellular MT to interfere with lymphocyte trafficking patterns. The results from the humoral response to collagen emphasize the point that there is no linear relationship between MT gene dose and T helper or humoral response patterns.

5.6 Conclusions

Recent studies investigating the role of ROS produced in response to TcR stimulation in $CD4^+$ T cells support the role of MT as an important redox mobilizable zinc pool with the potential to modify T cell signal transduction. Furthermore, oxidative signaling helps define the context in which MTs divergent roles in Zn buffering (zinc binding or zinc release) influence T cell function. In the absence of oxidative signaling, MT acts to bind and sequester Zn ions. The effect of increased MT expression in the absence of an oxidative signal is a decrease in intracellular labile $[Zn^{2+}]$ via binding of free Zn ions to unsaturated MT. The effect of MT expression during T cell signaling, however, appears to have the opposite effect, where MT expression increases intracellular labile $[Zn^{2+}]$. Additionally, the role of MT in modifying zinc dependent signal transduction pathways is not limited to release of Zn ions. MT facilitates the transfer of Zn to apo-proteins, even those with a lower binding affinity for zinc through a network of cooperative binding reactions involving selenium. Even when intracellular oxidants react with species other than MT, including glutathione or other protein thiols, the resulting disulfides are molecular targets for reduced or zinc bound MT. The complexity and unique biochemistry of MT's 20 vicinal cysteine residues impart this unique redox property that centrally places MT at the intersection of redox state and labile intracellular $[Zn^{2+}]$.

The consequence of increased intracellular labile $[Zn^{2+}]$ on the modification of T cell signaling pathways is only beginning to be understood. The role of zinc as a cofactor and allosteric regulator of enzyme activity is well established. It has been discovered only recently, however, that the inhibition (IC_{50}) values of relevant signaling

phosphatases are within the range of intracellular zinc fluctuations. This suggests that these signaling phosphatases are points of zinc-controlled regulation. In T cells, protein tyrosine phosphatases including MKP-1 are exceptionally sensitive to reversible inhibition by zinc. The effect of this inhibition is increased activation of phosphorylated MKP-1 substrates, including p38 MAPK. The regulation of p38 MAPK in the context of different MT gene backgrounds supports the role of zinc as an activator of p38 via inhibition of MKP-1. Furthermore, the MT associated increase in p38 activation can be inhibited by chelating zinc, or by loading the intracellular environment with a molar excess of the anti-oxidant NAC.

Studies investigating the role of MT in $CD4^+$ T cell mediated inflammatory autoimmune diseases have revealed a strong relationship between MT and the control of inflammation. There exists substantial contradiction in the literature regarding the effect of MT on the IL-10 expression and secretion from regulatory T cells, specifically Tr1 cells. Our findings suggest MT expression, in the context of Tr1 stimulation, is associated with an increase in intracellular labile [Zn^{2+}] and a decrease in IL-10 but no significant effect on IFN-gamma.

Previous studies have established the requirement of p38 activation for IL-10 expression, which suggests that MT-WT Tr1 cells should secrete more IL-10 than MT-KO based on p38 activation measurements. However, p38 is significantly activated following TcR or PMA stimulation of Tr1 cells from both MT-WT and MT-KO mice and cells from both strains secrete IL-10. The decrease in IL-10 secretion from MT-KO Tr1 cells following addition of Zn implies the regulation of IL-10 secretion, apart from sufficient activation of p38, is mediated by a zinc sensitive mechanism. This mechanism

may be inhibition of STAT3 activation, which has been observed in MT-WT Tr1 cells and is a known effect of zinc during TH17 development (Figure 5.7).

The association of the MT-KO genotype with increased IL-10 extends to the frequency of IL-10 producing Treg cells *in vivo.* Furthermore, the function of MT in modulating bioavailable zinc release and the association of this function with inflammation was discovered independently of a Zn-MT-inflammation hypothesis, based on the results of a GWAS study looking at IL-6 and control of inflammation. Taken together, these results suggest that MT's role in influencing the intracellular labile [Zn^{2+}] contributes to its effect on $CD4^+$ T cell function.

Figure 5.1 Metallothionein Gene Dose Affects Intracellular [Zn^{2+}] in Tr1 Cells Following TcR Stimulation

A.

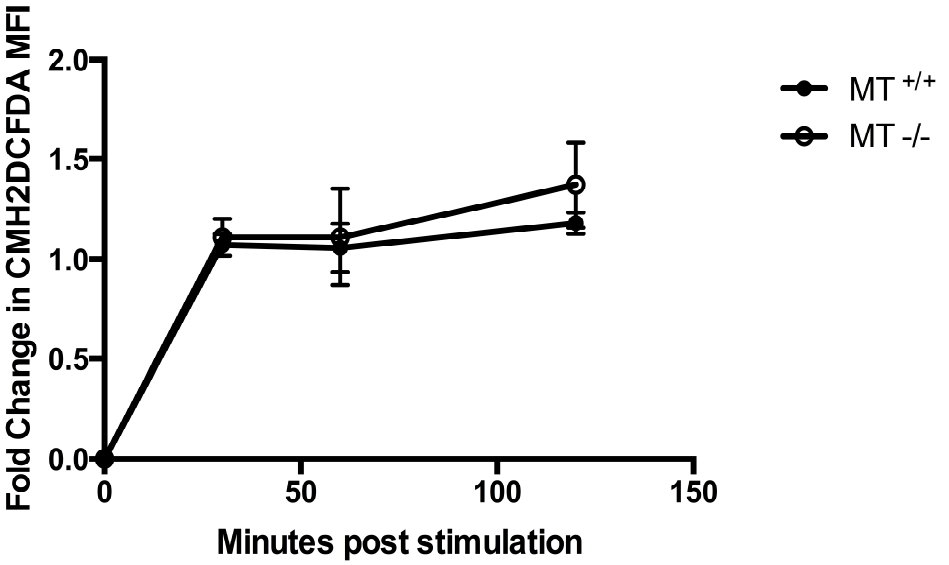

B.

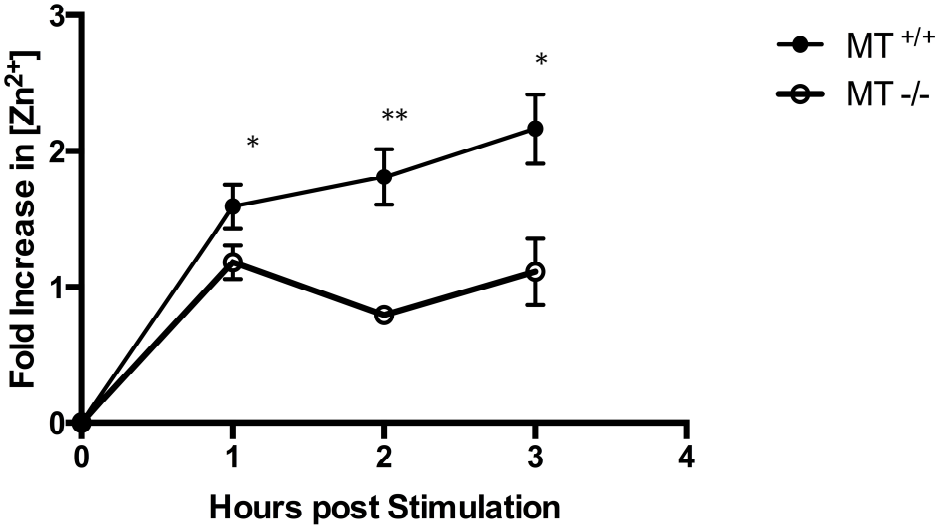

Tr1 induced splenocytes from metallothionein knockout ($MT^{-/-}$)(n=4) or wildtype controls ($MT^{+/+}$)(n=4) were stimulated with hamster anti-CD3 and anti-hamster IgG for 0-120 minutes. Cells were loaded with CMH_2DCFDA and labeled with anti-CD4 and propidium iodide. (A) The average fold change in CMH_2DCFDA fluorescence or (B) intracellular [Zn^{2+}] in treated $CD4^+$ PI^- T cells compared with untreated control cells each strain at 30, 60 and 120 minutes is shown. Error bars indicate standard deviation. *p<.05 **p<.01

Figure 5.2 Activation of p38 MAPK in Tr1 Cells Following TcR Stimulation

A.

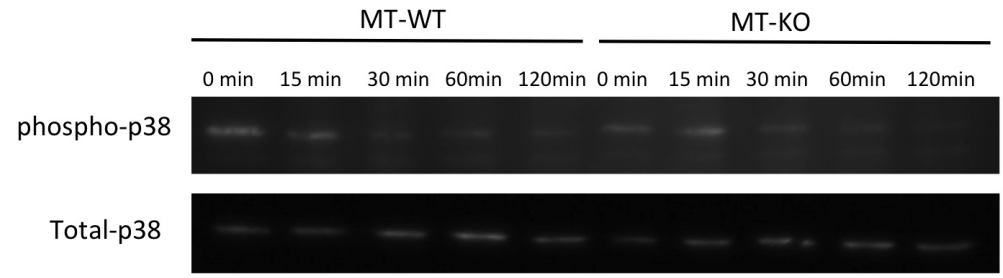

B.

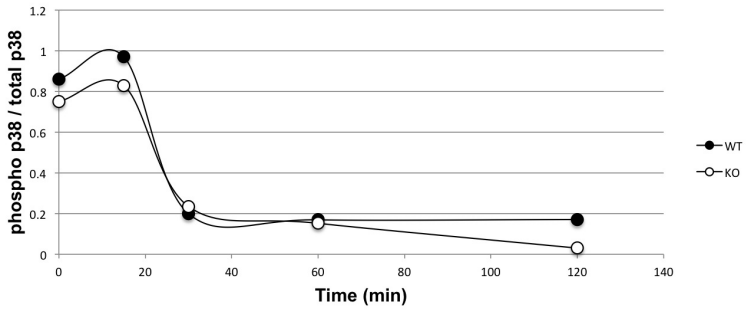

C.

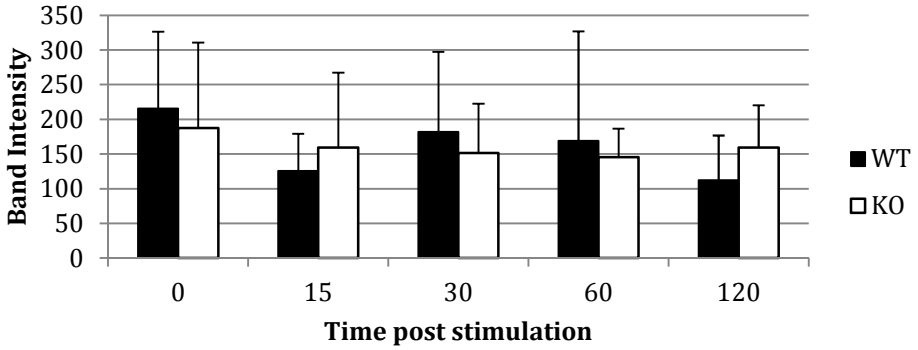

$CD4^+$ Tr1 cells from MT-WT (n=3) or MT-KO mice (n=3) were stimulated with hamster anti-CD3 and anti-hamster IgG for 0-120 minutes. Cell lysates from 3 samples per time point were pooled and protein concentration was measured by Bradford assay. (A) 24µg of cell lysate from each time point for each strain were then separated by SDS-PAGE and probed for phospho-p38 or total p38. Primary antibody binding was detected by chemiluminescence (B) The ratio of band intensity for phospho-p38 / total p38 over time is shown. (C) Total p38 was measured in MT-WT (n=3) and MT-KO (n=3) separately for each time point by western blot. Bars indicate mean band intensity. Error bars indicate standard deviation.

Figure 5.3 p38 MAPK Activity is Affected by MT Gene Dose or Zn in PMA Stimulated Tr1 Cells

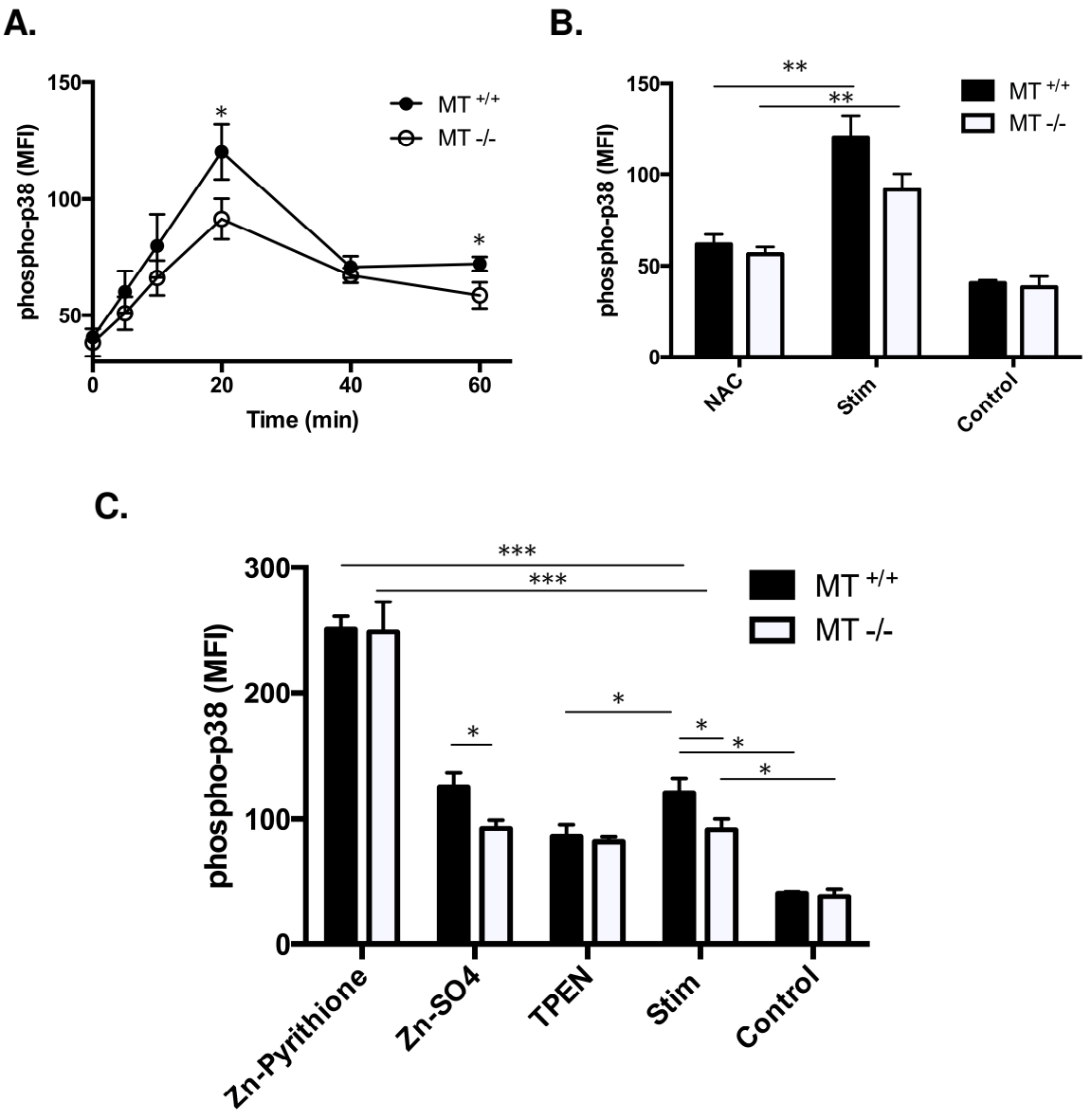

Tr1 induced splenocytes from metallothionein knockout ($MT^{-/-}$)(n=4) or wildtype controls ($MT^{+/+}$)(n=4) were stimulated with 100ng/mL PMA for 0-60 minutes. (A.) Cells were fixed and permeabilized and stained for CD4 and phospho-p38. (B.) Before PMA induced activation, cells were pretreated with N-acetyl cysteine [25mM] for 1 hour and then exposed to PMA [100ng/mL] (NAC) or PMA without pretreatment (Stim) or PBS alone (Control). (C) During PMA induced activation, cells were treated with a Zn chelator (TPEN, [5µM]) or Zn + ionophore (Zn-pyrithione [20µM]) or extracellular Zn alone (Zn-SO_4 [20µM]) or without PMA (control). The difference in phospho-p38 at 20 min post activation is shown. Error bars indicate standard deviation. *p<.05 **p<.01 ***p<.001

Figure 5.4 MT Gene Dose Affects Intracellular Labile [Zn^{2+}] and IL-10 Secretion from Tr1 Cells after TcR Restimulation

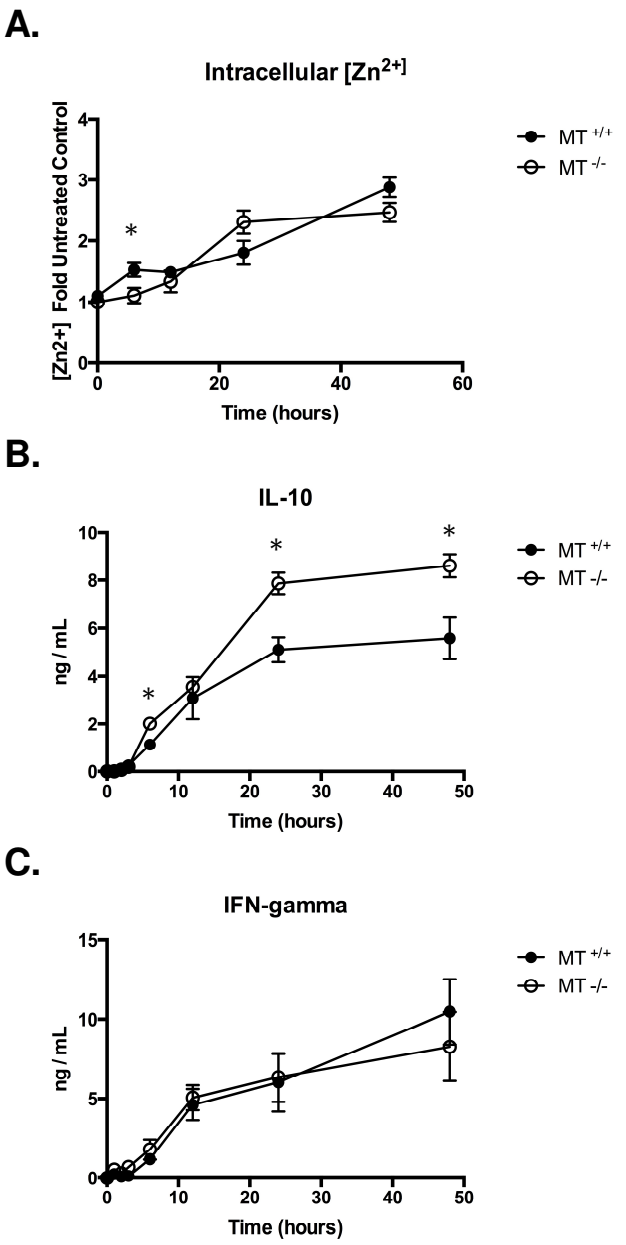

Tr1 induced splenocytes from metallothionein knockout ($MT^{-/-}$)(n=4) or wildtype controls ($MT^{+/+}$)(n=4) were restimulated with anti-CD3 for 48 hours. Cells were spun down at different time intervals and cells were loaded with Fluozin-3 and stained for CD4 and propidium iodide and (a) intracellular [Zn^{2+}] was measured in $CD4^+$ PI- cells. Supernatants from different timepoints were analyzed for the presence of (b) IL-10 and (c) IFN-gamma by ELISA. Error bars indicate standard deviation. Groups were analyzed by two-tailed T-test with Bonferoni correction for multiple comparisons *p<.05

Figure 5.5 Increasing [Zn^{2+}] Reduces IL-10 Secretion in Tr1 Cells from MT-KO mice

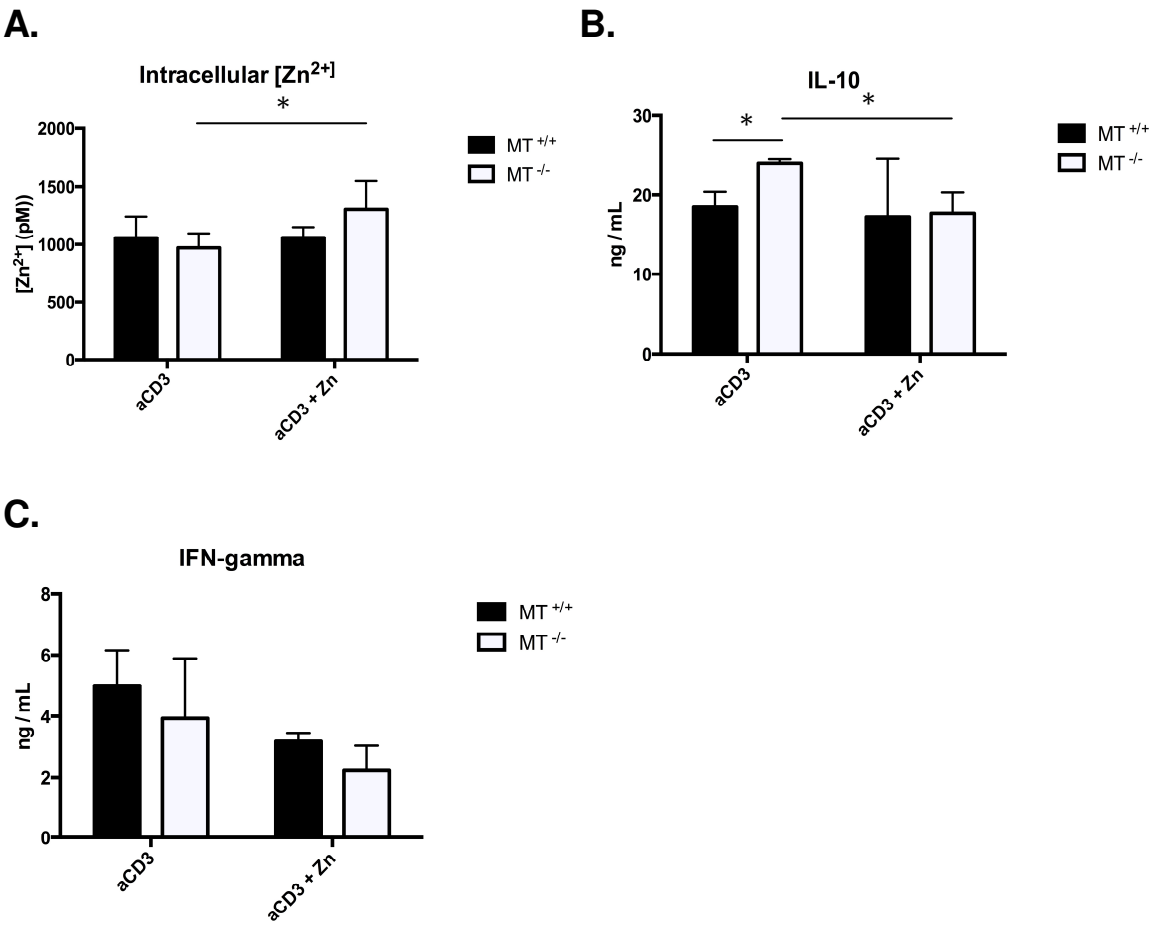

To determine if the effects of MT gene dose on Tr1 cytokine secretion are affected by [Zn^{2+}], 20µM $ZnSO_4$ was added to the media. Tr1 cells from metallothionein knockout ($MT^{-/-}$)(n=3) or wildtype mice ($MT^{+/+}$)(n=3) were restimulated with anti-CD3 [5µg/mL] for 48 hour with or without added $ZnSO_4$. Intracellular [Zn^{2+}] in $CD4^+$ PI- Tr1 cells after 48 hour restimulation was measured by flow cytometry. The concentration of secreted (B) IL-10 or (C) IFN-gamma in the culture media after 48 hours of restimulation was determined by ELISA. Bars indicate mean of 3 separate experiments. Error bars indicate standard deviation. *p<.05

Figure 5.6 MT Gene Dose Affects Circulating Treg Frequency

A. **B.**

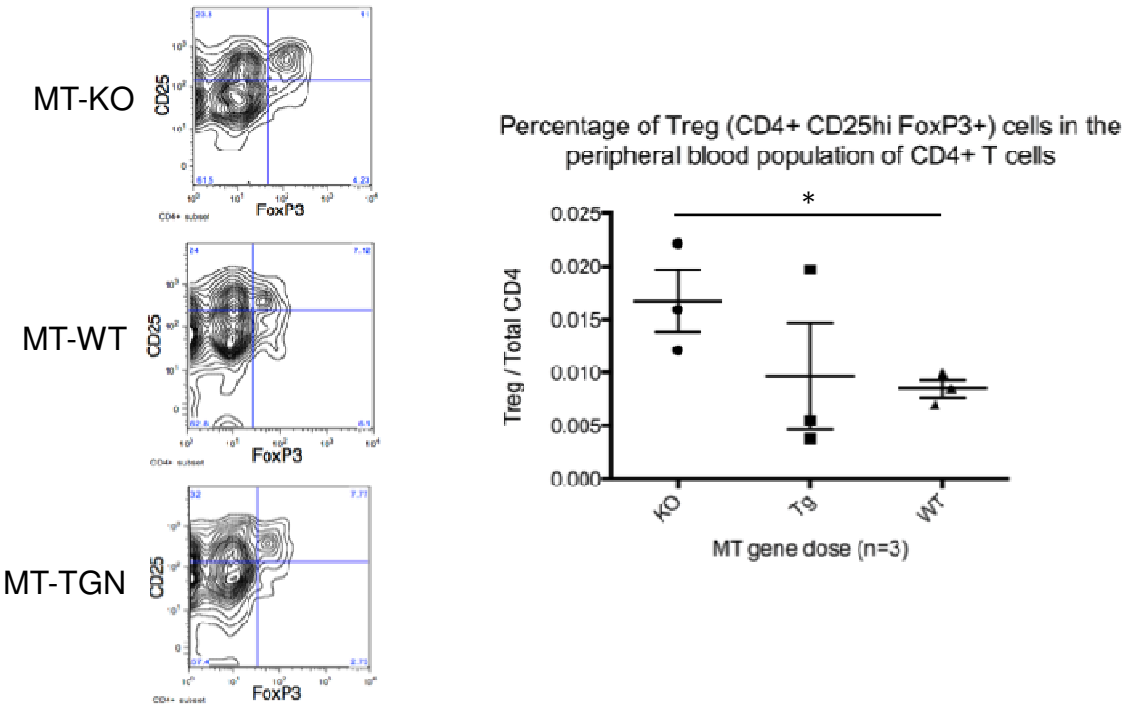

Peripheral Blood Mononuclear Cells were isolated from heparinized blood collected from MT-KO (n=3), MT-WT (n=3), and MT-TGN (n=3) mice. Cells were fixed and stained for the surface markers CD4 and CD25a. Cells were permeabilized and stained for the intracellular transcription factor FoxP3. Cells were gated on a lymphocyte scatter gate and $CD4^+$ marker. Tregs were identified as $CD4^+$ CD25hiFoxP3+ cells. (A) One representative mouse from each genotype is shown. (B) The frequency of Tregs / total $CD4^+$ T cells was plotted for each genotype. Points indicate frequencies in individual mice. Error bars indicate standard deviation. Groups were analyzed by one way ANOVA followed by Tukey's post test. *p<.05

Figure 5.7 MT Gene Dose Affects the Humoral Response to Type II Collagen

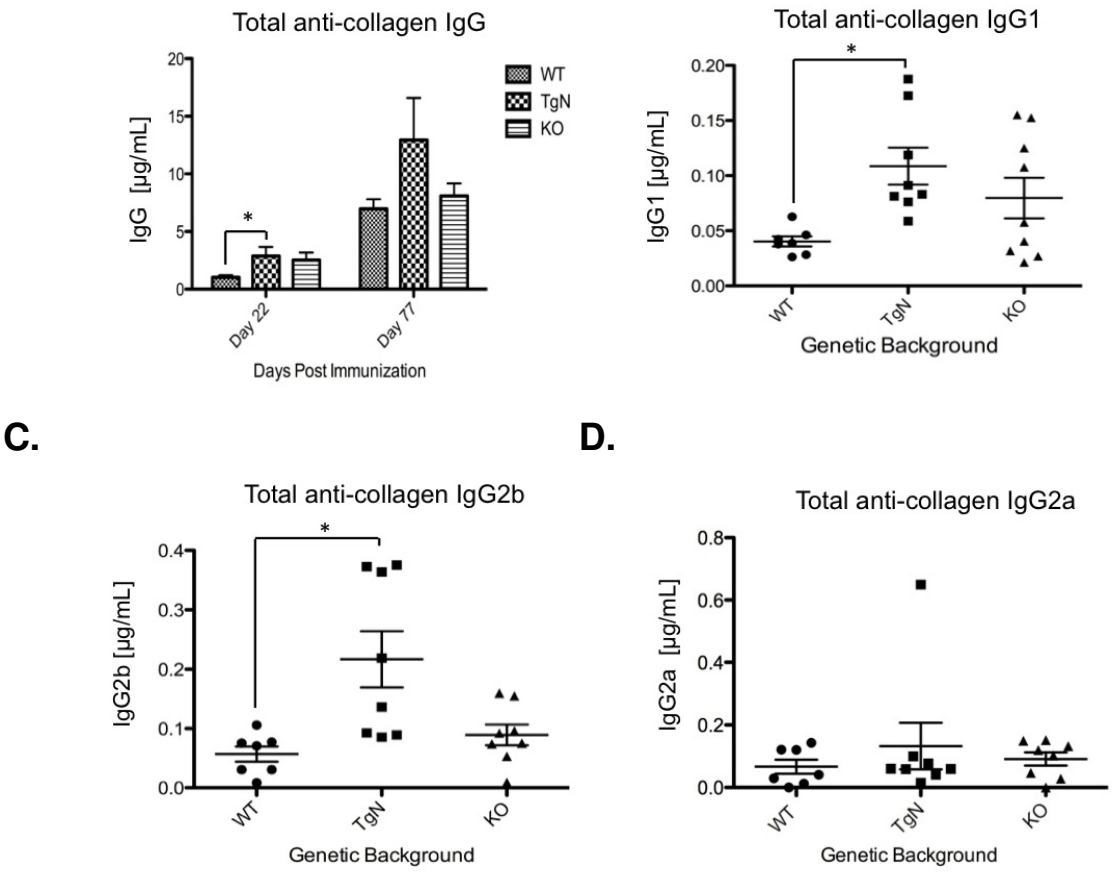

The humoral response to type II chicken collagen was assessed in MT-WT (n=7) MT-TGN (n=8) or MT-KO (n=8) mice. Mice were immunized with Type II collagen in CFA at Day 0 and given a booster immunization in IFA on day +14 and day +55. Serum was collected 22 days, 43 or 77 days after primary immunization and measured by ELISA. (A) Total anti-collagen IgG response on Day 22 and Day 77 are shown. (B-D) IgG subtype anti-collagen specific responses on day 43 are shown. Error bars indicate standard deviation. *p<.05, 1 way ANOVA followed by Tukey's Test.

Figure 5.8 Model: MT Transduces ROS Signals into Zn Signals and Affects $CD4^+$ T Cell Signaling

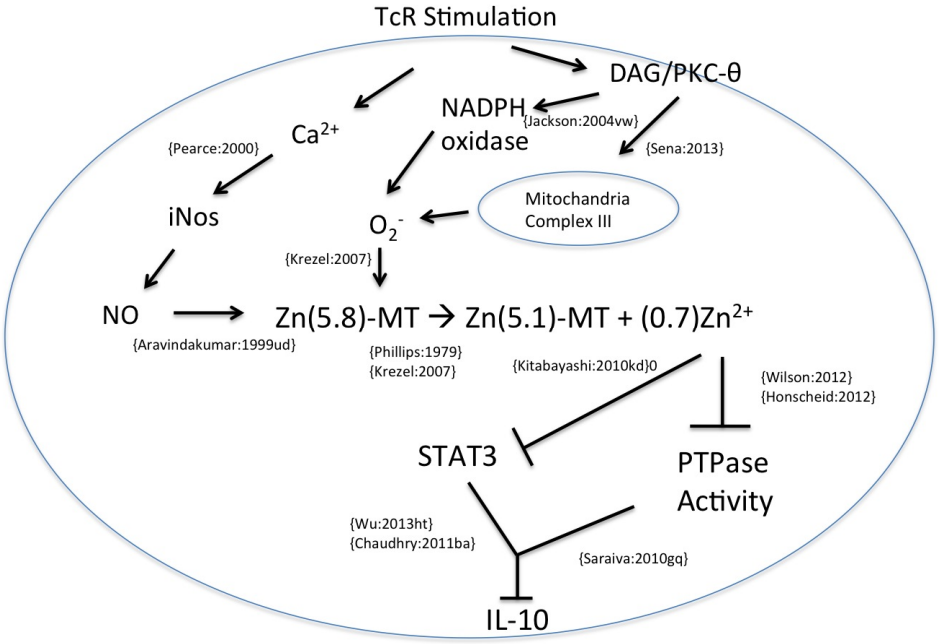

Chapter 6

6.1 Conclusions

The unique biochemistry of MT has always posed a challenge to studies designed to decipher its biological functions. Recently, with improved intracellular zinc sensors and techniques for investigating the redox state of MT in biological tissues, a role for MT at the intersection of redox and zinc biology has emerged. Specifically, the ultra low redox potential and unique zinc binding characteristics of MT suggest that it is capable of transducing intracellular oxidant signals into zinc signals by releasing bound zinc and increasing intracellular [Zn^{2+}]. Concurrently, a role for zinc in the modulation of T cell receptor signaling has been observed. In light of the recent observation that robust ROS production occurs following activation of $CD4^+$ T cells, the aims of this thesis were to address the following general questions:

1. When is MT expressed in $CD4^+$ T cells and is its expression affected by cytokine inducing conditions?
2. Does MT expression position $CD4^+$ T cells to respond differently to ROS in terms of intracellular zinc release?
3. Is activation of the zinc sensitive MAPK p38 affected by MT gene dose?
4. Does MT affect cytokine secretion patterns and are those effects zinc dependent?

To better understand the timing of MT expression and changes in intracellular [Zn^{2+}] during T cell activation, both parameters were measured over the course of primary T cell activation for 6 days. Prior to activation, resting naïve lymphocytes from

both MT-WT and MT-KO mice maintain a similar intracellular [Zn^{2+}], despite the fact that serum [Zn^{2+}] is higher in MT-WT mice. This coincides with very low levels of MT expression and suggests that under normal resting conditions MT does not play a significant role in zinc homeostasis in lymphocytes. Upon activation however, MT expression can be seen by day 3 and peaks on day 6, which coincides with the highest observed concentration of intracellular [Zn^{2+}]. Interestingly, MT expression did not affect the intracellular [Zn^{2+}] during this window of primary activation, suggesting other homeostatic zinc mechanisms dominate the control of intracellular [Zn^{2+}] during this time. Both MT expression and intracellular [Zn^{2+}] are affected by the presence of IL-27 during this activation, however, indicating zinc is a potential point of regulatory control in determining $CD4^+$ T cell fate during primary activation and differentiation. Specifically, the Tr1 effector phenotype inducing cytokine IL-27 promoted an increase in MT compared to TcR and CD28 co-stimulation without IL-27. These observations revealed definitively that MT is expressed following CD4+ T cell activation and its expression is increased when activation occurs in the presence of IL-27.

When the release of zinc following exposure to different concentration of H_2O_2 was compared between Tr1 cells expressing MT (MT-WT) and congenic MT knockout cells, a significant association between MT expression and increased release of zinc was observed. This difference was not due to total intracellular redox buffering capacity between the two genotypes, but rather was a consequence of the intracellular reduced thiol pool in MT-WT cells being comprised, in part, of MT. These results indicate that the expression of MT in Tr1 cells positions these cells to respond to ROS by efficiently

releasing zinc and increasing their intracellular labile [Zn^{2+}]. This result suggests a mechanism for MT mediated immunomodulation through the control and release of zinc.

The consequences of increased intracellular [Zn^{2+}] during T cell activation are complex, given the greater than 3000 known proteins that have at least one zinc binding domain. However, one general paradigm that has emerged recently is the inhibition of intracellular phosphatases by labile zinc, even at very low concentrations. One example of a zinc-sensitive phosphatase that is expressed in $CD4^+$ T cells and is important in T cell signaling following activation is MKP-1. One of the substrates of this enzyme is the p38 family of MAP kinases. Reactivation of Tr1 cells produces a robust ROS signal that is associated with an increase in intracellular [Zn^{2+}]. Similar to exposure to H2O2, cells that express MT release significantly more labile zinc following stimulation through the TcR and this is associated with an increased activation of p38. MT gene dose does not affect p38 activation when zinc is removed through chelation or added through the presence of an ionophore, however, suggesting the mechanism of MT mediated p38 regulation is zinc dependent.

The regulation of intracellular phosphatases and T cell signaling pathways by zinc released from MT has the potential to affect $CD4^+$ T cell effector function. To determine if there are differences in Tr1 cytokine secretion patterns between MT-WT and MT-KO $CD4^+$ T cells, IL-10 and IFN-γ were measured following restimulation of Tr1 cells. While IFN-γ secretion was similar between the two strains, IL-10 secretion was significantly increased in MT-KO cells compared with wildtype controls. Interestingly, wildtype levels of IL-10 secretion could be rescued by increasing the extracellular zinc concentration, once again suggesting that MT mediated affects on $CD4^+$ effector

function are, in part, zinc dependent. Taken together, these observations demonstrate a novel mechanism of MT mediated immunomodulation. By facilitating the release of zinc following TcR activation and the production of ROS, the potential of MT to affect intracellular phosphatase activity and associated $CD4^+$ T cell signaling pathways has been established. Furthermore, this mechanism has implications for MT mediated immunomodulation during inflammatory immune responses where oxidative stress is increased in the local environment. This type of pre-exposure to ROS prior to secondary activation would allow MT to prime $CD4^+$ T cells by increasing their intracellular $[Zn^{2+}]$ before signaling through the TcR. This has potential to alter the kinetics of signaling and potentially exacerbate inflammatory conditions by inhibiting intracellular phosphatases responsible for regulating TcR signaling. Additionally, this higher intracellular $[Zn^{2+}]$ would impart a cytoprotective effect on intracellular thiols, preventing further oxidation and preserving the proliferative capacity.

6.2 Future Directions

The experimental observations presented in this thesis open the door to further investigation into the role of MT in modifying intracellular signaling pathways in $CD4^+$ T cells. As a first step, the degree of MT oxidation by intracellular ROS can be investigated. Expression of the CFP-MT-YFP FRET sensor in $CD4^+$ T cells would allow the direct visualization of zinc release from MT by taking advantage of the structural changes in MT following zinc release and the resulting decreased FRET ratio. This would further confirm MT as the source of increased intracellular $[Zn^{2+}]$ following $CD4^+$ T

cell activation and control for the possibility that MT facilitates the release of zinc from another intracellular source.

The observation of increased p38 activation as a consequence of an MT mediated increase in intracellular [Zn^{2+}] and inhibition of the MKP-1 phosphatase warrants further investigation. As a proposed next step, the relationship between zinc concentration and global T cell phosphatase activity, measured by conversion of PNPP or other suitable substrate, should be assessed in the presence and absence of MT in a cell free system. Equivalent phosphatase activity in experiments with equivalent zinc concentrations, irrespective of the presence of MT, would demonstrate that the effect of MT on phosphatase activity is mediated through labile zinc and not through an interaction with MT directly.

Another important future direction of this research involves the contribution of $CD4^+$ T cells to MT mediated immunomodulation *in vivo*. While $CD4^+$ T cells are a requirement for the pathogenesis of several pro-inflammatory autoimmune diseases, it is not clear if MT mediated differences in disease pathology occur through an effect of $CD4^+$ T cell effector function. Employing a conditional knockout or knockdown model that takes advantage of the Cre-lox system to specifically prevent expression of MT in CD4+ T cells would address this question.

A more complete understanding of the role of MT and its influence on the regulation of labile zinc during T cell activation is an important step in determining how $CD4^+$ T cell responses are shaped during adaptive immune responses. This is especially true in for the development and function of protective type 1 regulatory T cells,

which could lead to therapeutic opportunities to more effectively control inflammatory autoimmune diseases.

Chapter 7

Appendix

7.1 Functional Phenotyping of T Cell Populations using SPR Based Immuno Microarrays

7.1.1 Introduction

The circulating population of peripheral T lymphocytes rapidly and frequently traffics throughout the body and is exposed to many different tissue microenvironments. Functional and phenotypic characterization of these T cells can indicate prior exposure to vaccines [295] infectious agents [296], and toxicants[297]. Furthermore, detection of certain self-antigen-specific T cells can help to confirm the presence of autoimmune disease [298] and may also reflect the propensity to develop autoimmune disease before the onset of symptoms. Detecting and characterizing antigen-specific T cells in peripheral blood, however, is a laborious, time-consuming, and costly activity. As a consequence, these types of analyses are usually done only after the appearance of clinically observable disease symptoms. At that point, damage to tissues may have progressed far enough to make treatment less effective than it might have been if started earlier.

The detection of antigen-specific T cells has previously been accomplished by specific labeling with fluorescently tagged oligimerized major histocompatibility complex (MHC) proteins that have been loaded with antigen-derived peptides (p/MHC). Cells that bind these complexes are subsequently identified by flow cytometry [299]. The allelic

form of the p/MHC complex must, in most cases, match the patient's MHC to promote a constructive interaction between the T cell receptor (TCR) and the fluorescently labeled p/MHC. Because MHC molecules in the human population are extremely polymorphic[300], the patient's MHC must be determined before T cell analysis can proceed. In flow cytometry, this approach is limited by the number of different fluorescent labels that can be differentiated in a single assay, as well as significant labor and reagent requirements for screening assays. By using pre-determined spatial coordinates rather than fluorescent tags on a sensor chip to identify specific interactions, microarrays are not constrained to the same multiplexing limits as flow cytometry. However, traditional fluorescence based cellular microarrays still require a labeling step during sample preparation to generate signal and remain technically challenging [301,302].

GCSPRI cellular microarrays retain the increased multiplexing capacity afforded by other microarray systems and do not require cells to be labeled. Cell binding to the sensor chip is quantified by measuring the change in SPR resonance angle at spatially defined regions of interest (ROIs) on the sensor chip (Chabot et al. 2009). Binding of a cell causes the resonance angle to shift, which results in a signal that is proportional to the number of cells captured [303]. In a GCSPRI system, the evanescent wave vector extends only about 200nm from the chip surface into the dielectric medium above [304] meaning that only cells directly in contact with the chip surface actually contribute to the GCSPRI measurement. This results in sufficient sensitivity to detect a single human T cell captured by an immobilized antibody ROI [303]. The incorporation of microfluidics makes this an ideal assay platform because small volumes of sample can be recirculated over the sensor surface to facilitate increased sampling of the cell

suspension. A GCSPRI sensor chip with 1 cm^2 active sensor surface area is capable of presenting more than 10^3 ROIs for potential cell capture in a 50µl flow cell volume [303]. The capacity to interrogate hundreds of peptide-MHC combinations in parallel in a single sample would allow screening for T cells that are specific for many putative disease-associated peptides in combination with multiple allelic variations of the MHC class I and class II molecules.

Using the dual mode GCSPRI/SPCE based microarray described in this report, T cell subsets bound to the chip surface can be assessed for cytokine secretion by co-immobilizing cell capture ligands and anti-cytokine antibodies on the same ROI microspot. After cells are selectively immobilized and enumerated by GCSPRI and cultured on the microarray, ROIs can be probed for the presence of secreted cytokines using secondary antibodies conjugated to a fluorescent tag. Low levels of fluorescence generated in this assay can be detected because of the increased signal to noise ratio resulting from surface plasmon coupled emission (SPCE) (Figure 7.1). By using the appropriate excitation wavelength, fluorophores within 200nm of the sensor chip surface are excited by both the excitation laser and the surface plasmon, rather than by the laser alone. Interaction of the fluorescent emission with the surface plasmon concentrates the fluorescence towards the path of the detector, increasing optical collection efficiency [305]. Together, increased excitation and collection efficiency improve the sensitivity of SPCE and allow for T cell activation status in response to stimulation to be characterized. By automating this process with programmed microfluidics, a dual mode GCSPRI/SPCE T cell detection/phenotyping assay is capable of assaying for the presence of hundreds of different antigen-specific T cells simultaneously and, when

present on the ROI in sufficient numbers, determining the functional status of the immobilized cells.

7.1.2 Protocol Optimization

In GCSPRI systems, the change in SPR angle over time is based on local refractive index changes that occur above the spatially defined ROIs on the biosensor chip [306] and is proportional to the density of cells bound to specific ROIs [303].To validate the utility of GCSPRI as a T cell detection platform, we compared two independent measurements of cell capture on the same GCSPRI chip. A $CD4^+$ T cell population was fluorescently labelled with the succinimidyl ester DDAO-SE, and then captured on 20 ROIs containing different concentrations of anti-CD3 antibody to facilitate a range of cell binding densities. Immobilization of antibodies for cell capture was mediated through a dithiobis-succinimidyl propionate (DSP) modified surface which acted as crosslinker between the gold chip and cell capture antibody. This surface was chosen for preliminary experiments because it is easily fabricated and results in uniform and reproducible immobilization of protein [307].The resulting GCSPRI angle shift was compared to the fluorescent signal for each ROI (Figure 7.3C). The high degree of of correlation (r^2= 0.9178) between the two measurements indicates that SPR angle shift provides an accurate measurement of captured cell populations that is comparable to direct detection of fluorescently labelled cells.

Non-specific binding (NSB) of protein and non-specific adhesion (NSA) of cells will influence the sensitivity of GCSPRI measurements by adding to background noise. Ideally, modifying the gold surface with a crosslinker will result in a more homogenous

and reproducible deposition of the capture ligand. This should lead to more target molecules or cells bound per unit area (higher activity), more reproducible analyte capture (less inter-assay variation), and a surface that is less sensitive to temperature and redox changes.

To test the activity of capture ligands immobilized via different surface modifications, we compared changes in the SPR angle using the Flexchip 8500 GCSPRI instrument after recirculation of CH7C17 T cells that recognize the influenza peptide (HA 306-318) presented by HLA-DR1 (HA-DR1). Anti-CD3 antibodies or HA-DR1 p/MHC complexes with a C-terminal cysteine were immobilized via passive physical adsorption to unmodified gold as a control surface strategy. Alternatively, immoblilization on the chip was facilitated using a 2-(pyridinyldithio) ethylcarbamoyl dextran (PDEC dextran) which forms a covalent bond to the capture ligand through a free sulfhydrl group and represents the use of a hydrogel matrix modification. Biotinylated anti-CD3 antibodies or HA-DR1 p/MHC complexes with a C-terminal biotin were also immobilized via a neutravidin modified gold surface that utilizes a self assembled monolayer (SAM) of alkane-dithiols as a crosslinker (Figure 7.2A). Cell capture activity of the immobilized HA-DR1 p/MHC complex was similar for both the biotin-neutravidin surface and sulfhydryl-PDEC dextran surface immobilization strategies. However, the PDEC dextran coated surface showed significantly lower non-specific binding to bovine serum albumin (BSA) negative control ROIs compared with the other surfaces tested (Figure 7.2B). Most non-specific cell and protein binding occurs through electrostatic or hydrophobic interactions with the surface [308] and the neutral, hydrophilic PDEC

dextran appeared to resist NSB which reduced background to less than 10% of signal. The coefficient of variation (CV) for p/MHC mediated cell capture on the PDEC dextran surface (CV<0.05) was lower than unmodified gold (CV<0.20) or neutravidin (CV<0.21) and is an indirect indicator of reproducible ROI spotting of the capture ligands.

The effect of sample flow rate was tested to determine the rate that produces the highest specific signal to background ratio. It has been reported by other groups that the rate constant for cell adhesion (e.g. the number of cells captured per unit time) increases with velocity under the range of flow conditions used in cellular microarray assays [309]. As the flow rate increases under these conditions, the encounter rate between cell surface markers and capture ligands increases but the duration of the interactions decreases. At very high flow rates, the adhesion rate begins to plateau as the two effects counterbalance each other [310]. We observed that faster sample flow rates increased the rate of cell adhesion up to a flow rate of 500µl min^{-1} (Figure 7.3A) for our system. Flow rates below 100 µl min^{-1} resulted in higher background signals at control ROIs due to increased non-specific cell adhesion, which lowerd the sensitivity of antigen-specific cell detection.

Optimal flow rate for the removal of non-specific cell adhesion by washing the chip surface with media was also investigated. At flow rates between 100 and 1000µl min^{-1}, removal of cells specifically bound to capture ligands was negligible, indicating that T cell capture via immobilized p/MHC or antibodies is a durable event. Removal of non-specifically bound cells was essentially equivalent for all flow rates above 1,000µl

min^{-1} after 15 min of wash (data not shown). For this reason, a flow rate of 1000µl min^{-1} was used for removal of unbound cells.

Using these flow-rate parameters, we investigated the amount of time needed to generate a maximum SPR angle shift at a given ROI. Using a sample flow rate of 500µl min^{-1} we found that a maximum SPR angle shift of between 320 and 400 resonance change units (RCU) was generated within 30 minutes of sample exposure at anti-CD3 or anti-CD28 containing ROIs (Figure 7.3B) on the dual mode GCSPRI/SPCE system. Variation in the rates of cell capture was observed when replicate ROIs were positioned near the center of the chip and near the flow cell edge, presumably due to laminar flow patterns. This positional effect disappeared when ROIs were placed more than 2mm from the flow cell edge and cell capture rates between 5 replicate ROIs placed at this minimum distance from the flow cell edge were similar (CV < 0.05) (data not shown). This spacing requirement was used in all cell capture microarray experiments reported here.

7.1.3 Antigen Specific T cell Capture and Functional Characterization

One application of GCSPRI technology is to interrogate a heterogeneous population of T cells and determine the presence of low-frequency T cells with specific antigen reactivity. To assess the limits of antigen-specific cell detection sensitivity, CH7C17 T cells were recirculated over a PDEC dextran biosensor chip as either a homogenous population, or in a mixed population with Jurkat T cells that do not recognize the HA-DR1 p/MHC construct. To test for non-specific binding to the DR1 MHC, we included a tetanus toxin derived control peptide also presented by DR1. There

was a strong linear correlation (r^2= 0.93) between antigen-specific T cell density and SPR angle shift (RCU). At the lower limit of detection, 0.1% HA-DR1 specific T cells in the pool of 6 x 10^6 total T cells resulted in cell capture signal that was significantly above signal from control peptide ROIs after 30 minutes of sample recirculation (Figure 7.4).

Another approach to further characterize T cells in a mixed population using SPR-based microarrays combines GCSPRI-based cell detection with an SPCE-based fluorescent measurement of cytokine secretion by captured cells. To test this application, we investigated whether T cell populations primed under different inducing conditions could be differentiated by a GCSPRI/SPCE cellular microarray. Jurkat T cells were exposed to TH1 inducing conditions (pre-cultured with anti-CD3, anti-CD28, IL-12 and IFN-gamma), TH2 inducing conditions (pre-cultured with anti-CD3, anti-CD28, IL-10 and IL-4), or control conditions (no stimulation) for 24 hours, followed by culture in media without cytokines for 24 hours. T cells were then stimulated with phytohemaglutanin (PHA) and captured on a dual mode GCSPRI/SPCE microarray sensor chip or incubated in wells for supernatant analysis by ELISA. For microarray experiments, antibodies against the T cell specific markers CD3 and CD28 were co-immobilized with a panel of anti-TH1 cytokine monoclonal antibodies to interrogate cell secretion. The fluorescent secretion signal was normalized to the density of captured cells at each ROI to determine a ratio of cytokine secretion per unit density of captured cells for each T cell sub population. In these experiments, cell capture signal for each of the three cell populations was roughly equivalent (CV < 0.08) because cells were passed over the chip surface until a monolayer of cells were immobilized on ROIs (Figure 7.5A).

Adjacent ROIs comprised of anti-TH1 cytokine antibody alone were not fluorescent, indicating secretion signals are specific to cells immobilized at a particular ROI (data not shown).

In TH1 cytokine secretion experiments, IL-2 secretion was increased when cells were exposed to TH1 versus control or TH2 inducing conditions and measured by SPCE or ELISA (Figure 7.5). This observation shows that the measured increase in IL-2 after pre-incubation with TH1 inducing conditions is independent of the assay format used to detect it. IFN-gamma secretion was also higher after TH1 compared with TH2 inducing conditions for both SPCE and ELISA based measurements. However, IFN-gamma levels were significantly higher for control versus TH2 conditions for both SPCE based assays but not in the supernatant used in the ELISA analysis. Similarly, increased secretion of TNF-alpha was observed after cells were induced under TH1 or control conditions compared with TH2 conditions and measured by SPCE. This difference was also not observed when the supernatant was measured by ELISA, where TNF-alpha secretion was only higher in TH1 compared with control conditions. We believe the differences in TH1 cytokine secretion profiles from SPCE versus ELISA experiments may reflect an additional stimulatory effect of cell capture by surface immobilized antibodies in the presence of PHA which is absent from cell incubation in wells. Furthermore, if higher levels of CD3 or CD28 surface expression correlate with increased IFN-gamma and TNF-alpha secretion, selecting these cells from the larger population could be responsible for the increased cytokine levels observed in the control induced populations in SPCE assays but not in ELISA experiments. In the ELISA experiments, secretion from these cells may have been diluted out in the larger

population and prevented differences being detected between TH2 and control induced populations. Alternatively, differences in microarray and ELISA cytokine profiles could be due, in part, to the release and capture of intra-cellular cytokines during cell lysis in microarray experiments.

Cells immobilized on anti-CD3 containing ROIs also produced less IL-2 after TH1 inducing conditions, and less TNF-alpha after control conditions compared by anti-CD28. Additionally, cells induced under TH2 versus control conditions secreted more IL-2 when captured by anti-CD28 (Figure 7.5C), but less IL-2 under TH2 versus control conditions when captured by anti-CD3 (Figure 7.5B). Preferential selection of cells expressing higher levels of CD3 or CD28 surface markers cannot explain the differences in secretion profiles under the same inducing conditions, indicating that the ligand used for capture can have an effect on captured cell activity. The significant differences in the functional phenotypes of T cells exposed to different inducing conditions and captured at either anti-CD3 or anti-CD28 containing ROIs demonstrates that T cell programming can be affected by exposure to different microenvironments, and that this programming contributes to a functional status that is distinct from the surface phenotype of the cell.

7.1.4 Conclusions

Because many autoimmune diseases are T cell mediated, detection and characterization of self-antigen reactive T cells is a more direct approach to specifically characterize an autoimmune disease and may be provide better predictive indicator of patient risk [311]. The frequency of a diabetes antigen-associated $CD8^+$ T cells in NOD

mice, for example, ranges from 0 – 0.76% of total $CD8^+$ T cells in peripheral blood [312] and correlates to disease with high specificity. The GCSPRI cellular microarray described here is sufficient to detect an antigen-specific T cell population in NOD mice after cells are positively selected for CD4 expression. The efficient screening of some T cell mediated autoimmune diseases, however, may require detection of very rare T cell populations and may have to overcome difficulties associated with very low avidity TCR – p/MHC interactions. To improve the detection sensitivity of a GCSPRI cellular microarray, strategies aimed at preventing non-specific cell binding or increasing the activity of the p/MHC reagents should be explored. Another potential approach would be to improve the molecular flexibility of the immobilized p/MHC complex by tethering it to a more flexible crosslinking surface. This could increase cell capture efficiency and result in more densely bound cells at p/MHC ROIs and a higher signal to noise ratio [301]. Self-assembled monolayers of functionalized oligo ethylene glycols may provide a scaffolding to optimize these parameters. Because the current GCSPRI optical configuration is sufficient to detect a single cell bound to an ROI, the challenge of improving sensitivity primarily involves reducing NSB and NSA to increase the signal to noise ratio. Lower background will result in higher sensitivity and a more accurate detection and quantification of specific cell populations. NSB reduction should also improve sensitivity of fluorescence based cell secretion assays by improving signal to noise ratio.

In some cases, detection of self-antigen reactive T cells alone may not be sufficient to predict or diagnose disease onset. $CD4^+$ GAD65 reactive T cells, for example, can be found at equivalent frequencies in healthy and type 1 diabetic

populations and it is their preferential activation in diabetic patients that is believed to be associated with disease [313]. In these cases, characterizing the activation status of specific T cell subsets may be needed to overcome high false-positive rates that would be associated with a T cell screening assay that only measured the presence of self-antigen reactive T cells. In rheumatoid arthritis patients, the ability to differentiate T cells based on their effector status and functional capacity has shown more promise in identifying individuals at risk to develop disease than the detection of antigen-specificity of T cells or the presence of peripheral blood cytokines alone [314].

The diagnostic information gained by interrogating circulating populations of lymphocytes is not limited to autoimmune disease. For example, exposure to various environmental stressors such as toxic heavy metals has been demonstrated to affect T cell development and the response to activation signals [315]. By integrating information about the presence of antigen-specific T cells and the functional status of immune cell subsets, GCSPRI/SPCE may therefore be able to screen for exposure to different environmental stressors. In this report, we have established the utility of GCSPRI for the detection of T cells on a p/MHC microarray. We have also established that mixed populations of T cells can be selectively sorted and detected and that selected populations can be interrogated for functional effector status by using SPCE. The broad applications of this combination T cell detection / functional characterization platform could extend from early diagnosis of T cell mediated autoimmune disease to exposure to environmental stresses or evaluation of therapeutic efficacy.

Figure 7.1. Schematic Representation of Surface Plasmon Coupled Emission Instrumentation

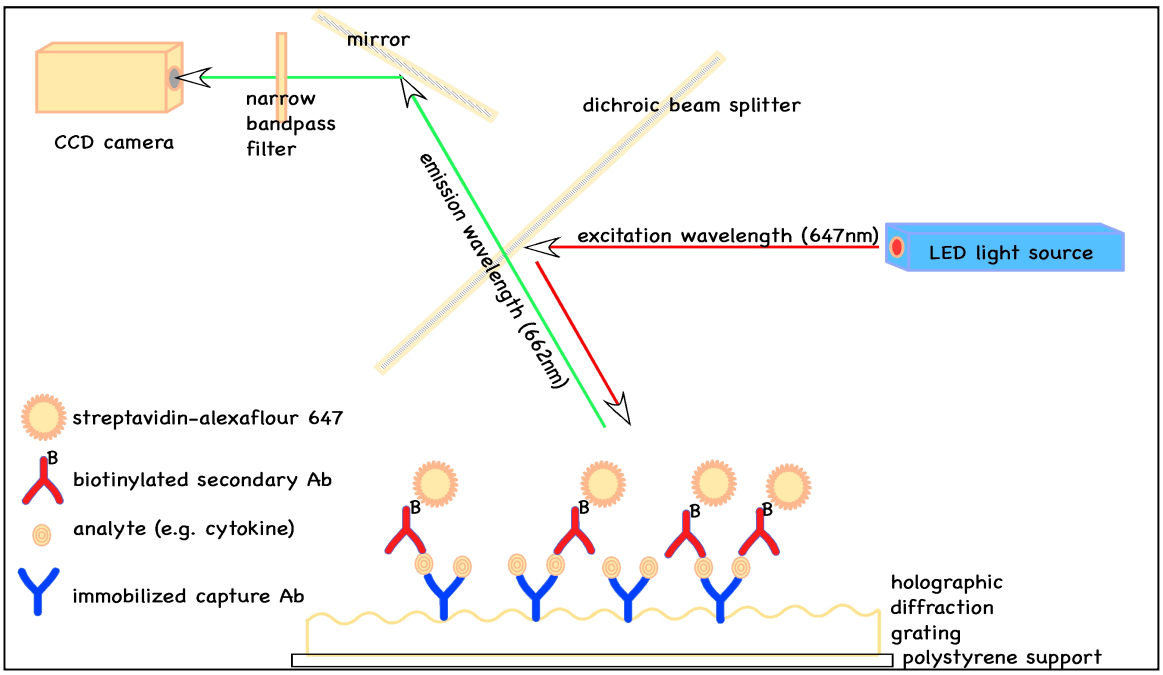

Figure 7.2. Surface Modification of SPR Sensor Chip

A.

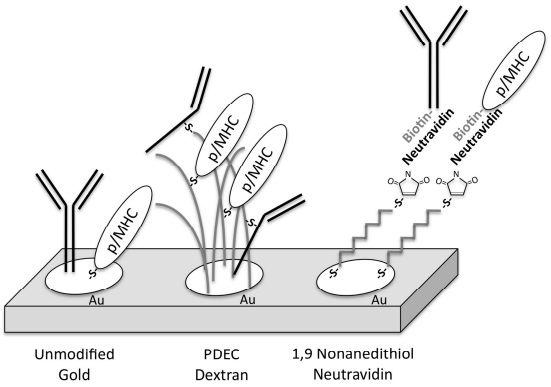

B.

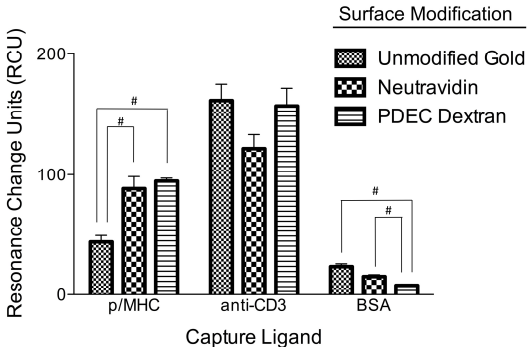

(A) Three distinct surface modification strategies were employed to test the specific activity of antibodies and p/MHC complexes to capture T cells on the microarray surface. As a control strategy (unmodified gold), antibodies were passively adsorbed to the gold sensor chip surface while p/MHC complexes with a C terminal cysteine residue (p/MHC – C) were covalently linked through a gold-thiolate bond. To evaluate a dextran hydrogel modification (PDEC Dextran), reduced antibodies and p/MHC – C complexes were immobilized through free sulfhydryl groups to modified dextran. To evaluate an self-assembled monolayer approach (1,9 Nonanedithiol Neutravidin), biotin labeled antibodies or p/MHC complexes were immobilized through neutravidin that was cross-linked to the gold surface through a 1,9 nonanedithiol monolayer and maleimide interaction. Diagram is not drawn to scale. (B) CH7C17 HA peptide specific T cells (1 x 10^6 cells ml $^{-1}$) in RPMI 1640 were recirculated over SPR sensor chips modified with neutravidin or PDEC dextran or left unmodified. The net SPR angle shift (RCU) after recirculation is shown. Bars are averages of 3 ROI ± S.D. $^{\#}$ indicates a significant difference between groups ($p \leq .05$).

Figure 7.3 Cell Capture Kinetics

A.

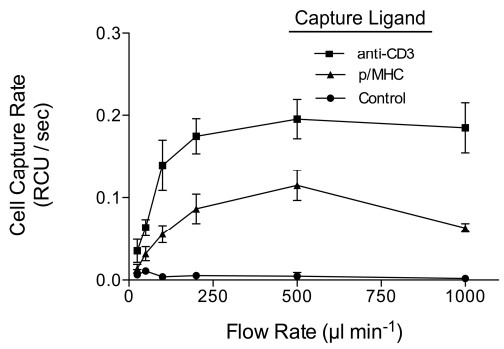

B.

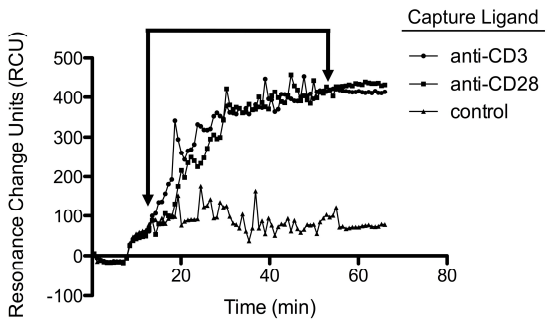

C.

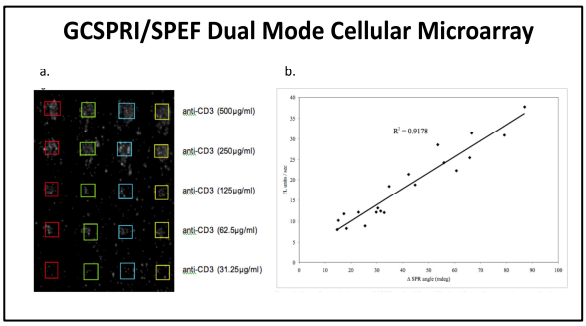

*

(A)Anti-CD3 antibody (squares), HA-DR1 monomers (triangles), or TT-DR1 negative control monomers (circles) were immobilized on a SPR sensor surface in regions of interest. HA peptide specific CH7C17 cells (2 x 10^6 cells ml^{-1}) were passed over a PDEC dextran treated SPR sensor chip for 10 minutes at indicated flow rates. The net shift in SPR angle from before and after cell sample exposure was divided by the time of sample exposure to determine cell capture rate. Points are the average of 3 separate ROIs and error bars indicate ± S.D. (B) Anti-CD3 antibodies (circles), anti-CD28 antibodies (squares) or isotype matched negative control antibodies (triangles) were immobilized on a DSP modified GCSPRI sensor chip. Chips were washed with PBS (10 min) and a media baseline was established (5 min). Chips were exposed to a suspension of Jurkat E6 T cells (2 x 10^6 cells ml^{-1}) at 500 µl min^{-1} for 40 minutes. Each line represents one ROI on the microarray. Arrows indicate the duration of cell suspension exposure to the sensor chip surface. (C) Jurkat E6 T cells (1 x 10^6 cells ml^{-1}) were fluorescently labeled with DDAO-SE and passed over a SPR sensor chip microarray containing a dilution series of anti-CD3 antibody spotted in quadruplicate(left). The net shift in GCSRPI angle (RCU) was compared to fluorescence (AFU) measured by SPCE for 20 individual regions of interest (ROIs) (right). Linear correlation is represented as r^2.

Figure 7.4 Limits of HA-DR1 reactive T cell detection by GCSPRI microarray.

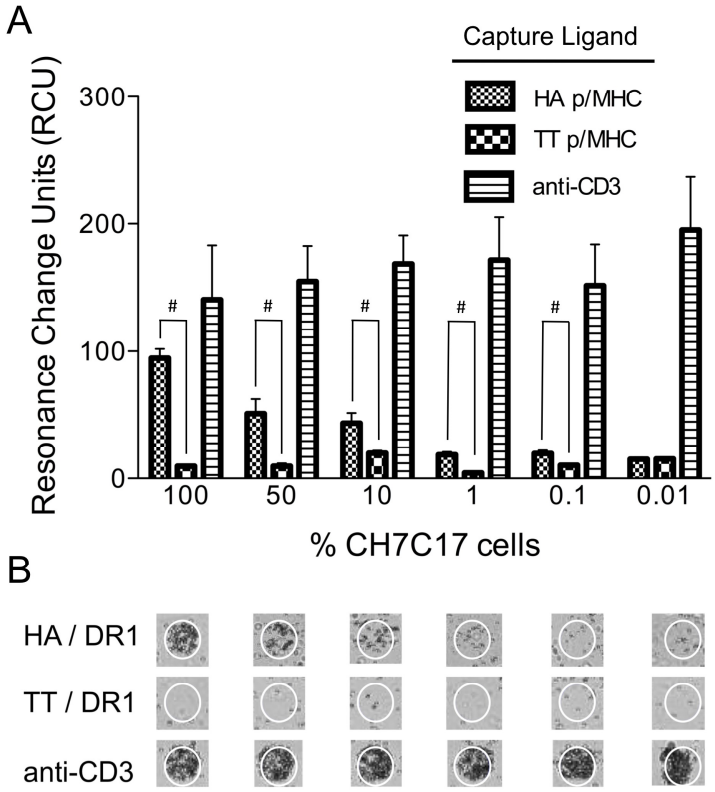

CH7C17 HA-DR1 reactive T cells were mixed with Jurkat E6 T cells and the percentage of reactive cells in a cell sample of 6 x 10^6 total cells was varied from 100 to 0.01%. (A) A mixed T cell suspension was recirculated over a PDEC dextran modified SPR biosensor chip for 30 minutes and net GCSPRI angle shift (RCU) at ROIs containing cognate p/MHC (HA / DR1), negative control p/MHC (TT / DR1), or anti-CD3 antibody was determined. Bars are the average of 3 separate experiments ± S.D.. (B) Images of representative ROIs after T cell sample exposure from each condition are shown. #indicates a significant difference between groups ($p \leq .05$).

Figure 7.5 Cytokine release from T cells exposed to different inducing conditions can be differentiated by GCSPRI/SPCE microarray

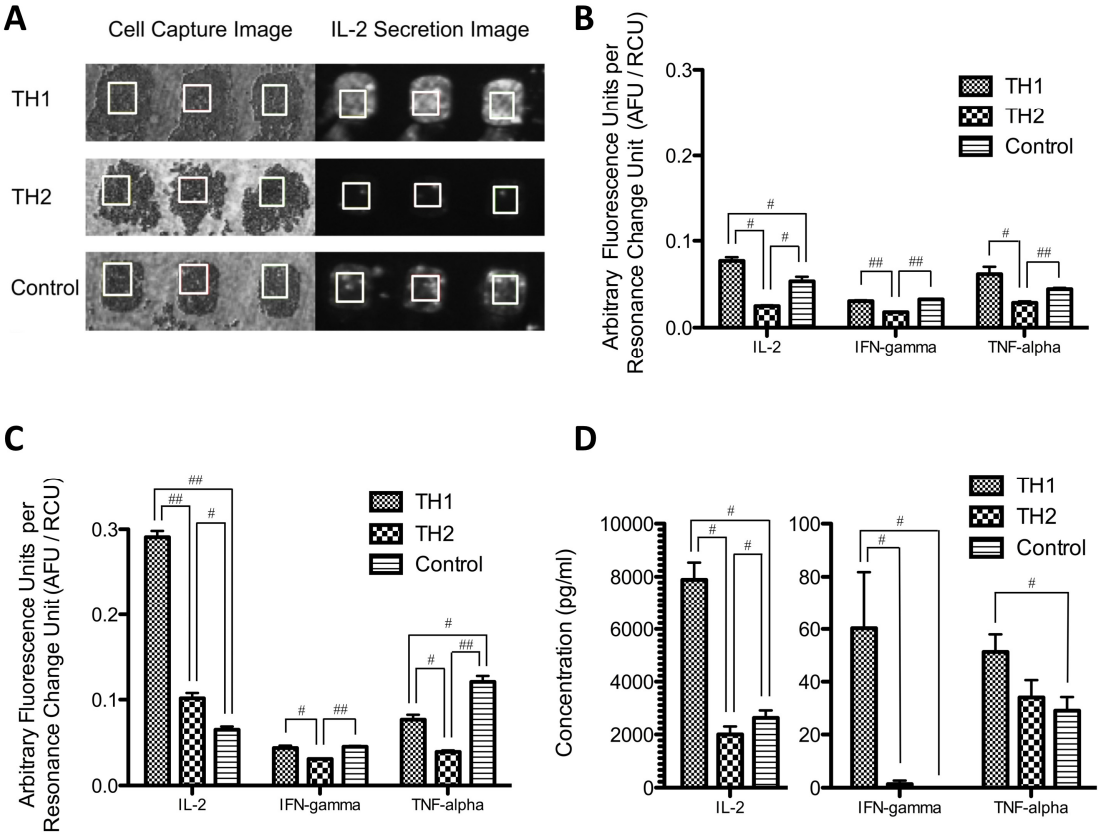

Jurkat E6 T cells were stimulated under TH1 or TH2 inducing conditions or control conditions (no stimulation) for 48 hours and then cultured for 24 hours in media without cytokines. (A) Cells were then captured at ROIs containing anti-CD3 or anti-CD28 antibody and anti-TH1 cytokine antibodies and incubated on the chip in the presence of PHA for 3 hours to allow for cytokine secretion and capture. Cells were then lysed and ROIs were probed for the presence of secreted cytokines using fluorescently labeled secondary antibodies. (B,C) Fluorescence per unit of cell density was measured using a ratio of the surface plasmon coupled emission (SPCE) measurement (AFU) divided by the GCSPRI measurement (RCU). (D) Cells were incubated in wells of a 24 well tissue culture plate in the presence of PHA for 3 hours before cells were spun down and the supernatant was analyzed for the presence of 3 cytokines by ELISA. Bars are the average of 3 independent experiments ± S.D. $^{\#}$indicates a significant difference between groups ($p \leq .05$), $^{\#\#}$($p \leq .002$)

Chapter 8

References

1. Coyle, P., Philcox, J. C., Carey, L. C. & Rofe, A. M. Metallothionein: the multipurpose protein. *Cellular and Molecular Life Sciences (CMLS)* **59,** 627–647 (2002).
2. Huh, S. *et al.* Functions of metallothionein generating interleukin-10-producing regulatory CD4+ T cells potentiate suppression of collagen-induced arthritis. *J. Microbiol. Biotechnol.* **17,** 348–358 (2007).
3. ESPEJO, C. The role of methallothioneins in experimental autoimmune encephalomyelitis and multiple sclerosis. *Annals of the New York …* (2005).
4. Role of metallothioneins as danger signals in the pathogenesis of colitis. **233,** 89–100 (2014).
5. Wu, C. *et al.* Metallothioneins negatively regulate IL-27-induced type 1 regulatory T-cell differentiation. *Proceedings of the National Academy of Sciences* **110,** 7802–7807 (2013).
6. Hönscheid, A., Rink, L. & Haase, H. T-lymphocytes: a target for stimulatory and inhibitory effects of zinc ions. *Endocr Metab Immune Disord Drug Targets* **9,** 132–144 (2009).
7. Yu, M. *et al.* Regulation of T cell receptor signaling by activation-induced zinc influx. *J. Exp. Med.* **208,** 775–785 (2011).
8. Kaltenberg, J. *et al.* Zinc signals promote IL-2-dependent proliferation of T cells. **40,** 1496–1503 (2010).
9. Brieger, A., Rink, L. & Haase, H. Differential regulation of TLR-dependent MyD88 and TRIF signaling pathways by free zinc ions. *J. Immunol.* **191,** 1808–1817 (2013).
10. Liu, M.-J. *et al.* ZIP8 Regulates Host Defense through Zinc-Mediated Inhibition of NF-κB. *Cell Reports* **3,** 386–400 (2013).
11. Kitabayashi, C. *et al.* Zinc suppresses Th17 development via inhibition of STAT3 activation. *International Immunology* **22,** 375–386 (2010).
12. Wilson, M., Hogstrand, C. & Maret, W. Picomolar Concentrations of Free Zinc(II) Ions Regulate Receptor Protein-tyrosine Phosphatase Activity. **287,** 9322–9326 (2012).
13. Hönscheid, A., Dubben, S., Rink, L. & Haase, H. Zinc differentially regulates mitogen-activated protein kinases in human T cells. *The Journal of Nutritional Biochemistry* **23,** 18–26 (2012).
14. Maret, W. Metals on the move: zinc ions in cellular regulation and in the coordination dynamics of zinc proteins. *Biometals* **24,** 411–418 (2011).
15. Aydemir, T. B., Liuzzi, J. P., McClellan, S. & Cousins, R. J. Zinc transporter ZIP8 (SLC39A8) and zinc influence IFN-gamma expression in activated human T cells. *J. Leukoc. Biol.* **86,** 337–348 (2009).
16. Stoye, D. *et al.* Zinc aspartate suppresses T cell activation in vitro and relapsing experimental autoimmune encephalomyelitis in SJL/J mice. **25,** 529–539 (2012).
17. Tanaka, S., Akaishi, E., Hosaka, K., Okamura, S. & Kubohara, Y. Zinc ions

suppress mitogen-activated interleukin-2 production in Jurkat cells. *Biochemical and Biophysical Research Communications* **335,** 162–167 (2005).
18. Krezel, A. A., Hao, Q. Q. & Maret, W. W. The zinc/thiolate redox biochemistry of metallothionein and the control of zinc ion fluctuations in cell signaling. *Arch Biochem Biophys* **463,** 188–200 (2007).
19. Krezel, A. A. & Maret, W. W. Zinc-buffering capacity of a eukaryotic cell at physiological pZn. *J Biol Inorg Chem* **11,** 1049–1062 (2006).
20. Maret, W. Zinc coordination environments in proteins as redox sensors and signal transducers. *Antioxid Redox Signal* **8,** 1419–1441 (2006).
21. Quesada, A. Direct Reaction of H2O2with Sulfhydryl Groups in HL-60 Cells: Zinc-Metallothionein and Other Sites. *Arch Biochem Biophys* **334,** 241–250 (1996).
22. Maret, W. Redox biochemistry of mammalian metallothioneins. *J Biol Inorg Chem* **16,** 1079–1086 (2011).
23. Margoshes, M. & Vallee, B. L. A CADMIUM PROTEIN FROM EQUINE KIDNEY CORTEX. *J. Am. Chem. Soc.* **79,** 4813–4814 (1957).
24. Kägi, J. & Kojima, Y. Chemistry and biochemistry of metallothionein. *Metallothionein II* (1987).
25. Binz, P.-A. & Kägi, J. H. R. in *Metallothionein IV* 7–13 (Birkhäuser Basel, 1999). doi:10.1007/978-3-0348-8847-9_2
26. Kagi, J. H. & Nordberg, M. *Metallothionein; Proceedings*. (1979).
27. Masters, B. A., Quaife, C. J. & Erickson, J. C. Metallothionein III is expressed in neurons that sequester zinc in synaptic vesicles. *The Journal of …* (1994).
28. Hoey, J. G., Garrett, S. H., Sens, M. A., Todd, J. H. & Sens, D. A. Expression of MT-3 mRNA in human kidney, proximal tubule cell cultures, and renal cell carcinoma. *Toxicology Letters* **92,** 149–160 (1997).
29. MOFFATT, P. & SÉGUIN, C. Expression of the Gene Encoding Metallothionein-3 in Organs of the Reproductive System. *http://dx.doi.org/10.1089/dna.1998.17.501* **17,** 501–510 (2009).
30. Quaife, C. J. *et al.* Induction of a New Metallothionein Isoform (MT-IV) Occurs during Differentiation of Stratified Squamous Epithelia. *Biochemistry* **33,** 7250–7259 (2002).
31. Jahroudi, N., Foster, R., Price-Haughey, J., Beitel, G. & Gedamu, L. Cell-type specific and differential regulation of the human metallothionein genes. Correlation with DNA methylation and chromatin structure. *J. Biol. Chem.* **265,** 6506–6511 (1990).
32. Nath, R., Paliwal, V. K., Prasad, R. & Kambadur, R. Role of metallothionein in metal detoxification and metal tolerance in protein calorie malnutrition and calcium deficient monkeys (Macaca mulatta). *Metallothionein II* (1987). doi:10.1007/978-3-0348-6784-9_67
33. Henry, R. B., Liu, J., Choudhuri, S. & Klaassen, C. D. Species variation in hepatic metallothionein. *Toxicology Letters* **74,** 23–33 (1994).
34. Mesna, O. J., Steffensen, I. L., Hjertholm, H. & Andersen, R. A. Accumulation of metallothionein and its multiple forms by zinc, cadmium and dexamethasone in human peripheral T and B lymphocytes and monocytes. *Chem. Biol. Interact.* **94,** 225–242 (1995).

35. Lynes, M. A., Garvey, J. S. & Lawrence, D. A. Extracellular metallothionein effects on lymphocyte activities. *Molecular Immunology* **27,** 211–219 (1990).
36. Won-Woo Lee, D. C. M. C.-G. R. Z. N. V. I. S. A. A. C. M. W. J. J. G. Age-Dependent Signature of Metallothionein Expression in Primary CD4 T Cell Responses Is Due to Sustained Zinc Signaling. *Rejuvenation Res* **11,** 1001 (2008).
37. Miles, A. T., Hawksworth, G. M., Beattie, J. H. & Rodilla, V. Induction, regulation, degradation, and biological significance of mammalian metallothioneins. *Critical Reviews in Biochemistry and Molecular Biology* **35,** 35–70 (2000).
38. Nakajima, K., Suzuki, K., Otaki, N. & Kimura, M. Epitope mapping of metallothionein antibodies. *Meth. Enzymol.* **205,** 174–189 (1991).
39. Masters, B. A., Kelly, E. J., Quaife, C. J., Brinster, R. L. & Palmiter, R. D. Targeted disruption of metallothionein I and II genes increases sensitivity to cadmium. *Proc. Natl. Acad. Sci. U.S.A.* **91,** 584–588 (1994).
40. Palmiter, R. D., Sandgren, E. P., Koeller, D. M. & Brinster, R. L. Distal regulatory elements from the mouse metallothionein locus stimulate gene expression in transgenic mice. **13,** 5266–5275 (1993).
41. Silver, L. M. *Mouse genetics: concepts and applications.* (Oxford University Press, 1995).
42. Haq, F., Mahoney, M. & Koropatnick, J. Signaling events for metallothionein induction. *Mutation Research/Fundamental and Molecular Mechanisms of Mutagenesis* **533,** 211–226 (2003).
43. Quaife, C., Hammer, R. E., Mottet, N. K. & Palmiter, R. D. Glucocorticoid regulation of metallothionein during murine development. *Developmental Biology* **118,** 549–555 (1986).
44. Searle, P. F. *et al.* Regulation, linkage, and sequence of mouse metallothionein I and II genes. *Mol. Cell. Biol.* **4,** 1221–1230 (1984).
45. Sadhu, C. & Gedamu, L. Regulation of human metallothionein (MT) genes. Differential expression of MTI-F, MTI-G, and MTII-A genes in the hepatoblastoma cell line (HepG2). *J. Biol. Chem.* **263,** 2679–2684 (1988).
46. Laukens, D., Waeytens, A., De Bleser, P., Cuvelier, C. & De Vos, M. Human metallothionein expression under normal and pathological conditions: mechanisms of gene regulation based on in silico promoter analysis. *Crit. Rev. Eukaryot. Gene Expr.* **19,** 301–317 (2009).
47. Yang, Y. Y., Robbins, P. D. & Lazo, J. S. Differential transactivation of human metallothionein-IIa in cisplatin-resistant and -sensitive cells. *Oncol. Res.* **10,** 85–98 (1998).
48. Heuchel, R. *et al.* The transcription factor MTF-1 is essential for basal and heavy metal-induced metallothionein gene expression. *EMBO J.* **13,** 2870–2875 (1994).
49. Yamada, H. & Koizumi, S. Metallothionein induction in human peripheral blood lymphocytes by heavy metals. *Chem. Biol. Interact.* **78,** 347–354 (1991).
50. Koizumi, S., Suzuki, K., Ogra, Y., Yamada, H. & Otsuka, F. Transcriptional activity and regulatory protein binding of metal□responsive elements of the human metallothionein□IIA gene. *Eur J Biochem* **259,** 635–642 (1999).
51. Bopp, T. *et al.* Cyclic adenosine monophosphate is a key component of regulatory T cell-mediated suppression. *Journal of Experimental Medicine* **204,**

1303–1310 (2007).
52. Dalton, T. P., Li, Q., Bittel, D., Liang, L. & Andrews, G. K. Oxidative Stress Activates Metal-responsive Transcription Factor-1 Binding Activity OCCUPANCY IN VIVO OF METAL RESPONSE ELEMENTS IN THE METALLOTHIONEIN-I GENE PROMOTER. *J. Biol. Chem.* **271,** 26233–26241 (1996).
53. Imbert, J., Zafarullah, M. & Culotta, V. C. Transcription factor MBF-I interacts with metal regulatory elements of higher eucaryotic metallothionein genes. *… and cellular biology* (1989). doi:10.1128/MCB.9.12.5315
54. Searle, P. F. Zinc dependent binding of a liver nuclear factor to metal response element MRE-a of the mouse metallothionein-I gene and variant sequences. *Nucl. Acids Res.* **18,** 4683–4690 (1990).
55. Remondelli, P., Moltedo, O. & Leone, A. Regulation of ZiRF1 and basal SP1 transcription factor MRE-binding activity by transition metals. *FEBS Letters* **416,** 254–258 (1997).
56. Stuart, G. W., Searle, P. F. & Palmiter, R. D. Identification of multiple metal regulatory elements in mouse metallothionein-I promoter by assaying synthetic sequences. *, Published online: 31 October 1985; | doi:10.1038/317828a0* **317,** 828–831 (1985).
57. Lu, N. Z. *et al.* International Union of Pharmacology. LXV. The pharmacology and classification of the nuclear receptor superfamily: glucocorticoid, mineralocorticoid, progesterone, and androgen receptors. *Pharmacol. Rev.* **58,** 782–797 (2006).
58. Varshney, U., Jahroudi, N., Foster, R. & Gedamu, L. Structure, organization, and regulation of human metallothionein IF gene: differential and cell-type-specific expression in response to heavy metals and glucocorticoids. *Mol. Cell. Biol.* **6,** 26–37 (1986).
59. Andrews, G. K. Regulation of metallothionein gene expression by oxidative stress and metal ions. *Biochem. Pharmacol.* **59,** 95–104 (2000).
60. Dalton, T., Palmiter, R. D. & Andrews, G. K. Transcriptional induction of the mouse metallothionein-I gene in hydrogen peroxide-treated Hepa cells involves a composite major late transcription factor/antioxidant response element and metal response promoter elements. *Nucl. Acids Res.* **22,** 5016–5023 (1994).
61. Regulation of Zinc Homeostasis by Inducible NO Synthase-Derived NO: Nuclear Metallothionein Translocation and Intranuclear Zn^{2+} Release. **100,** 13952–13957 (2003).
62. Katakai, K., Liu, J., Nakajima, K., Keefer, L. K. & Waalkes, M. P. Nitric oxide induces metallothionein (MT) gene expression apparently by displacing zinc bound to MT. *Toxicology Letters* **119,** 103–108 (2001).
63. Um, H.-C., Jang, J.-H., Kim, D.-H., Lee, C. & Surh, Y.-J. Nitric oxide activates Nrf2 through S-nitrosylation of Keap1 in PC12 cells. *Nitric Oxide* **25,** 161–168 (2011).
64. Coto, J. A., Hadden, E. M., Sauro, M., Zorn, N. & Hadden, J. W. Interleukin 1 regulates secretion of zinc-thymulin by human thymic epithelial cells and its action on T-lymphocyte proliferation and nuclear protein kinase C. *Proc. Natl. Acad. Sci. U.S.A.* **89,** 7752–7756 (1992).

65. Ghoshal, K. & Jacob, S. T. Regulation of metallothionein gene expression. *Progress in nucleic acid research and molecular …* (2000). doi:10.1016/S0079-6603(00)66034-8
66. Kasutani, K., Itoh, N., Kanekiyo, M., Muto, N. & Tanaka, K. Requirement for cooperative interaction of interleukin-6 responsive element type 2 and glucocorticoid responsive element in the synergistic activation of mouse metallothionein-I gene by interleukin-6 and glucocorticoid. *Toxicol. Appl. Pharmacol.* **151,** 143–151 (1998).
67. Sato, M., Sasaki, M. & Hojo, H. Differential induction of metallothionein synthesis by interleukin-6 and tumor necrosis factor-alpha in rat tissues. *Int. J. Immunopharmacol.* **16,** 187–195 (1994).
68. Majumder, S., Ghoshal, K., Gronostajski, R. M. & Jacob, S. T. Downregulation of Constitutive and Heavy Metal-Induced Metallothionein-I Expression by Nuclear Factor I. (2001). doi:10.3727/000000001783992588
69. Tang, C. M., Westling, J. & Seto, E. trans repression of the human metallothionein IIA gene promoter by PZ120, a novel 120-kilodalton zinc finger protein. *Mol. Cell. Biol.* **19,** 680–689 (1999).
70. Majumder, S., Ghoshal, K., Li, Z., Bo, Y. & Jacob, S. T. Silencing of metallothionein-I gene in mouse lymphosarcoma cells by methylation. *Oncogene* **18,** 6287–6295 (1999).
71. Andrews, G. K. & Adamson, E. D. Butyrate selectively activates the metallothionein gene in teratocarcinoma cells and induces hypersensitivity to metal induction. *Nucl. Acids Res.* **15,** 5461–5475 (1987).
72. Birren, B. W. & Herschman, H. R. Regulation of the rat metallothionein-I gene by sodium butyrate. *Nucl. Acids Res.* **14,** 853–867 (1986).
73. Transcriptional regulation of the mouse metallothionein-I gene by heavy metals. (1981). at <http://www.jbc.org/content/256/11/5712.short>
74. Sadhu, C. & Gedamu, L. Metal-specific posttranscriptional control of human metallothionein genes. *Mol. Cell. Biol.* **9,** 5738–5741 (1989).
75. Vasconcelos, M. H., Tam, S. C., Beattie, J. H. & Hesketh, J. E. Evidence for differences in the post-transcriptional regulation of rat metallothionein isoforms. *Biochem. J.* **315 (Pt 2),** 665–671 (1996).
76. Vasconcelos, M. H., Tam, S.-C., Hesketh, J. E., Reid, M. & Beattie, J. H. Metal- and tissue-dependent relationship between metallothionein mRNA and protein. *Toxicol. Appl. Pharmacol.* **182,** 91–97 (2002).
77. Ogra, Y. & Suzuki, K. T. Biological significance of non-acetylated metallothionein. *Journal of Chromatography B: Biomedical Sciences …* (1999).
78. Brouwer, M., Hoexum-Brouwer, T. & Cashon, R. E. A putative glutathione-binding site in CdZn-metallothionein identified by equilibrium binding and molecular-modelling studies. *Biochem. J.* **294 (Pt 1),** 219–225 (1993).
79. Jiang, L. J., Maret, W. & Vallee, B. L. The glutathione redox couple modulates zinc transfer from metallothionein to zinc-depleted sorbitol dehydrogenase. *Proc. Natl. Acad. Sci. U.S.A.* **95,** 3483–3488 (1998).
80. Choudhuri, S., McKim, J. M., Jr. & Klaassen, C. D. Role of hepatic lysosomes in the degradation of metallothionein. *Toxicol. Appl. Pharmacol.* **115,** 64–71 (1992).
81. McKim, J. M., Jr., Choudhuri, S. & Klaassen, C. D. In vitro degradation of apo-,

zinc-, and cadmium-metallothionein by cathepsins B, C, and D. *Toxicol. Appl. Pharmacol.* **116,** 117–124 (1992).
82. Feldman, S. L., Failla, M. L. & Cousins, R. J. Degradation of rat liver metallothioneins in vitro. *Biochimica et Biophysica Acta (BBA) - General Subjects* **544,** 638–646 (1978).
83. Steinebach, O. M. & Wolterbeek, B. T. Metallothionein biodegradation in rat hepatoma cells: a compartmental analysis aided 35S-radiotracer study. *Biochimica et Biophysica Acta (BBA) - General Subjects* **1116,** 155–165 (1992).
84. Degradation of zinc-metallothionein in monolayer cultures of rat hepatocytes. *Proc. Soc. Exp. Biol. Med.* **191,** 130–138 (1989).
85. Klaassen, C. D., Choudhuri, S., James M McKim, S. J. S., Lehman-McKeeman, L. D. & Kershaw, W. C. In Vitro and In Vivo Studies on the Degradation of Metallothionein. *Environmental Health Perspectives* **102,** 141–146 (1994).
86. Saito, S. & Hunziker, P. E. Differential sensitivity of metallothionein-1 and -2 in liver of zinc-injected rat toward proteolysis. *Biochimica et Biophysica Acta (BBA) - General Subjects* **1289,** 65–70 (1996).
87. Woo, E. Nucleophilic Distribution of Metallothionein in Human Tumor Cells. *Exp. Cell Res.* **224,** 365–371 (1996).
88. Woo, E. S., Dellapiazza, D., Wang, A. S. & Lazo, J. S. Energy□dependent nuclear binding dictates metallothionein localization. *J. Cell. Physiol.* **182,** 69–76 (2000).
89. Nagano, T. *et al.* The transport mechanism of metallothionein is different from that of classical NLS□bearing protein. *J. Cell. Physiol.* **185,** 440–446 (2000).
90. Takahashi, Y., Ogra, Y. & Suzuki, K. T. Nuclear trafficking of metallothionein requires oxidation of a cytosolic partner. *J. Cell. Physiol.* **202,** 563–569 (2005).
91. Armario, A. *et al.* Age-dependent effects of acute and chronic intermittent stresses on serum metallothionein. *Physiology & Behavior* **39,** 277–279 (1987).
92. Hidalgo, J., Giralt, M., Garvey, J. S. & Armario, A. Physiological role of glucocorticoids on rat serum and liver metallothionein in basal and stress conditions. *Am J Physiol* (1988).
93. Tang, W. *et al.* Measurement of Cadmium-Induced Metallothionein in Urine by ELISA and Prevention of Overestimation Due to Polymerization. *J Anal Toxicol* **23,** 153–158 (1999).
94. Hart, B. A. & Garvey, J. S. Detection of metallothionein in bronchoalveolar cells and lavage fluid following repeated cadmium inhalation. *Environ. Res.* **40,** 391–398 (1986).
95. Suzuki, T. *et al.* Metallothionein of prostatic tissues and fluids in rats and humans. *Tohoku J Exp Med* **166,** 251–257 (1992).
96. Danielson, K. G., Ohi, S. & Huang, P. C. Immunochemical localization of metallothionein in rat liver and kidney. *J Histochem Cytochem* **30,** 1033–1039 (1982).
97. De Lisle, R. C., Sarras, M. P., Hidalgo, J. & Andrews, G. K. Metallothionein is a component of exocrine pancreas secretion: implications for zinc homeostasis. *Am J Physiol* **271,** C1103–C1110 (1996).
98. Milnerowicz, H. & Chmarek, M. Influence of smoking on metallothionein level and other proteins binding essential metals in human milk. *Acta Paediatr.* **94,**

402–406 (2005).
99. Shapiro, S. G. & Cousins, R. J. Induction of rat liver metallothionein mRNA and its distribution between free and membrane-bound polyribosomes. *Biochemical Journal* **190,** 755–764 (1980).
100. Nickel, W. Unconventional Secretory Routes: Direct Protein Export Across the Plasma Membrane of Mammalian Cells. *Traffic* **6,** 607–614 (2005).
101. Backhaus, R. *et al.* Unconventional protein secretion: Membrane translocation of FGF-2 does not require protein unfolding. *Journal of Cell Science* **117,** 1727–1736 (2004).
102. Nickel, W. The mystery of nonclassical protein secretion. *Eur J Biochem* **270,** 2109–2119 (2003).
103. Cannon, J. G., Evans, W. J. & Hughes, V. A. Physiological mechanisms contributing to increased interleukin-1 secretion. *J Appl …* (1986).
104. Wolff, N. A. Megalin-Dependent Internalization of Cadmium-Metallothionein and Cytotoxicity in Cultured Renal Proximal Tubule Cells. *Journal of Pharmacology and Experimental Therapeutics* **318,** 782–791 (2006).
105. Klassen, R. B. Megalin mediates renal uptake of heavy metal metallothionein complexes. *AJP: Renal Physiology* **287,** F393–F403 (2004).
106. Knecht, D. & Lynes, M. Metallothionein mediates leukocyte chemotaxis. *BMC Immunol* (2005).
107. Hamer, D. H. Metallothionein [1,2]. *Annu. Rev. Biochem.* **55,** 913–951 (1986).
108. Li, Y. & Maret, W. Human metallothionein metallomics. *Journal of Analytical Atomic Spectrometry* **23,** 1055–1062 (2008).
109. Aoki, Y. & Suzuki, K. T. Detection of metallothionein by western blotting. *Meth. Enzymol.* **205,** 108–114 (1991).
110. Zhang, X. *et al.* Structure of the Neurospora SET domain protein DIM-5, a histone H3 lysine methyltransferase. *Cell* **111,** 117–127 (2002).
111. Min, J., Zhang, X., Cheng, X., Grewal, S. I. S. & Xu, R.-M. Structure of the SET domain histone lysine methyltransferase Clr4. *Nature Structural & Molecular Biology* **9,** 828–832 (2002).
112. Berg, J. M. & Shi, Y. The Galvanization of Biology: A Growing Appreciation for the Roles of Zinc. *Science* **271,** 1081–1085 (1996).
113. Vallee, B. L. & Falchuk, K. H. The biochemical basis of zinc physiology. *Physiol. Rev.* **73,** 79–118 (1993).
114. Dinkova-Kostova, A. T. & Holtzclaw, W. D. Keap1, the sensor for electrophiles and oxidants that regulates the phase 2 response, is a zinc metalloprotein. *Biochemistry* (2005).
115. Winterbourn, C. C. & Hampton, M. B. Thiol chemistry and specificity in redox signaling. *Free Radic. Biol. Med.* **45,** 549–561 (2008).
116. Wouters, M. A., Fan, S. W. & Haworth, N. L. Disulfides as Redox Switches: From Molecular Mechanisms to Functional Significance. *http://dx.doi.org/10.1089/ars.2009.2510* **12,** 53–91 (2009).
117. Maret, W. & Vallee, B. L. Thiolate ligands in metallothionein confer redox activity on zinc clusters. *Proc. Natl. Acad. Sci. U.S.A.* **95,** 3478–3482 (1998).
118. Vašák, M. & Kägi, J. Spectroscopic properties of metallothionein. *Metal ions in biological systems* (1983).

119. Otvos, J. D. & Armitage, I. M. Cadmium-113 NMR of metallothionein: direct evidence for the existence of polynuclear metal binding sites. *J. Am. Chem. Soc.* **101,** 7734–7736 (1979).
120. Krezel, A. & Maret, W. Dual Nanomolar and Picomolar Zn(II) Binding Properties of Metallothionein. *J. Am. Chem. Soc.* **129,** 10911–10921 (2007).
121. Jacob, C., Maret, W. & Vallee, B. L. Control of zinc transfer between thionein, metallothionein, and zinc proteins. *Proc. Natl. Acad. Sci. U.S.A.* **95,** 3489–3494 (1998).
122. Maret, W. The function of zinc metallothionein: a link between cellular zinc and redox state. *J. Nutr.* **130,** 1455S–8S (2000).
123. Krezel, A. & Maret, W. Different redox states of metallothionein/thionein in biological tissue. *Biochem. J.* **402,** 551–558 (2007).
124. Irani, K. *et al.* Mitogenic signaling mediated by oxidants in Ras-transformed fibroblasts. *Science* (1997). doi:10.1126/science.275.5306.1649
125. S-Glutathionylation of metallothioneins by nitrosative/oxidative stress. (2008). at <http://www.sciencedirect.com/science/article/pii/S0531556507002689>
126. Thornalley, P. J. & Vašák, M. Possible role for metallothionein in protection against radiation-induced oxidative stress. Kinetics and mechanism of its reaction with superoxide and hydroxyl radicals. *Biochimica et Biophysica Acta (BBA) - Protein Structure and Molecular Enzymology* **827,** 36–44 (1985).
127. Pearce, L. L. *et al.* Role of metallothionein in nitric oxide signaling as revealed by a green fluorescent fusion protein. *Proc. Natl. Acad. Sci. U.S.A.* **97,** 477–482 (2000).
128. Khatai, L., Goessler, W., Lorencova, H. & Zangger, K. Modulation of nitric oxide-mediated metal release from metallothionein by the redox state of glutathione in vitro. *Eur J Biochem* **271,** 2408–2416 (2004).
129. Kröncke, K. D., Fehsel, K., Schmidt, T. & Zenke, F. T. Nitric oxide destroys zinc-sulfur clusters inducing zinc release from metallothionein and inhibition of the zinc finger-type yeast transcription activator LAC9. *Biochemical and …* (1994).
130. Yu Chen, Yoshifumi Irie, Wing Ming Keung, A. & Maret, W. S-Nitrosothiols React Preferentially with Zinc Thiolate Clusters of Metallothionein III through Transnitrosation†. *Biochemistry* **41,** 8360–8367 (2002).
131. Pluth, M. D., Tomat, E. & Lippard, S. J. Biochemistry of mobile zinc and nitric oxide revealed by fluorescent sensors. *Annu. Rev. Biochem.* **80,** 333–355 (2011).
132. Chen, Y. & Maret, W. Catalytic selenols couple the redox cycles of metallothionein and glutathione. *Eur J Biochem* **268,** 3346–3353 (2001).
133. Maret, W. Metallothionein redox biology in the cytoprotective and cytotoxic functions of zinc. *Exp Gerontol* **43,** 363–369 (2008).
134. Sagher, D., Brunell, D. & Hejtmancik, J. F. Thionein can serve as a reducing agent for the methionine sulfoxide reductases. *Proc. Natl. Acad. Sci. U.S.A.* **103,** 8656–8661 (2006).
135. Vallee, D. B. L. in *Metallothionein II* **52,** 5–16 (Birkhäuser Basel, 1987).
136. Lynes, M. A. Metallothionein and Anti-Metallothionein, Complementary Elements of Cadmium-Induced Renal Disease. *Toxicological Sciences* **91,** 1–3 (2006).
137. Lynes, M. A. *et al.* The physiological roles of extracellular metallothionein.

Experimental Biology and Medicine **231,** 1548–1554 (2006).
138. Devisscher, L., Hindryckx, P. & Olievier, K. Metallothionein, an emerging danger signal during experimental colitis. *25th Belgian Week of …* (2013).
139. Youn, J. & Lynes, M. A. Metallothionein-induced suppression of cytotoxic T lymphocyte function: An important immunoregulatory control. *Toxicological Sciences* **52,** 199–208 (1999).
140. Membrane-Bound Metallothionein 1 of Murine Dendritic Cells Promotes the Expansion of Regulatory T Cells In Vitro. (2013). at <http://toxsci.oxfordjournals.org/content/early/2013/12/22/toxsci.kft268.short>
141. Canpolat, E. & Lynes, M. A. In Vivo Manipulation of Endogenous Metallothionein with a Monoclonal Antibody Enhances a T-Dependent Humoral Immune Response. *Toxicological Sciences* **62,** 61–70 (2001).
142. Distinct roles of reactive nitrogen and oxygen species to control infection with the facultative intracellular bacterium Francisella tularensis. (2004). at <http://iai.asm.org/content/72/12/7172.short>
143. An inducible nitric oxide synthase-luciferase reporter system for in vivo testing of anti-inflammatory compounds in transgenic mice. (2003). at <http://www.jimmunol.org/content/170/12/6307.short>
144. Sena, L. A. *et al.* Mitochondria Are Required for Antigen-Specific T Cell Activation through Reactive Oxygen Species Signaling. *Immunity* **38,** 225–236 (2013).
145. Crowthers, K. C., Kline, V., Giardina, C. & Lynes, M. A. Augmented humoral immune function in metallothionein-null mice. *Toxicology and applied …* (2000).
146. Sakurai, A. *et al.* Regulatory role of metallothionein in NF-κB activation. *FEBS Letters* (1999).
147. Kröncke, K.-D. & Klotz, L.-O. Zinc fingers as biologic redox switches? *Antioxid Redox Signal* **11,** 1015–1027 (2009).
148. Fukada, T., Yamasaki, S., Nishida, K., Murakami, M. & Hirano, T. Zinc homeostasis and signaling in health and diseases: Zinc signaling. *J Biol Inorg Chem* **16,** 1123–1134 (2011).
149. Murakami, M. & Hirano, T. Intracellular zinc homeostasis and zinc signaling. *Cancer Science* **99,** 1515–1522 (2008).
150. Youn, J. *et al.* Metallothionein suppresses collagen-induced arthritis via induction of TGF-beta and down-regulation of proinflammatory mediators. *Clin. Exp. Immunol.* **129,** 232–239 (2002).
151. *Suppression of arthritis by metallothionein*. (Arthritis …, 2002). at <http://scholar.google.com#>
152. Park, L. *et al.* Tat-enhanced delivery of metallothionein can partially prevent the development of diabetes. *Free Radic. Biol. Med.* **51,** 1666–1674 (2011).
153. Treatment with metallothionein prevents demyelination and axonal damage and increases oligodendrocyte precursors and tissue repair during experimental …. (2003). at <http://onlinelibrary.wiley.com/doi/10.1002/jnr.10615/full>
154. Banu, N. & Meyers, C. M. IFN-gamma and LPS differentially modulate class I... [Kidney Int. 1999] - PubMed - NCBI. *Kidney Int* **55,** 2250–2263 (1999).
155. Jorgensen, P. F. *et al.* Peptidoglycan and lipoteichoic acid modify monocyte phenotype in human whole blood. *Clin. Diagn. Lab. Immunol.* **8,** 515–521 (2001).

156. Harding, F. A., McArthur, J. G., Gross, J. A., Raulet, D. H. & Allison, J. P. CD28-mediated signalling co-stimulates murine T cells and prevents induction of anergy in T-cell clones. *Nature* **356,** 607–609 (1992).
157. Lenschow, D. J., and, T. L. W. & Bluestone, J. A. CD28/B7 SYSTEM OF T CELL COSTIMULATION. **14,** 233–258 (2003).
158. Itano, A. A. & Jenkins, M. K. Antigen presentation to naive CD4 T cells in the lymph node. *Nat. Immunol.* **4,** 733–739 (2003).
159. Rao, P. S., Jaggi, M., Smith, D. J., Hemstreet, G. P. & Balaji, K. C. Metallothionein 2A interacts with the kinase domain of PKCμ in prostate cancer. *Biochemical and Biophysical Research Communications* **310,** 1032–1038 (2003).
160. Zhu, J. & Paul, W. E. CD4 T cells: Fates, functions, and faults. *Blood* **112,** 1557–1569 (2008).
161. Rincón, M. MAP-kinase signaling pathways in T cells. *Curr Opin Immunol* **13,** 339–345 (2001).
162. Son, Y. *et al.* Mitogen-Activated Protein Kinases and Reactive Oxygen Species: How Can ROS Activate MAPK Pathways? *Journal of Signal Transduction* **2011,** 1–6 (2011).
163. Clark, A. Crosstalk between glucocorticoids and mitogen-activated protein kinase signalling pathways. *Current Opinion in Pharmacology* **3,** 404–411 (2003).
164. Raingeaud, J. *et al.* Pro-inflammatory cytokines and environmental stress cause p38 mitogen-activated protein kinase activation by dual phosphorylation on tyrosine and threonine. *J. Biol. Chem.* **270,** 7420–7426 (1995).
165. Beyersmann, D. & Haase, H. Functions of zinc in signaling, proliferation and differentiation of mammalian cells. *Biometals* **14,** 331–341 (2001).
166. Olsen, J. V. *et al.* Global, In Vivo, and Site-Specific Phosphorylation Dynamics in Signaling Networks. *Cell* **127,** 635–648 (2006).
167. Haase, H. & Maret, W. Intracellular zinc fluctuations modulate protein tyrosine phosphatase activity in insulin/insulin-like growth factor-1 signaling. *Exp. Cell Res.* **291,** 289–298 (2003).
168. Williams, M. S. & Kwon, J. T cell receptor stimulation, reactive oxygen species, and cell signaling. **37,** 1144–1151 (2004).
169. Haynes, B. F., Telen, M. J., Hale, L. P. & Denning, S. M. CD44 — A molecule involved in leukocyte adherence and T-cell activation. *Immunology Today* **10,** 423–428 (1989).
170. Caruso, A. *et al.* Flow cytometric analysis of activation markers on stimulated T cells and their correlation with cell proliferation. *Cytometry* **27,** 71–76 (1997).
171. Zhu, J., Yamane, H. & Paul, W. E. Differentiation of Effector CD4 T Cell Populations *. *Annu Rev Immunol* **28,** 445–489 (2010).
172. Zhu, J. & Paul, W. E. Peripheral CD4+ T-cell differentiation regulated by networks of cytokines and transcription factors. *Immunol. Rev.* **238,** 247–262 (2010).
173. Mosmann, T. R., Cherwinski, H. & Bond, M. W. Two types of murine helper T cell clone. I. Definition according to profiles of lymphokine activities and secreted proteins. *The Journal of …* (1986).
174. Hsieh, C. S. *et al.* Development of TH1 CD4+ T cells through IL-12 produced by Listeria-induced macrophages. *Science* **260,** 547–549 (1993).

175. SZABO, S. A Novel Transcription Factor, T-bet, Directs Th1 Lineage Commitment. **100,** 655–669 (2000).
176. Le Gros, G., Ben-Sasson, S. Z., Seder, R., Finkelman, F. D. & Paul, W. E. Generation of interleukin 4 (IL-4)-producing cells in vivo and in vitro: IL-2 and IL-4 are required for in vitro generation of IL-4-producing cells. *Journal of Experimental Medicine* **172,** 921–929 (1990).
177. Swain, S. L., Weinberg, A. D., English, M. & Huston, G. IL-4 directs the development of Th2-like helper effectors. *J. Immunol.* **145,** 3796–3806 (1990).
178. Stockinger, B. & Veldhoen, M. Differentiation and function of Th17 T cells. *Curr Opin Immunol* (2007).
179. Bilate, A. M. & Lafaille, J. J. Induced CD4+Foxp3+ regulatory T cells in im... [Annu Rev Immunol. 2012] - PubMed - NCBI. *Annu Rev Immunol* **30,** 733–758 (2012).
180. Weaver, C. T. & Hatton, R. D. Interplay between the TH17 and TReg cell lineages: a (co-) evolutionary perspective. *Nat. Rev. Immunol.* (2009).
181. Grazia Roncarolo, M. *et al.* Interleukin□10□secreting type 1 regulatory T cells in rodents and humans. *Immunol. Rev.* **212,** 28–50 (2006).
182. Foussat, A. *et al.* A comparative study between T regulatory type 1 and CD4+CD25+ T cells in the control of inflammation. *The Journal of Immunology* **171,** 5018–5026 (2003).
183. Barrat, F. J. *et al.* In vitro generation of interleukin 10-producing regulatory CD4(+) T cells is induced by immunosuppressive drugs and inhibited by T helper type 1 (Th1)- and Th2-inducing cytokines. *J. Exp. Med.* **195,** 603–616 (2002).
184. Akbari, O., DeKruyff, R. H. & Umetsu, D. T. Pulmonary dendritic cells producing IL-10 mediate tolerance induced by respiratory exposure to antigen. *Nat. Immunol.* **2,** 725–731 (2001).
185. O'Neill, E. J., Nicolson, K. S. & Wraith, D. C. Role for IL-10 in suppression mediated by peptide-induced regulatory T cells in vivo. *The Journal of …* (2003). doi:10.4049/jimmunol.170.3.1240
186. Jonuleit, H., Schmitt, E., Schuler, G., Knop, J. & Enk, A. H. Induction of interleukin 10-producing, nonproliferating CD4(+) T cells with regulatory properties by repetitive stimulation with allogeneic immature human dendritic cells. *J. Exp. Med.* **192,** 1213–1222 (2000).
187. Pot, C., Apetoh, L., Awasthi, A. & Kuchroo, V. K. Induction of regulatory Tr1 cells and inhibition of T< sub> H</sub> 17 cells by IL-27. *Seminars in Immunology* (2011).
188. Chen, C., Lee, W.-H., Yun, P., Snow, P. & Liu, C.-P. Induction of autoantigen-specific Th2 and Tr1 regulatory T cells and modulation of autoimmune diabetes. *The Journal of Immunology* **171,** 733–744 (2003).
189. Maret, W. Molecular aspects of human cellular zinc homeostasis: redox control of zinc potentials and zinc signals. *Biometals* **22,** 149–157 (2009).
190. Williams, R. J. P. & Fraústo da Silva, J. J. R. The distribution of elements in cells. **200-202,** 247–348 (2000).
191. Cousins, R. J., Liuzzi, J. P. & Lichten, L. A. Mammalian zinc transport, trafficking, and signals. **281,** 24085–24089 (2006).

192. Colvin, R. A., Holmes, W. R., Fontaine, C. P. & Maret, W. Cytosolic zinc buffering and muffling: their role in intracellular zinc homeostasis. *Metallomics* **2,** 306–317 (2010).
193. Zalewski, P. *et al.* Use of a zinc fluorophore to measure labile pools of zinc in body fluids and cell-conditioned media. *BioTechniques* **40,** 509–520 (2006).
194. Haase, H., Hebel, S., Engelhardt, G. & Rink, L. Flow cytometric measurement of labile zinc in peripheral blood mononuclear cells. *Anal. Biochem.* **352,** 222–230 (2006).
195. Daaboul, D., Rosenkranz, E., Uciechowski, P. & Rink, L. Repletion of zinc in zinc-deficient cells strongly up-regulates IL-1β-induced IL-2 production in T-cells. *Metallomics* **4,** 1088–1097 (2012).
196. Giacconi, R. *et al.* Comparison of intracellular zinc signals in nonadherent lymphocytes from young-adult and elderly donors: role of zinc transporters (Zip family) and proinflammatory cytokines. *The Journal of Nutritional Biochemistry* **23,** 1256–1263 (2012).
197. Cipriano, C. *et al.* Polymorphisms in MT1a gene coding region are associated with longevity in Italian Central female population. *Biogerontology* **7,** 357–365 (2006).
198. Moroni, F. *et al.* Interrelationship among neutrophil efficiency, inflammation, antioxidant activity and zinc pool in very old age. *Biogerontology* **6,** 271–281 (2005).
199. Warner, G. L. & Lawrence, D. A. Stimulation of murine lymphocyte responses by cations. *Cellular Immunology* **101,** 425–439 (1986).
200. Mann, J. J. & Fraker, P. J. Zinc pyrithione induces apoptosis and increases expression of Bim. *Apoptosis* **10,** 369–379 (2005).
201. Matsui, H. *et al.* Low micromolar zinc exerts cytotoxic action under H2O2-induced oxidative stress: Excessive increase in intracellular Zn2+ concentration. *Toxicology* **276,** 27–32 (2010).
202. Shen, C. *et al.* Relating Cytotoxicity, Zinc Ions, and Reactive Oxygen in ZnO Nanoparticle-Exposed Human Immune Cells. *Toxicological Sciences* (2013). doi:10.1093/toxsci/kft187
203. Bao, B. *et al.* Intracellular free zinc up-regulates IFN-[gamma] and T-bet essential for Th1 differentiation in Con-A stimulated HUT-78 cells. *Biochemical and Biophysical Research Communications* (2011).
204. Aydemir, T. B., Blanchard, R. K. & Cousins, R. J. Zinc supplementation of young men alters metallothionein, zinc transporter, and cytokine gene expression in leukocyte populations. *Proc. Natl. Acad. Sci. U.S.A.* **103,** 1699–1704 (2006).
205. Shankar, A. H. & Prasad, A. S. Zinc and immune function: the biological basis of altered resistance to infection. *Am J Clin Nutr* **68,** 447S–463S (1998).
206. Frasca, D. *et al.* Protein phosphatase 2A (PP2A) is increased in old murine B cells and mediates p38 MAPK/tristetraprolin dephosphorylation and E47 mRNA instability. *Mech. Ageing Dev.* **131,** 306–314 (2010).
207. Che, K. F. *et al.* p38 mitogen-activated protein kinase/signal transducer and activator of transcription-3 pathway signaling regulates expression of inhibitory molecules in T Cells activated by HIV-1-exposed dendritic cells. *Molecular Medicine* **18,** 1169–1182 (2012).

208. Jarnicki, A. G. *et al.* Attenuating Regulatory T Cell Induction by TLR Agonists through Inhibition of p38 MAPK Signaling in Dendritic Cells Enhances Their Efficacy as Vaccine Adjuvants and Cancer Immunotherapeutics.
209. SAKLATVALA, J. The p38 MAP kinase pathway as a therapeutic target in inflammatory disease. *Current Opinion in Pharmacology* **4,** 372–377 (2004).
210. IL-27 induces the differentiation of Tr1-like cells from human naive CD4+T cells via the phosphorylation of STAT1 and STAT3. **136,** 21–28 (2011).
211. Kamiński, M. M. *et al.* T cell Activation Is Driven by an ADP-Dependent Glucokinase Linking Enhanced Glycolysis with Mitochondrial Reactive Oxygen Species Generation. *Cell Reports* **2,** 1300–1315 (2012).
212. Malaiyandi, L. M., Dineley, K. E. & Reynolds, I. J. Divergent consequences arise from metallothionein overexpression in astrocytes: Zinc buffering and oxidant-induced zinc release. *Glia* **45,** 346–353 (2004).
213. Kawano, Y., Noma, T. & Yata, J. Regulation of human IgG subclass production by cytokines. IFN-gamma and IL-6 act antagonistically in the induction of human IgG1 but additively in the induction of IgG2. *The Journal of Immunology* **153,** 4948–4958 (1994).
214. Stüber, E. & Strober, W. The T cell-B cell interaction via OX40-OX40L is necessary for the T cell-dependent humoral immune response. *J. Exp. Med.* **183,** 979–989 (1996).
215. Bossie, A. & Vitetta, E. S. IFN-gamma enhances secretion of IgG2a from IgG2a-committed LPS-stimulated murine B cells: implications for the role of IFN-gamma in class switching. *Cellular Immunology* **135,** 95–104 (1991).
216. Lettesjö, H. & Möller, E. IgG2b inducing factor from rheumatoid arthritis synovial fluid activates antibody production in highly purified mouse B lymphocytes. *Scand J Immunol* **45,** 43–49 (1997).
217. Wedderburn, L. R., Searle, S. J., Rees, A. R., Lamb, J. R. & Owen, M. J. Mapping T cell recognition: the identification of a T cell receptor residue critical to the specific interaction with an influenza hemagglutinin peptide. *Eur. J. Immunol.* **25,** 1654–1662 (1995).
218. Devadas, S., Zaritskaya, L., Rhee, S. G., Oberley, L. & Williams, M. S. Discrete generation of superoxide and hydrogen peroxide by T cell receptor stimulation: Selective regulation of mitogen-activated protein kinase activation and Fas ligand expression. *Journal of Experimental Medicine* **195,** 59–70 (2002).
219. Ayers, F. C., Warner, G. L., Smith, K. L. & Lawrence, D. A. Fluorometric quantitation of cellular and nonprotein thiols. *Anal. Biochem.* **154,** 186–193 (1986).
220. Inglis, J. J., Šimelyte, E., McCann, F. E., Criado, G. & Williams, R. O. Protocol for the induction of arthritis in C57BL/6 mice. *Nature Protocols* **3,** 612–618 (2008).
221. Li, Y., Hawkins, B. E., DeWitt, D. S., Prough, D. S. & Maret, W. The relationship between transient zinc ion fluctuations and redox signaling in the pathways of secondary cellular injury: Relevance to traumatic brain injury. *Brain Research* **1330,** 131–141 (2010).
222. Plum, L. M. *et al.* PTEN-inhibition by zinc ions augments interleukin-2-mediated Akt phosphorylation. *Metallomics* (2014). doi:10.1039/c3mt00197k

223. Rhee, I. & Veillette, A. Protein tyrosine phosphatases in lymphocyte activation and autoimmunity. *Nat. Immunol.* **13,** 439–447 (2012).
224. Ra, H. J. & Parks, W. C. Control of matrix metalloproteinase catalytic activity. *Matrix Biology* **26,** 587–596 (2007).
225. Lim, N. C., Freake, H. C. & Br ckner, C. Illuminating Zinc in Biological Systems. *Chem. Eur. J.* **11,** 38–49 (2005).
226. Qiao, W. *Development of in Vivo Cytosolic and Organellar Zinc Probes Using Zinc-binding Proteins in Saccharomyces Cerevisiae*. (2008).
227. Snitsarev, V., Budde, T., Stricker, T. P., Cox, J. M. & Krupa, D. J. Fluorescent Detection of Zn< sup> 2+</sup>-Rich Vesicles with Zinquin: Mechanism of Action in Lipid Environments. *Biophys J* **80,** 1538–1546 (2001).
228. Slepchenko, K. G. & Li, Y. V. Rising intracellular zinc by membrane depolarization and glucose in insulin-secreting clonal HIT-T15 beta cells. *Experimental Diabetes Research* **2012,** 1–8 (2012).
229. Zhao, J., Bertoglio, B. A., Gee, K. R. & Kay, A. R. The zinc indicator FluoZin-3 is not perturbed significantly by physiological levels of calcium or magnesium. *Cell Calcium* **44,** 422–426 (2008).
230. Feske, S., Skolnik, E. Y. & Prakriya, M. Ion channels and transporters in lymphocyte function and immunity. *Nat. Rev. Immunol.* **12,** 532–547 (2012).
231. Devinney, M. J., Reynolds, I. J. & Dineley, K. E. Simultaneous detection of intracellular free calcium and zinc using fura-2FF and FluoZin-3. *Cell Calcium* **37,** 225–232 (2005).
232. Lebedeva, I. V., Pande, P. & Patton, W. F. Sensitive and Specific Fluorescent Probes for Functional Analysis of the Three Major Types of Mammalian ABC Transporters. *PLoS ONE* **6,** e22429 (2011).
233. Scott, B. J. & Bradwell, A. R. Identification of the serum binding proteins for iron, zinc, cadmium, nickel, and calcium. *Clinical Chemistry* **29,** 629–633 (1983).
234. Kimura, M. Metallothioneins of monocytes and lymphocytes. *Meth. Enzymol.* **205,** 291–302 (1991).
235. Overbeck, S., Uciechowski, P., Ackland, M. L., Ford, D. & Rink, L. Intracellular zinc homeostasis in leukocyte subsets is regulated by different expression of zinc exporters ZnT-1 to ZnT-9. **83,** 368–380 (2008).
236. Mandar A Aras, E. A. Redox Regulation of Intracellular Zinc: Molecular Signaling in the Life and Death of Neurons. *Antioxid Redox Signal* **15,** 2249–2263 (2011).
237. Buttke, T. M. & Sandstrom, P. A. Redox regulation of programmed cell death in lymphocytes. *Free radical research* (1995). doi:10.3109/10715769509147548
238. Treves, S. Apoptosis Is Dependent on Intracellular Zinc and Independent of Intracellular Calcium in Lymphocytes. *Exp. Cell Res.* **211,** 339–343 (1994).
239. Dietary zinc deficiency and expression of T lymphocyte signal transduction proteins. **78,** 823–828 (2000).
240. Hadzic, T. *et al.* The role of low molecular weight thiols in T lymphocyte proliferation and IL-2 secretion. *The Journal of Immunology* **175,** 7965–7972 (2005).
241. Cayota, A., Vuillier, F., Gonzalez, G. & Dighiero, G. In vitro antioxidant treatment recovers proliferative responses of anergic CD4+ lymphocytes from human immunodeficiency virus-infected individuals. *Blood* **87,** 4746–4753 (1996).

242. Monick, M. M. *et al.* Intracellular thiols contribute to Th2 function via a positive role in IL-4 production. *The Journal of Immunology* **171,** 5107–5115 (2003).
243. Pedersen-Lane, J. H., Zurier, R. B. & Lawrence, D. A. Analysis of the thiol status of peripheral blood leukocytes in rheumatoid arthritis patients. *J. Leukoc. Biol.* **81,** 934–941 (2007).
244. Lawrence, D. A., Song, R. & Weber, P. Surface thiols of human lymphocytes and their changes after in vitro and in vivo activation. *J. Leukoc. Biol.* **60,** 611–618 (1996).
245. Dominici, S., Valentini, M., Maellaro, E. & Del Bello, B. Redox modulation of cell surface protein thiols in U937 lymphoma cells: the role of γ-glutamyl transpeptidase-dependent H 2 O 2 \ldots. *Free Radical Biology \ldots* (1999).
246. Banerjee, R. Redox Remodeling as an Immunoregulatory Strategy - Biochemistry (ACS Publications). *Biochemistry* (2010).
247. Langmade, S. J., Ravindra, R., Daniels, P. J. & Andrews, G. K. The Transcription Factor MTF-1 Mediates Metal Regulation of the Mouse ZnT1 Gene. *J. Biol. Chem.* **275,** 34803–34809 (2000).
248. Palmiter, R. D. Protection against zinc toxicity by metallothionein and zinc transporter 1. in *Proc. Natl. Acad. Sci. U.S.A.* **101,** 4918–4923 (National Acad Sciences, 2004).
249. Eide, D. J. Zinc transporters and the cellular trafficking of zinc. **1763,** 711–722 (2006).
250. Dodeller, F. & Schulze-Koops, H. The p38 mitogen-activated protein kinase signaling cascade in CD4 T cells. *Arthritis Res. Ther.* (2006).
251. Lu, B. *et al.* GADD45γ Mediates the Activation of the p38 and JNK MAP Kinase Pathways and Cytokine Production in Effector TH1 Cells. *Immunity* **14,** 583–590 (2001).
252. Maneechotesuwan, K., Xin, Y. & Ito, K. Regulation of Th2 cytokine genes by p38 MAPK-mediated phosphorylation of GATA-3. *The Journal of …* **178,** 2491–2498 (2007).
253. Noubade, R. *et al.* Activation of p38 MAPK in CD4 T cells controls IL-17 production and autoimmune encephalomyelitis. at <http://www.ncbi.nlm.nih.gov/pubmed/21791428>
254. Sato, K., Nagayama, H., Tadokoro, K., Juji, T. & Takahashi, T. A. Extracellular signal-regulated kinase, stress-activated protein kinase/c-Jun N-terminal kinase, and p38mapk are involved in IL-10-mediated selective repression of TNF-alpha-induced activation and maturation of human peripheral blood monocyte-derived dendritic cells. *The Journal of Immunology* **162,** 3865–3872 (1999).
255. Koprak, S., Staruch, M. J. & Dumont, F. J. A specific inhibitor of the p38 mitogen activated protein kinase affects differentially the production of various cytokines by activated human T cells: dependence on CD28 signaling and preferential inhibition of IL-10 production. *Cellular Immunology* **192,** 87–95 (1999).
256. Veiopoulou, C. *et al.* IL-2 and IL-10 production by human CD4+T cells is differentially regulated by p38: mode of stimulation-dependent regulation of IL-2. *Gynecol Obstet Invest* **11,** 199–208 (2004).
257. Salvador, J. M. *et al.* Alternative p38 activation pathway mediated by T cell receptor-proximal tyrosine kinases. *Nat. Immunol.* **6,** 390–395 (2005).

258. Holler, P. D. & Kranz, D. M. Quantitative analysis of the contribution of TCR/pepMHC affinity and CD8 to T cell activation. *Immunity* **18,** 255–264 (2003).
259. Noel, P. J., Boise, L. H., Green, J. M. & Thompson, C. B. CD28 costimulation prevents cell death during primary T cell activation. *J. Immunol.* **157,** 636–642 (1996).
260. Linsley, P. S. & Ledbetter, J. A. The role of the CD28 receptor during T cell responses to antigen. *Annu Rev Immunol* (1993).
261. Goldberg, R., Wildbaum, G., Zohar, Y., Maor, G. & Karin, N. Suppression of ongoing adjuvant-induced arthritis by neutralizing the function of the p28 subunit of IL-27. *The Journal of Immunology* **173,** 1171–1178 (2004).
262. LeBel, C. P., Ischiropoulos, H. & Bondy, S. C. Evaluation of the probe 2‘,7’-dichlorofluorescin as an indicator of reactive oxygen species formation and oxidative stress. *Chem. Res. Toxicol.* **5,** 227–231 (1992).
263. Krezel, A. & Bal, W. Studies of zinc(II) and nickel(II) complexes of GSH, GSSG and their analogs shed more light on their biological relevance. *Bioinorg Chem Appl* 293–305 (2004). doi:10.1155/S1565363304000172
264. Jackson, S. H., Devadas, S., Kwon, J., Pinto, L. A. & Williams, M. S. T cells express a phagocyte-type NADPH oxidase that is activated after T cell receptor stimulation. *Nat. Immunol.* **5,** 818–827 (2004).
265. Zhao, B. L., Duan, S. J. & Xin, W. J. Lymphocytes can produce respiratory burst and oxygen radicals as polymorphonuclear leukocytes. *Cell Biophys.* **17,** 205–211 (1990).
266. Efimova, O., Szankasi, P. & Kelley, T. W. Ncf1 (p47phox) is essential for direct regulatory T cell mediated suppression of CD4+ effector T cells. **6,** (2011).
267. Prakriya, M. & Lewis, R. S. CRAC channels: activation, permeation, and the search for a molecular identity. *Cell Calcium* (2003).
268. Vig, M., Srivastava, S., Kandpal, U. & Sade, H. Inducible nitric oxide synthase in T cells regulates T cell death and immune memory. *The Journal of …* (2004). doi:10.1172/JCI20225
269. Liew, F. Y. Regulation of lymphocyte functions by nitric oxide. *Curr Opin Immunol* **7,** 396–399 (1995).
270. Koncz, A. *et al.* Nitric oxide mediates T cell cytokine production and signal transduction in histidine decarboxylase knockout mice. *The Journal of Immunology* **179,** 6613–6619 (2007).
271. Wei, X.-Q. *et al.* Altered immune responses in mice lacking inducible nitric oxide synthase. *, Published online: 01 June 1995; | doi:10.1038/375408a0* **375,** 408–411 (1995).
272. Niedbala, W. Nitric oxide preferentially induces type 1 T cell differentiation by selectively up-regulating IL-12 receptor beta 2 expression via cGMP. *Proceedings of the National Academy of Sciences* **99,** 16186–16191 (2002).
273. Huang, F. P. *et al.* Nitric oxide regulates Th1 cell development through the inhibition of IL-12 synthesis by macrophages. *Eur. J. Immunol.* **28,** 4062–4070 (1998).
274. Ruiz-Stewart, I. *et al.* Guanylyl cyclase is an ATP sensor coupling nitric oxide signaling to cell metabolism. in *Proc. Natl. Acad. Sci. U.S.A.* **101,** 37–42 (National Acad Sciences, 2004).

275. Szabó, C., Ischiropoulos, H. & Radi, R. Peroxynitrite: biochemistry, pathophysiology and development of therapeutics. *Nature Reviews Drug Discovery* **6,** 662–680 (2007).
276. St Croix, C. M. *et al.* Nitric oxide-induced changes in intracellular zinc homeostasis are mediated by metallothionein/thionein. **282,** L185–L192 (2002).
277. Aravindakumar, C. T., Ceulemans, J. & De Ley, M. Nitric oxide induces Zn2+ release from metallothionein by destroying zinc-sulphur clusters without concomitant formation of S-nitrosothiol. *Biochem. J.* **344 Pt 1,** 253–258 (1999).
278. Kassim, R., Ramseyer, C. & Enescu, M. Oxidation of Zinc–Thiolate Complexes of Biological Interest by Hydrogen Peroxide: A Theoretical Study. *Inorg. Chem.* **50,** 5407–5416 (2011).
279. Wolfgang Maret, C. J. B. L. V. E. H. F. Inhibitory sites in enzymes: Zinc removal and reactivation by thionein. *Proceedings of the National Academy of Sciences* **96,** 1936–1940 (1999).
280. Ren, F., Chen, X., Hesketh, J., Gan, F. & Huang, K. Selenium promotes T-cell response to TCR-stimulation and ConA, but not PHA in primary porcine splenocytes. *PLoS ONE* **7,** e35375 (2012).
281. Hoffmann, F. W. *et al.* Dietary selenium modulates activation and differentiation of CD4+ T cells in mice through a mechanism involving cellular free thiols. *J. Nutr.* **140,** 1155–1161 (2010).
282. Lee, K. & Esselman, W. J. Inhibition of PTPs by H2O2 regulates the activation of distinct MAPK pathways. *Free Radic. Biol. Med.* **33,** 1121–1132 (2002).
283. Simon, A. R., Rai, U., Fanburg, B. L. & Cochran, B. H. Activation of the JAK-STAT pathway by reactive oxygen species. *Am J Physiol* **275,** C1640–C1652 (1998).
284. Gloire, G., Legrand-Poels, S. & Piette, J. NF-κB activation by reactive oxygen species: Fifteen years later. *Biochem. Pharmacol.* **72,** 1493–1505 (2006).
285. Varin, A. *et al.* In vitro and in vivo effects of zinc on cytokine signalling in human T cells. *Exp Gerontol* **43,** 472–482 (2008).
286. Krutzik, P. O., Irish, J. M., Nolan, G. P. & Perez, O. D. Analysis of protein phosphorylation and cellular signaling events by flow cytometry: techniques and clinical applications. *Clin Immunol* (2004).
287. Krezel, A. & Maret, W. Thionein/metallothionein control Zn(II) availability and the activity of enzymes. *J Biol Inorg Chem* **13,** 401–409 (2007).
288. Penkowa, M. & Hidalgo, J. Metallothionein Treatment Reduces Proinflammatory Cytokines IL-6 and TNF-[alpha] and Apoptotic Cell Death during Experimental Autoimmune Encephalomyelitis (EAE). *Experimental neurology* **170,** 1–14 (2001).
289. O'Garra, A., Vieira, P. L., Vieira, P. & Goldfeld, A. E. IL-10-producing and naturally occurring CD4+Tregs: Limiting collateral damage. *Journal of Clinical Investigation* **114,** 1372–1378 (2004).
290. Parker, D. C. T cell-dependent B cell activation. *Annu Rev Immunol* **11,** 331–360 (1993).
291. Catchpole, B., Staines, N. A. & Hamblin, A. S. Antigen presentation of Type II collagen in rats. *Clin. Exp. Immunol.* **125,** 478–484 (2001).
292. Emeny, R. T. *et al.* Manipulations of metallothionein gene dose accelerate the

response to Listeria monocytogenes. *Chem. Biol. Interact.* **181,** 243–253 (2009).
293. Klouche, M., Wilhelm, D. & Kirchner, H. Cytokines, immunoglobulins, and IgG subclasses in patients with IgG plasmacytomas. *Immun. Infekt.* **22,** 149–151 (1994).
294. King, C. L. & Nutman, T. B. IgE and IgG subclass regulation by IL-4 and IFN-gamma in human helminth infections. Assessment by B cell precursor frequencies. *The Journal of Immunology* **151,** 458–465 (1993).
295. Whiteside, T. L. *et al.* Enzyme-linked immunospot, cytokine flow cytometry, and tetramers in the detection of T-cell responses to a dendritic cell-based multipeptide vaccine in patients with melanoma. *Clin Cancer Res* **9,** 641–649 (2003).
296. Lalvani, A. *et al.* Rapid detection of Mycobacterium tuberculosis infection by enumeration of antigen-specific T cells. *Am. J. Respir. Crit. Care Med.* **163,** 824–828 (2001).
297. Raulf-Heimsoth, M. *et al.* T-cell receptor repertoire expression in workers with occupational asthma due to platinum salt. *Eur Respir J* **16,** 871–878 (2000).
298. Cernea, S. & Herold, K. C. Monitoring of antigen-specific CD8 T cells in patients with type 1 diabetes treated with antiCD3 monoclonal antibodies. *Clin Immunol* **134,** 121–129 (2010).
299. Reijonen, H., Kwok, W. W. & Nepom, G. T. Detection of CD4+ autoreactive T cells in T1D using HLA class II tetramers. *Annals of the New York Academy of Sciences* **1005,** 82–87 (2003).
300. Reche, P. A. & Reinherz, E. L. Sequence variability analysis of human class I and class II MHC molecules: functional and structural correlates of amino acid polymorphisms. *J. Mol. Biol.* **331,** 623–641 (2003).
301. Deviren, G., Gupta, K., Paulaitis, M. E. & Schneck, J. P. Detection of antigen-specific T cells on p/MHC microarrays. *J Mol Recognit* **20,** 32–38 (2007).
302. Soen, Y., Chen, D. S., Kraft, D. L., Davis, M. M. & Brown, P. O. Detection and characterization of cellular immune responses using peptide-MHC microarrays. *PLoS Biol* **1,** E65–E65 (2003).
303. Unfricht, D. W., Colpitts, S. L., Fernandez, S. M. & Lynes, M. A. Grating-coupled surface plasmon resonance: a cell and protein microarray platform. *Proteomics* **5,** 4432–4442 (2005).
304. Chabot, V. *et al.* Biosensing based on surface plasmon resonance and living cells. *Biosens Bioelectron* **24,** 1667–1673 (2009).
305. Reilly, M., Sr, Nessing, P. & Guignon, E. SPR surface enhanced fluorescence with a gold-coated corrugated sensor chip. in (2006).
306. Jin, G. B., Unfricht, D. W., Fernandez, S. M. & Lynes, M. A. Cytometry on a chip: Cellular phenotypic and functional analysis using grating-coupled surface plasmon resonance. *Biosens Bioelectron* **22,** 200–206 (2006).
307. Schmid, A. H., Stanca, S. E., Thakur, M. S., Thampi, K. R. & Suri, C. R. Site-directed antibody immobilization on gold substrate for surface plasmon resonance sensors. *Sens Actuators B Chem* **113,** 297–303 (2006).
308. Andersson, L. O., Rehnström, A. & Eaker, D. L. Studies on 'nonspecific' binding. *Eur J Biochem* **20,** 371–380 (1971).
309. Pierres, A., Tissot, O., Malissen, B. & Bongrand, P. Dynamic adhesion of CD8-

positive cells to antibody-coated surfaces: The initial step is independent of microfilaments and intracellular domains of cell-binding molecules. *J. Cell Biol.* **125,** 945–953 (1994).
310. Chang, K.-C. & Hammer, D. A. The Forward Rate of Binding of Surface-Tethered Reactants: Effect of Relative Motion between Two Surfaces. *Biophys J* **76,** 1280–1292 (1999).
311. Trudeau, J. D., Chandler, T., Soukhatcheva, G., Verchere, C. B. & Tan, R. Prospective prediction of spontaneous but not recurrent autoimmune diabetes in the non-obese diabetic mouse. *Diabetologia* **50,** 1015–1023 (2007).
312. Trudeau, J. D. Prediction of spontaneous autoimmune diabetes in NOD mice by quantification of autoreactive T cells in peripheral blood. **111,** 217–223 (2003).
313. Danke, N. A., Yang, J., Greenbaum, C. & Kwok, W. W. Comparative study of GAD65-specific CD4+ T cells in healthy and type 1 diabetic subjects. *J. Autoimmun.* **25,** 303–311 (2005).
314. Davis, J. M. *et al.* Analysis of complex biomarkers for human immune-mediated disorders based on cytokine responsiveness of peripheral blood cells. *The Journal of Immunology* **184,** 7297–7304 (2010).
315. Mishra, K. P. *et al.* Effect of lead exposure on the immune response of some occupationally exposed individuals. *Toxicology* **188,** 251–259 (2003).